X-RAY DIFFRACTION STUDIES AT VERY HIGH PRESSURE ABOVE 100 KBAR

by

Akihito OHTANI

Department of Material Physics
Faculty of Engineering Science
Osaka University

February 1979

CONTENTS

ACKNOWLEDGMENT

The author expresses his cordial thanks to Professor N. Kawai for valuable guidance and advices in the entire course of the study. He also expresses his appreciation to Professor S. Kume and Dr. A. Onodera for critical reading of the manuscript and helpful discussions. The excellent technical support of Mr. K. Tanaka is gratefully acknowledged. Thanks are due to Professor S. Narita, Dr. S. Block and Dr. J. A. Van Vechten for the supply of the crystals.

ABSTRACT

A new pressure device is developed. It consists of an octahedral assemblage of anvils and a pair of guide blocks driven by a uniaxial hydraulic press. Hydrostatic pressures higher than 250 kbar can be applied on a sample.

Using this device, the x-ray diffractions are undertaken. Simultaneous measurements of electrical resistance are also attempted. Pressures required for metallic transitions of several semiconductors are determined by the correlations of lattice shrinkage of NaCl due to compression, which is theoretically evaluated by an equation of state of this substance. The results are shown to be accurate enough to use these values as the fixed points on the universal scale of pressure standard.

The present investigation also makes it possible to add the transition point of GaP at 253 kbar as a new fixed point on the scale.

GENERAL INTRODUCTION

Temperature and pressure are the most fundamental and virtual parameters upon which physical and chemical properties are influenced. Measurements of temperature are undertaken with high accuracy but the determination of pressure usually meets a difficulty above 100 kbar. The reason is mainly attributed to the lack of absolute scale to which the pressure worked on a specimen is correlated and calibrated.

Recently success is seen in the x-ray diffractions of specimens under pressures. A loosely packed crystal, in general, transforms into a new polymorphic phase, with both higher density and also in most cases higher coordination number. The x-ray analysis is necessary to know the structure of the high-pressure phase, especially in the case when the high-pressure phase cannot be quenched to room temperature and ordinary pressure. Although the transition is detectable with various methods (e.g., dilatometric, resistometric, or optical), x-ray diffraction analysis can confirm the real existence of the transition. The volume change associated with the transition can also be measured.

Another use of x-ray diffraction is to measure a change of lattice parameter of substance by compression.

When the substance is compressed, the distance between the constituent atoms or ions decreases and it follows the shrinkage of volume. If the lattice energies of both potential and vibrational are theoretically evaluated, the force which is required to shrink the crystal is obtained. Consequently, the magnitude of pressure compressing a specimen is estimated by the observation of change of lattice parameter determined by the x-ray diffraction.

The practical application of relation between the compressibility and the pressure is useful to solve the above-stated difficulty and this is, at present, only the way to know the absolute value of working pressure.

There have been a number of pressure vessels with which one can carry out x-ray diffraction studies. They are roughly classified into three categories, namely, (a) the piston-cylinder type, (b) the opposed anvil type, and (c) the multianvil type, respectively. In the piston-cylinder vessels, gas and liquid media are mostly used, and hence the pressure is hydrostatic. Since the solid media are compressed in the opposed anvil and multianvil vessels, especially at pressures above 100 kbar, the generated pressure in the solid is by no means hydrostatic. Multianvils driven by the respective forces

multiaxial in directions can be expected to generate more isotropic pressure compared to the use of uniaxial apparatus. Thus the pressure in the multianvil devices is said to be quasi-hydrostatic despite the solid is medium for pressure transmitting. Hydrostatic condition is expected to be enhanced with increasing number of anvils which compress the medium.

In part I of this paper is first discribed the design of a new device in which an octahedral specimen medium is used and which is capable of x-ray diffraction studies. Secondly, the advantages of this device and the comparison of pressure transmitting media of different kinds are shown.

In part II, the experiments of simultaneous observations of x-ray diffraction of NaCl and of electric resistance change of several semiconductors are shown. The threshold pressures, at which the phase transformations of semiconductor to metallic state commence, are determined and these results are combined with those of x-ray diffraction to discuss a possibility of use of the transition points as a new scale of pressure standards.

Part I. PRESSURE VESSEL OF SPLIT-OCTAHEDRON TYPE FOR X-RAY DIFFRACTION STUDIES

1. Introduction

In 1933, Cohn started x-ray diffraction studies at elevated pressures (Cohn, 1933). The films were arranged outside a Be window of the pressure bomb. The pressure was generated up to 3 kbar. In 1935, Frevel measured the compressibility of CsI up to 1 kbar using pyrex glass capillary tube (Frevel, 1935). It was Jacobs (1938) who first succeeded in identifying the crystallographic structure of high-pressure phase of AgI. Until 1950, piston-cylinder apparatuses made of Be or diamond as the cylinder were used (Lawson and Riley, 1949; Lawson and Tang, 1950). The x-ray films were located again outside of the cylinders and the materials to be tested were pressurized with various liquids in the piston-cylinder. The pressures worked on the samples, therefore, were hydrostatic but the available pressure was very much restricted because of the low tensile strengths in both Be and diamond.

Since 1959, high-pressure x-ray analyses have been extensively studied in the solid pressure transmitting media, and a wide variety of pressure devices has been

used. The devices can be classified into four groups :

(i) opposed anvil device (Jamieson et al., 1959; Jamieson and Lawson, 1962; Bassett et al., 1967; Kapitanov et al., 1975),

(ii) supported opposed anvil device (Drickamer type) (Perez-Albuerne et al., 1964),

(iii) supported piston device (Belt type) (Freud and LaMori, 1969; Freud and Sclar, 1969),

(iv) multianvil device (Barnett and Hall, 1964; Contre, 1969; Inoue and Asada, 1973; Ohtani et al., 1977).

The prerequisites in each device are that the pressure medium should be transparent to x-rays and that a clearance should be left between the anvils or pistons for the path of the x-rays. The pressure medium is made of materials having low average atomic number and less x-ray absorption characteristics, such as B or LiH. In the opposed anvil devices, the anvil is made of diamond, c-BN*, or WC. When the gem-quality diamond or c-BN is used, the x-ray beam can penetrate through the axis of opposed anvils. In the other devices of (ii), (iii), and (iv), the anvils or pistons are made of WC. The x-rays are radiated into the specimen through the clearance left between the

---

* cubic zincblende form of BN

adjoining anvils or pistons.

The volume of the pressure medium, that of the specimen, and the attainable pressure in each type of device are tabulated in Table 1-1. Figure 1-1 shows the volume of specimen and the attainable pressure. The obtainable volume is relatively large in the multianvil devices as well as in the supported anvil or supported piston devices, whereas it becomes extremely small in the opposed anvil device. Although high pressures are attainable in the diamond-anvil cell, the pressure generated in the space between the opposed anvil faces become nonhydrostatic, and an anisotropic deformation of the specimen is accompanied as shown in Fig. 1-2.

In the multianvil devices, the generated pressures are expected to be more hydrostatic than in any other type of vessels (Fig. 1-2). According to this request, four (Barnett and Hall, 1964), six (Contre, 1969; Inoue and Asada, 1973), and eight (Ohtani et al., 1977) anvils have been designed to compress tetrahedral, hexahedral, and octahedral pressure media and the injections of beam have been attempted through the clearance between the adjoining anvils. The x-rays diffracted by a specimen are collected on the curved surface on which either a film or a counter is mounted.

Table 1-1. Attainable pressure and working volume in various x-ray apparatuses.

Apparatus	Pressure (kbar)	Volume of specimen (cc)	Volume of chamber (cc)	References
Diamond anvil	1,000	1×10^{-8}	1×10^{-8}	Mao et al., (1978)
WC Bridgman anvil	165	2×10^{-5}	1×10^{-3}	Mii et al., (1973)
WC Drickamer anvil	450	4×10^{-5}	2×10^{-3}	Perez-Albuerne et al., (1964)
Belt	100	7×10^{-5}	5×10^{-2}	Freud et al., (1969)
Cubic anvil	233	1×10^{-3}	5×10^{-2}	Yagi and Akimoto, (1977)
Octahedral anvil	256	2×10^{-4}	6×10^{-3}	Present work

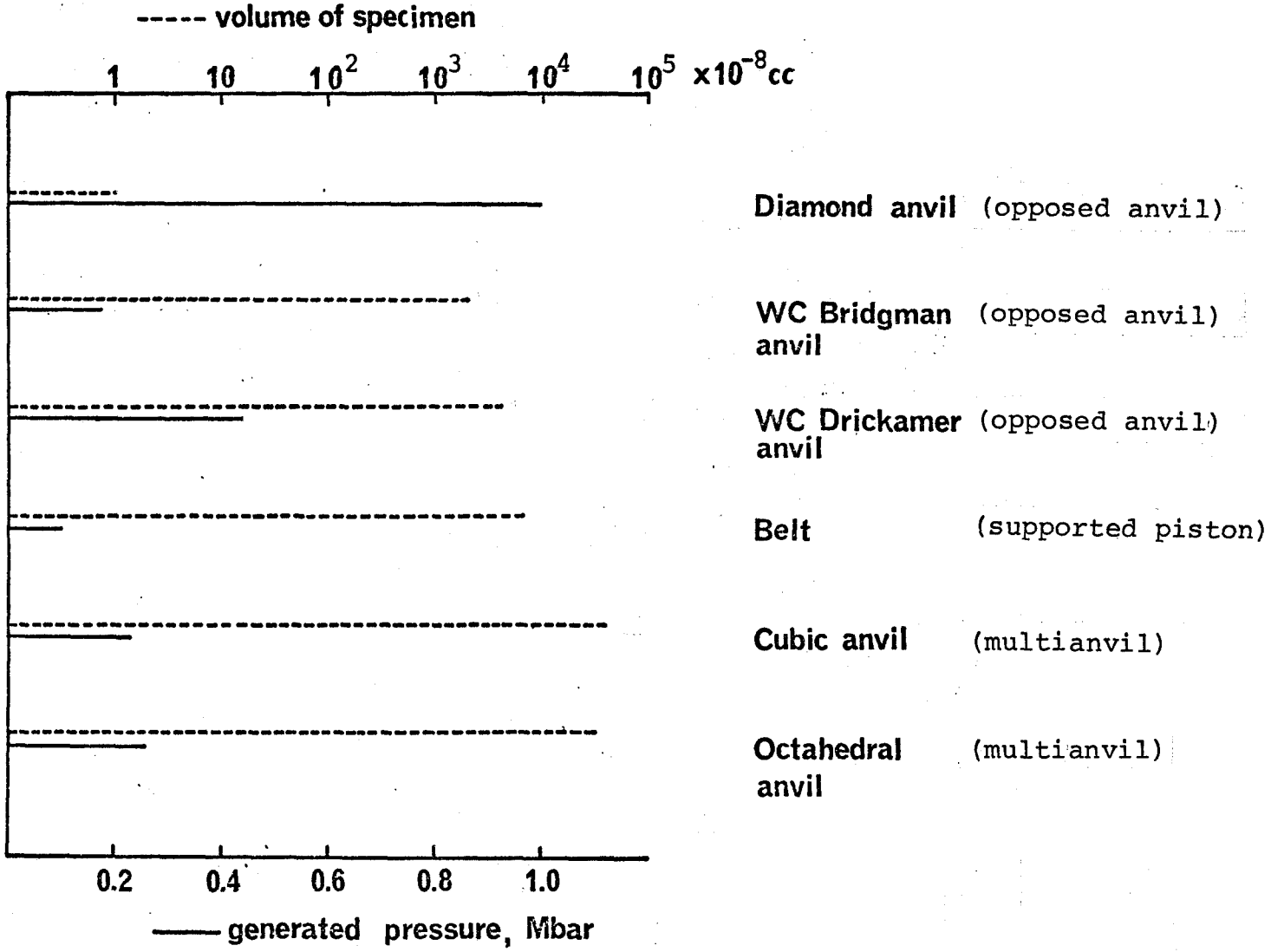

Fig. 1-1. Volume of specimen(dashed line) and generated pressure(solid line) in various types of x-ray apparatus.

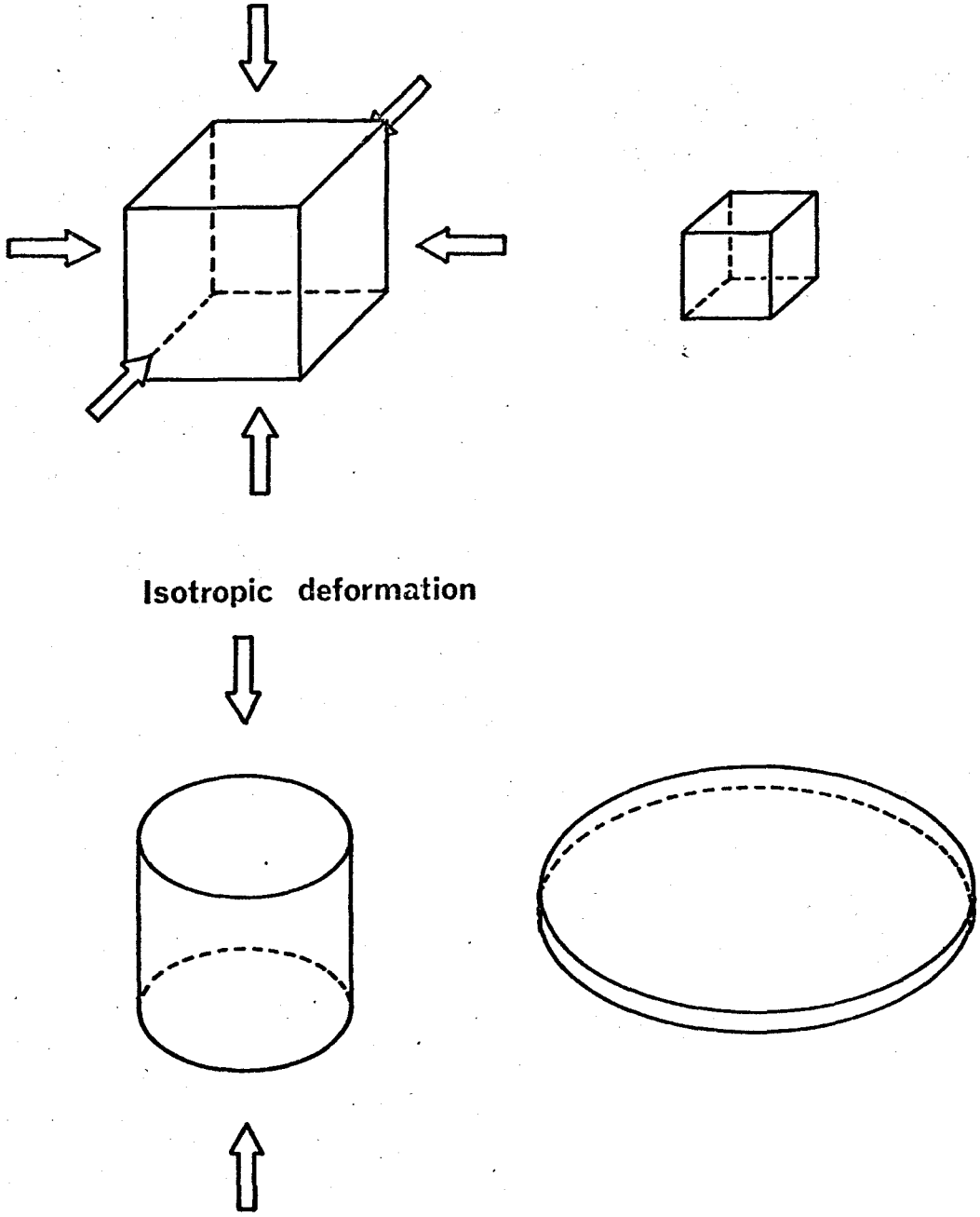

Fig. 1-2. Schema showing isotropic deformation in cubic press and uniaxial deformation in opposed anvil apparatus, respectively.

Amongst the three types of the multianvil devices, the octahedral anvil device is expected to generate the most hydrostatic pressure, since the pressure medium is compressed with the highest number of anvils.

Until the author developed a new device, a split-cone type apparatus as shown in Fig. 1-3 had been used for x-ray diffraction studies in our laboratory. Two cones, each divided into four anvils, were enclosed into rubber caps, on the outer surface of which was applied a load pressure using compressed oil. This system had unavoidable error in the accuracy of the shrinkage. The anvils, for example, showed a misalignment as shown in Fig. 1-4. The advancement of anvils got stagnated and the x-ray beam was intercepted by the adjacent anvils. Besides, the system could not resist the eventual intrusion of the rubber cap into gaps between the anvils. Consequently, very high pressure was hardly producible. It also occurred that the center of the specimen frequently shifted from the original position to which the x-ray beam should have been irradiated.

In order to avoid the above-mentioned defects, the design of the vessel has completely been changed.

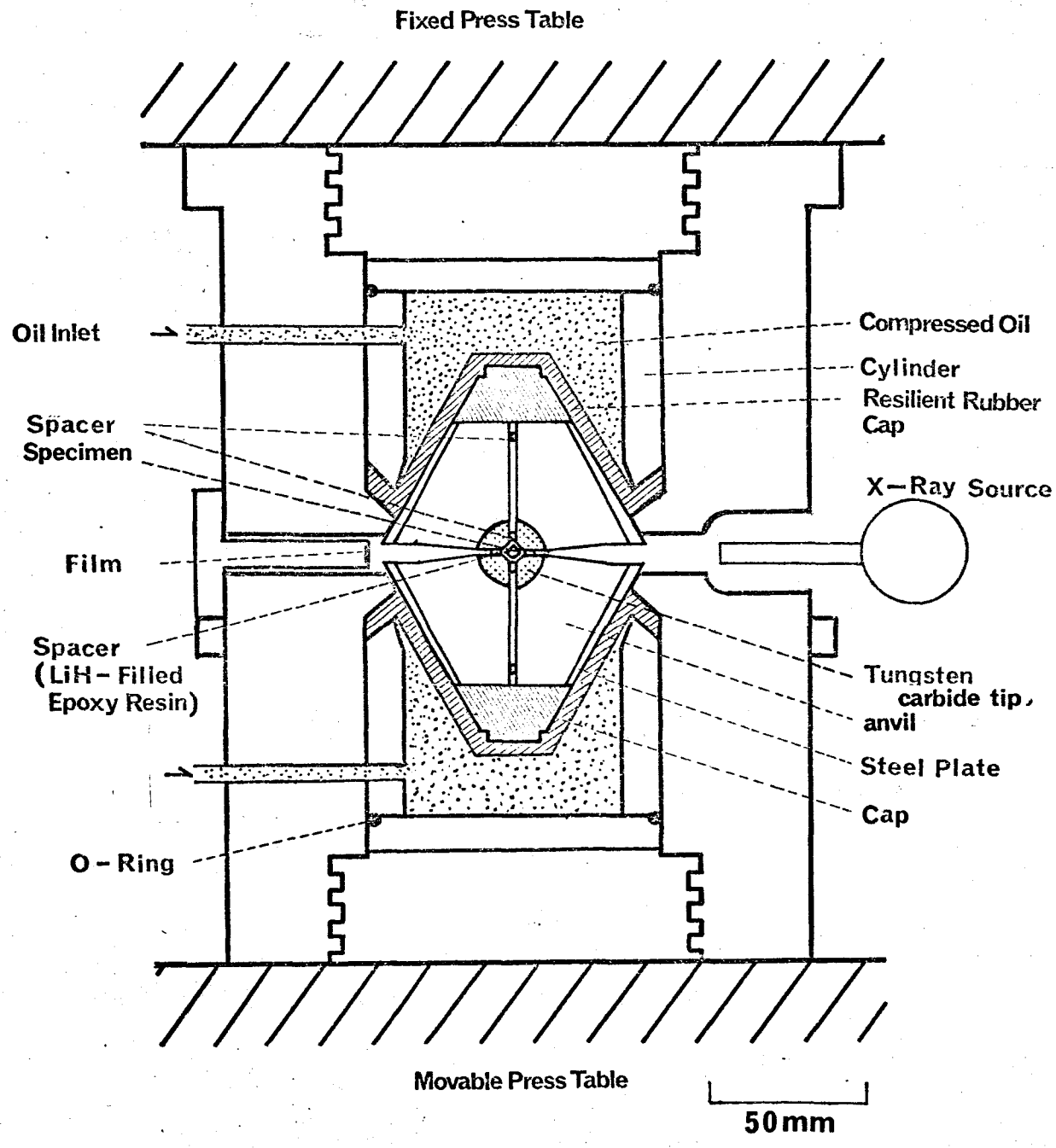

Fig. 1-3. Cross section of split-cone type apparatus.

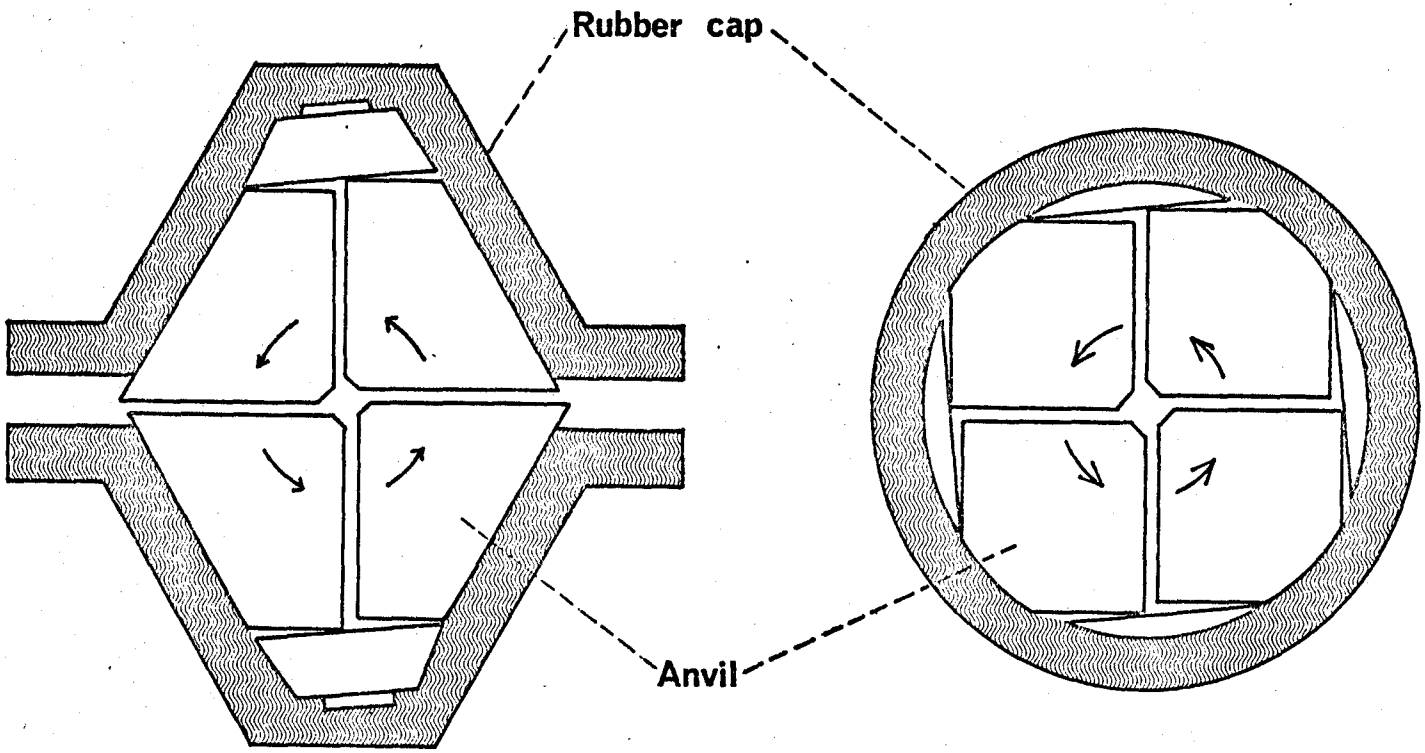

Fig. 1-4. Inappropriate movement of anvils in the split-cone apparatus.

2. Design of Anvil Assemblage of Split-Octahedron Type

The present apparatus consists of a uniaxial hydraulic press, a pair of guide blocks, an octahedral assemblage of anvils, and an octahedral pressure transmitting medium together with a specimen to be studied.

There are three types of octahedral assemblage of multianvils with which the x-ray studies are made, as shown in Fig. 1-5. In all cases of the octahedrons, the x-ray beam can be induced to the specimen in center through the equatorial plane.

In the case of both A and B, the octahedron is equally divided by the three planes through the center. Although the equatorial plane is common to both octahedrons A and B, the remaining two planes in octahedron B differ from the two planes in octahedron A by $\pi/4$.

The octahedron C is divided into six pieces. The shape formed by the two of six pieces is different from that formed by the remaining four pieces.

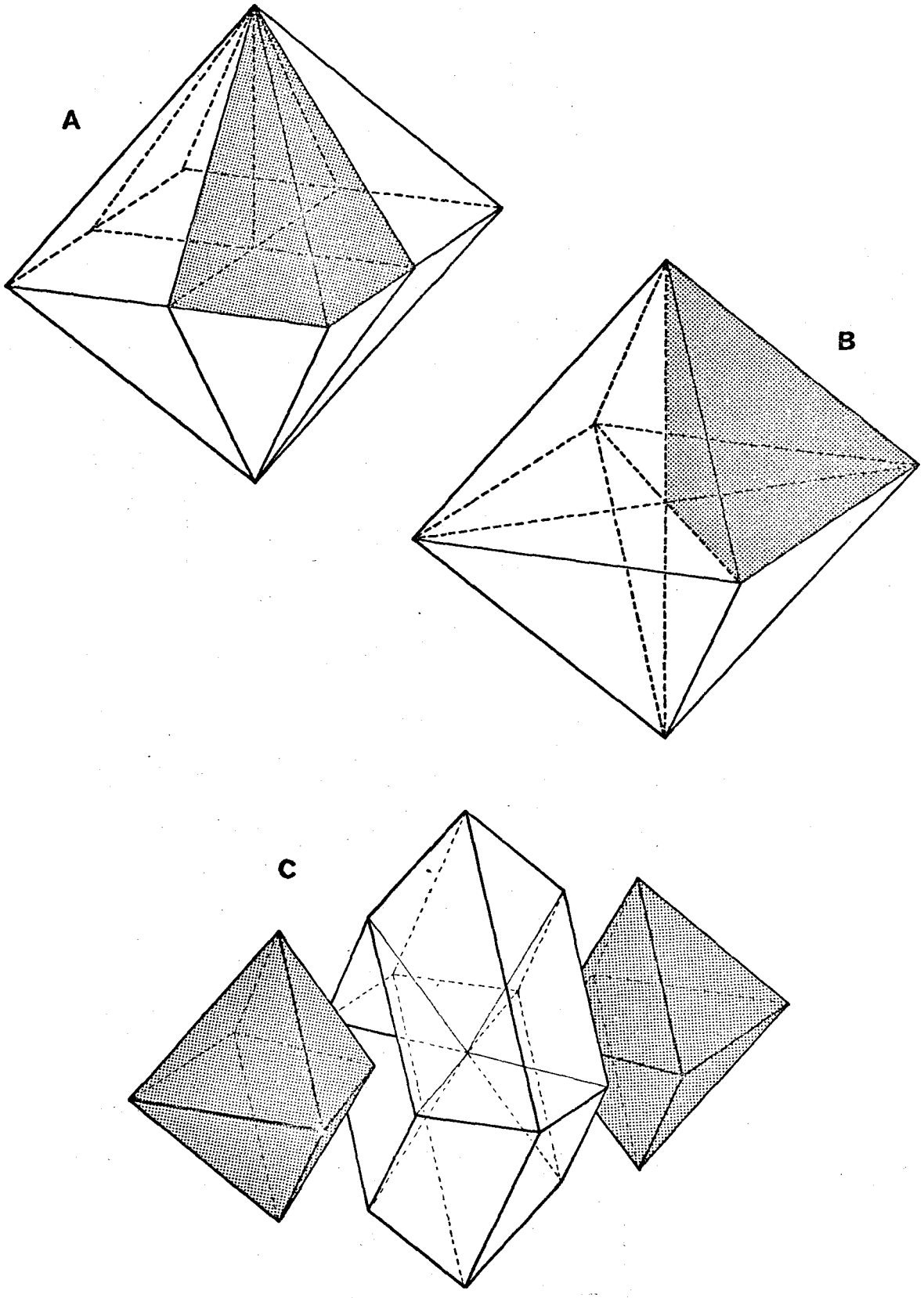

Fig. 1-5. Three types of splitting an octahedron.

3. Experiment

3.1) Configuration of octahedral anvil assemblage

Both A and B types of assemblage were examined, but the C type of assemblage was not used in the present experiment. In each type, three kinds of anvil assemblage were examined as follows : (1) an assemblage consisting of eight main anvils only, (2) an assemblage consisting of eight main anvils and two auxiliary anvils, and (3) an assemblage consisting of eight main anvils and six auxiliary anvils, respectively (Fig. 1-6).

A cross section of the anvil assemblage (3) is shown in Fig. 1-7. Cardboard spacers were placed in the clearance between the main anvils, and also on the rear faces of auxiliary anvils. In order to keep electrical insulation, mica sheets were placed on the outer surfaces of octahedral assemblage and also between main anvils and auxiliary anvils.

A corner of each main anvil was truncated to form a triangular face. When the anvils were assembled, the assemblage had an octahedral hollow space in the center. Into this space was placed an octahedral pressure chamber containing a specimen to be compressed.

The dimension and materials of components in the assemblage are listed in Table 1-2.

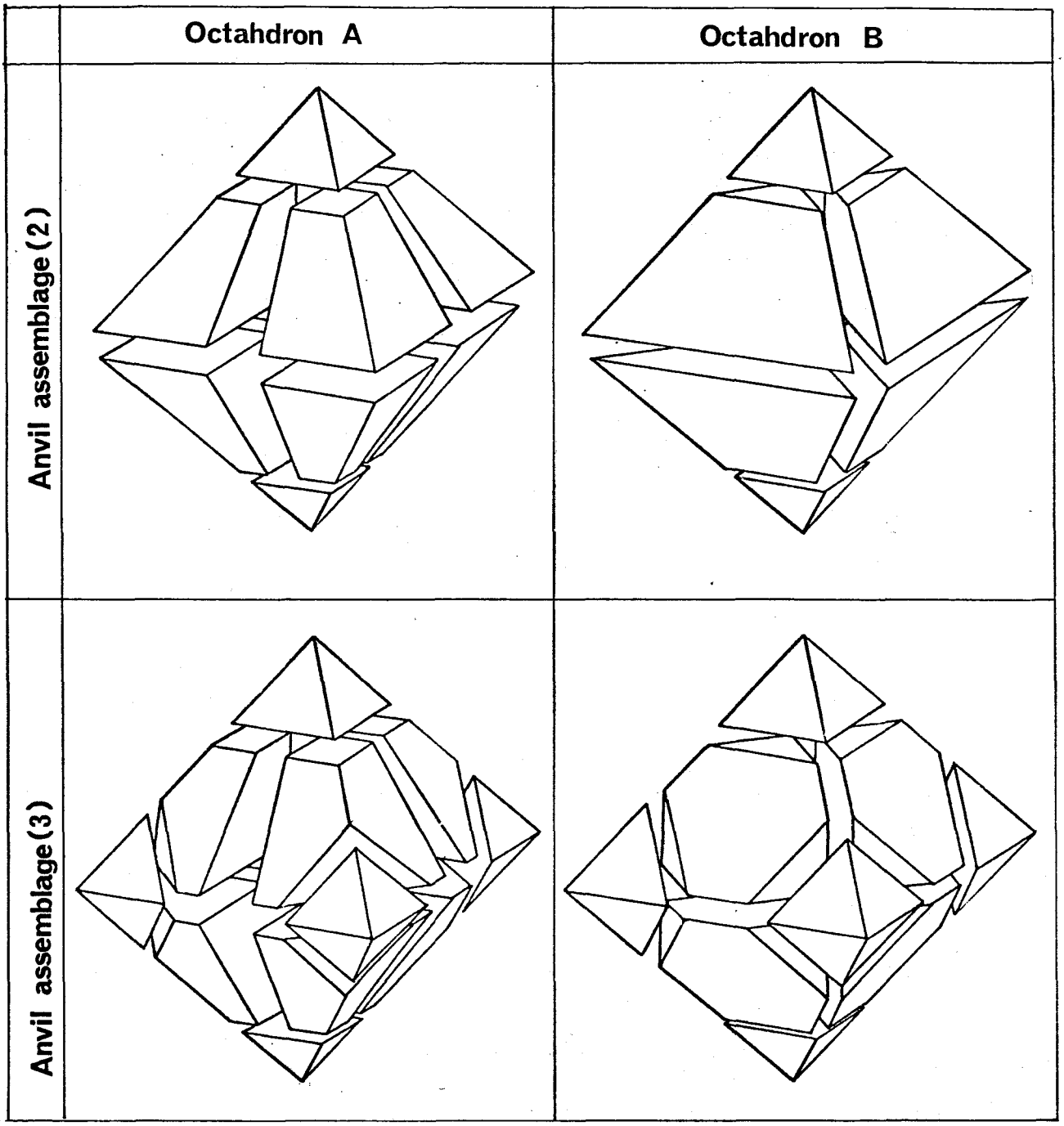

Fig. 1-6. Anvil assemblages (2) and (3), each in octahedrons A and B. The assemblage (2) consists of eight main anvils and two auxiliary anvils. The assemblage (3) consists of eight main anvils and six auxiliary anvils.

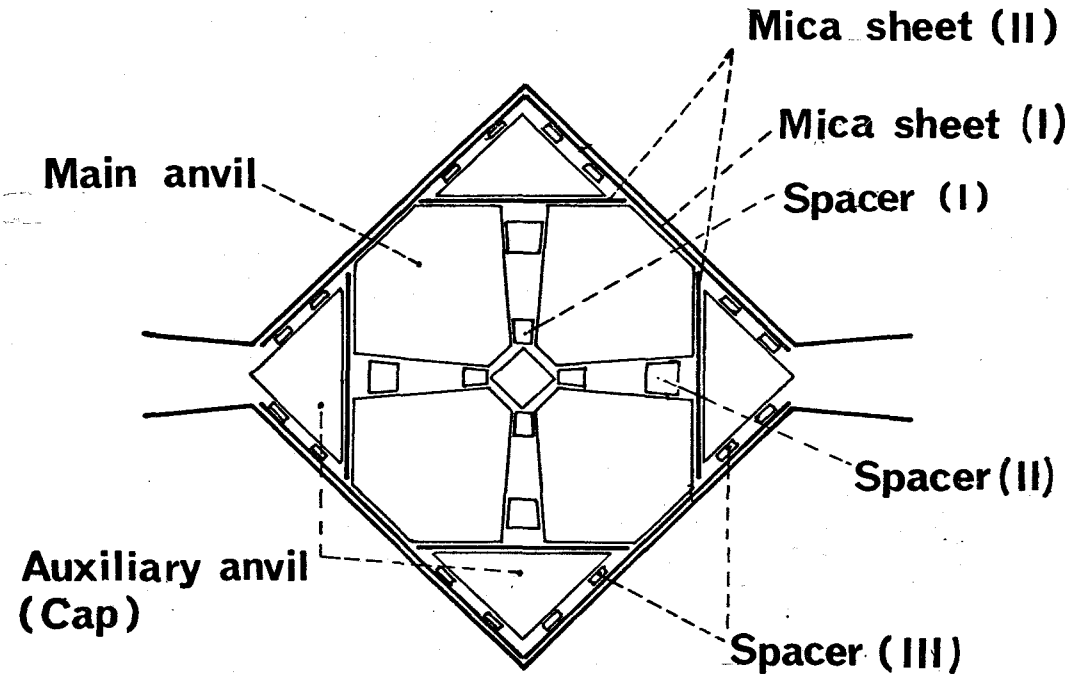

Fig. 1-7. Cross section of the assemblage (3).

Table 1-2. Description of components in the assemblage.

Component	Dimension (mm)	Material
Main anvil*	a : 10.270 b : 11.270 f : 1.0	WC
Auxiliary anvil*	c : 9.00	WC
Mica sheet†	I : 0.20 thick II : 0.15 thick	
Spacer†	I : 1.3 x 1.3 x 1.5 II : 1.0 x 1.0 x 1.3 III : 1.0 x 1.0 x 0.7	Cardboard

* Each is shown in the figure below.

† Each is shown in Fig. 1-7.

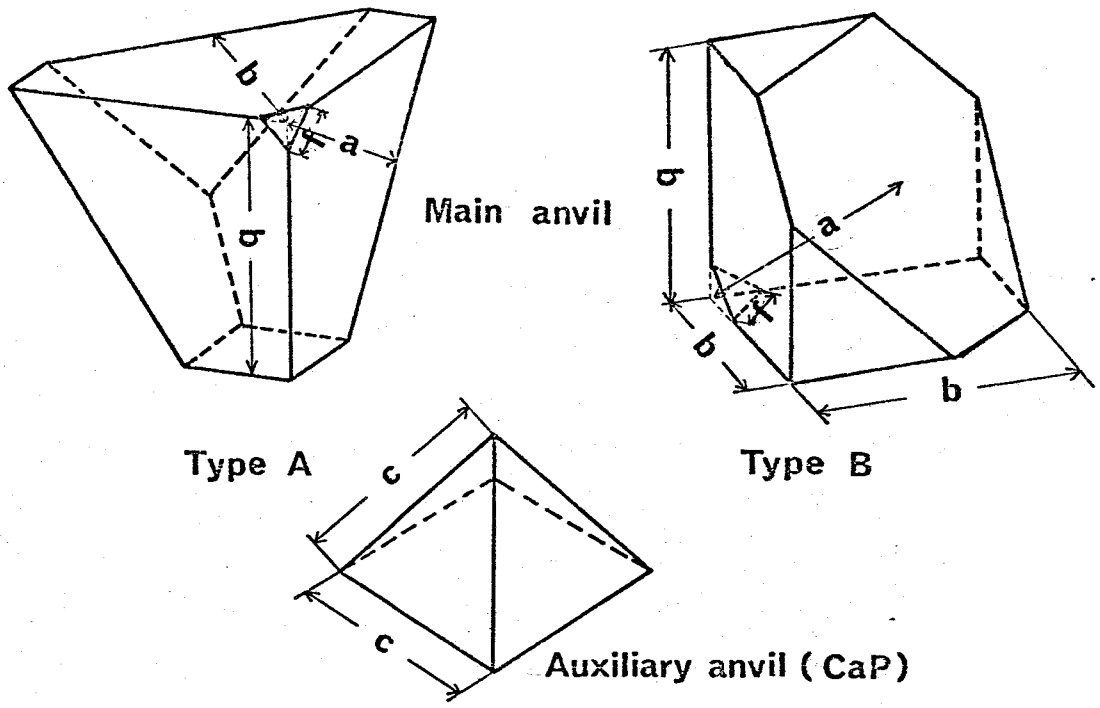

When we used the auxiliary anvils whose size was 10 % smaller than that listed in Table 1-2, the main anvils did not advance synchronously. Larger auxiliary anvils, on the other hand, improved the advancement of main anvils. Instead of the advantage, this type of assemblage lead to a break of main anvils, since the main anvils were supported only by the auxiliary anvils at the later stage of compression. An insertion of soft material such as In metal on the auxiliary anvils resulted in a poor alignment of main anvils. An increase of amount of cardboard spacer was also followed by a break of the main anvils.

3.2) Pressure-transmitting medium and specimen

An admixture of B powder and epoxy resin in the ratio 4 : 1 in weight was prepared. The admixture was poured into a cast having pyramidal hollow space and a medium block with pyramidal shape as shown in Fig. 1-8 (a) was consolidated. A hemispherical hollow was drilled in the center of the basal plane of the pyramid. Into this hollow was filled either an admixture of diamond and eposy resin or admixture of B and epoxy resin. Another pyramid was prepared and a small ditch was made. A pressure calibrant was embedded in it as shown in Fig. 1-8 (b). Two electrodes made of Pt foil were placed on both ends of the calibrant. When the basal planes of pyramids (a) and (b) were put together, an octahedral medium was completed. The description of sample assemblage is tabulated in Table 1-3.

Table 1-3. Description of sample assemblage.

Edge length of octahedron	: 2.5 mm
Diameter of spherical pressure transmitting medium	: 1.2 mm
Thickness of Pt foil	: 0.02 mm
Dimension of calibrant (needle)	: ~0.1x0.1x0.6 mm^3

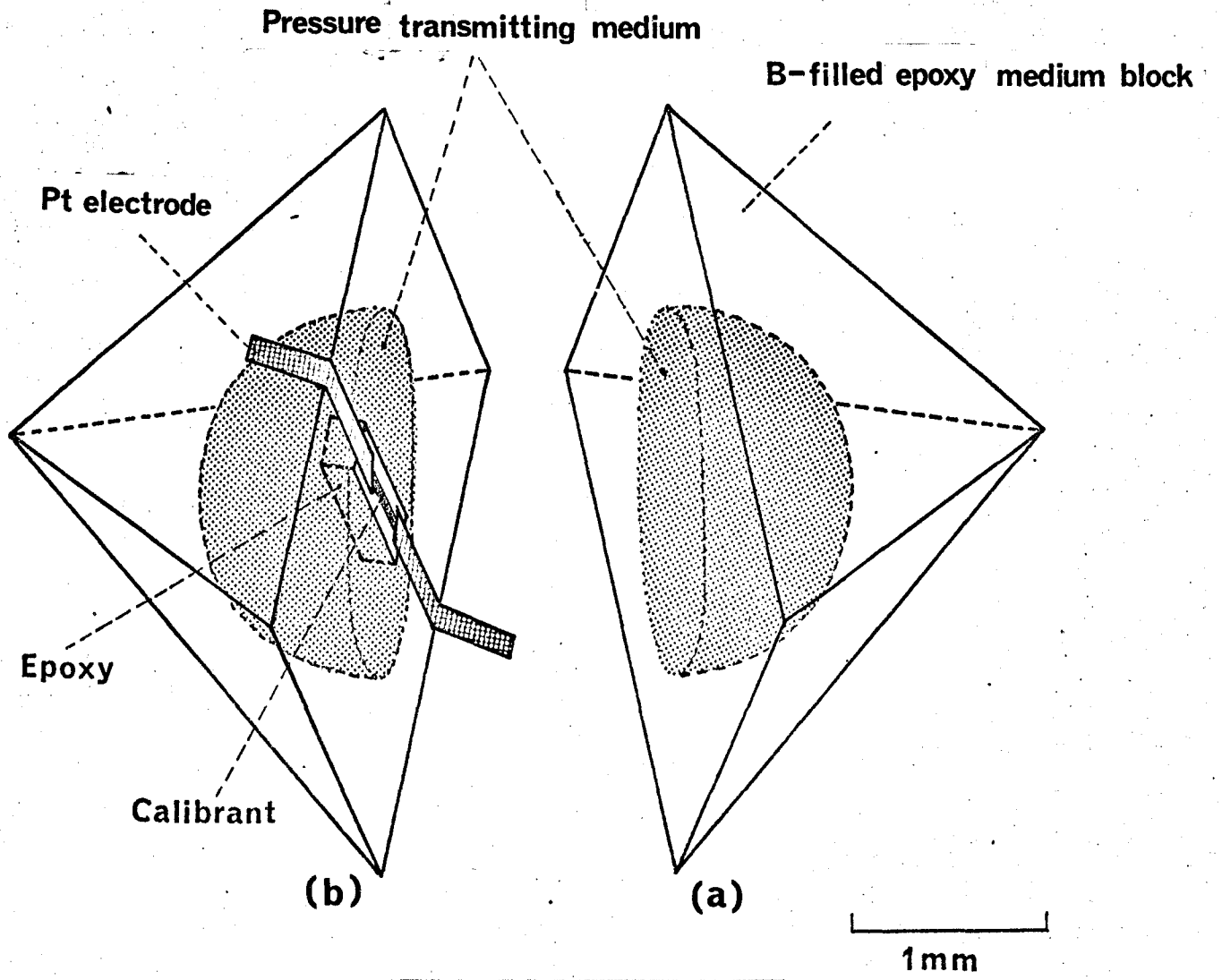

Fig. 1-8. Sample assembly.

3.3) Construction of guide blocks

A sphere made of WC was divided into eight blocks by three planes, being mutually perpendicular to each other. By truncating the center of each block, the guide blocks were made. Four blocks out of eight were put together so that a hemisphere was formed. This hemisphere was then placed into a hemispherical hollow space prepared on the upper part of one cylinder as shown in Fig. 1-9. A pyramidal hollow space was formed in the center. A similar cylinder containing another hemisphere was made.

Two cylinders were joined as shown in Fig. 1-10. The anvil assemblage containing the pressure transmitting medium and calibrant was finally compressed within an octahedral space surrounded by the guide blocks.

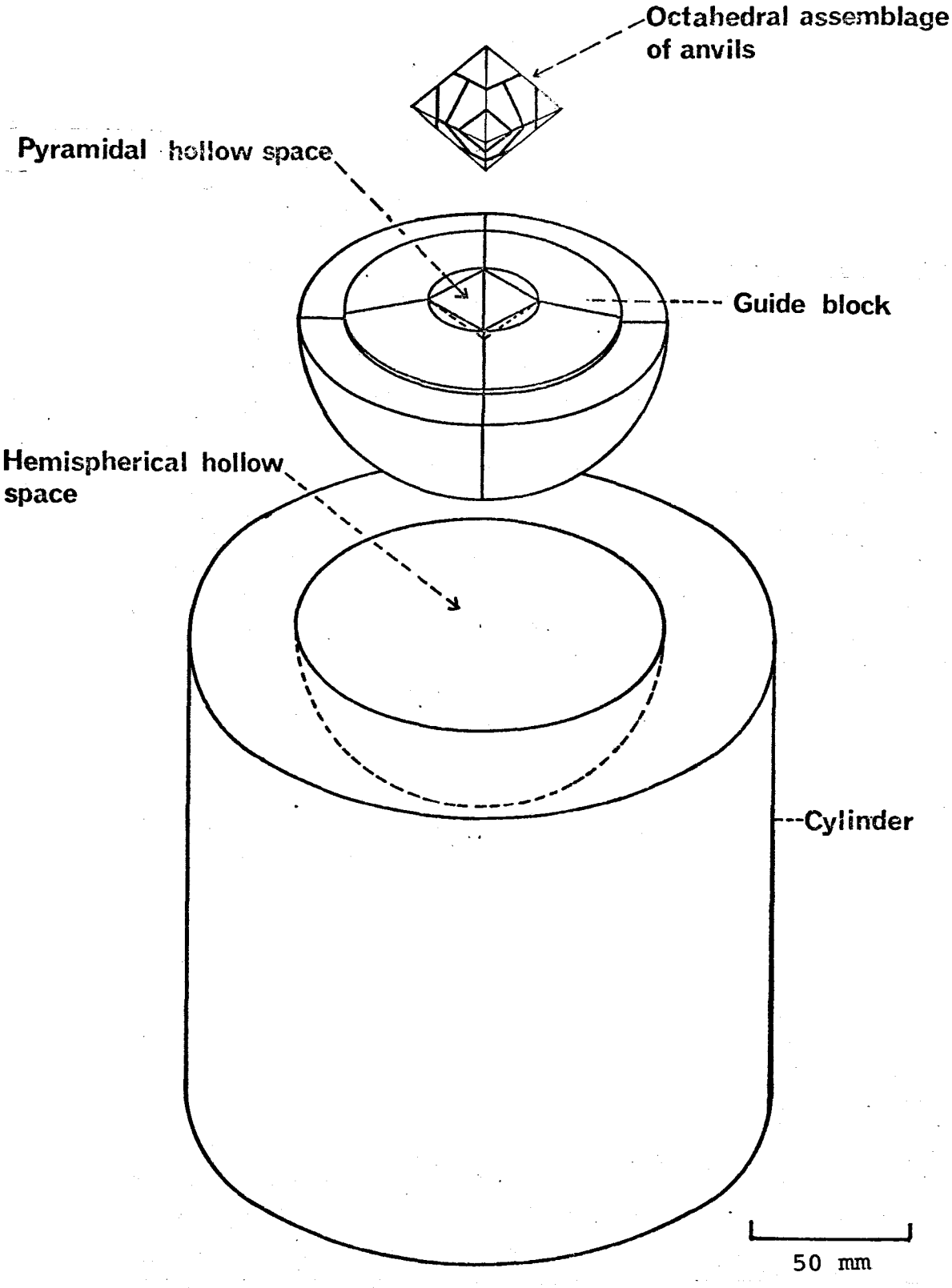

Fig. 1-9. Construction of guide block.

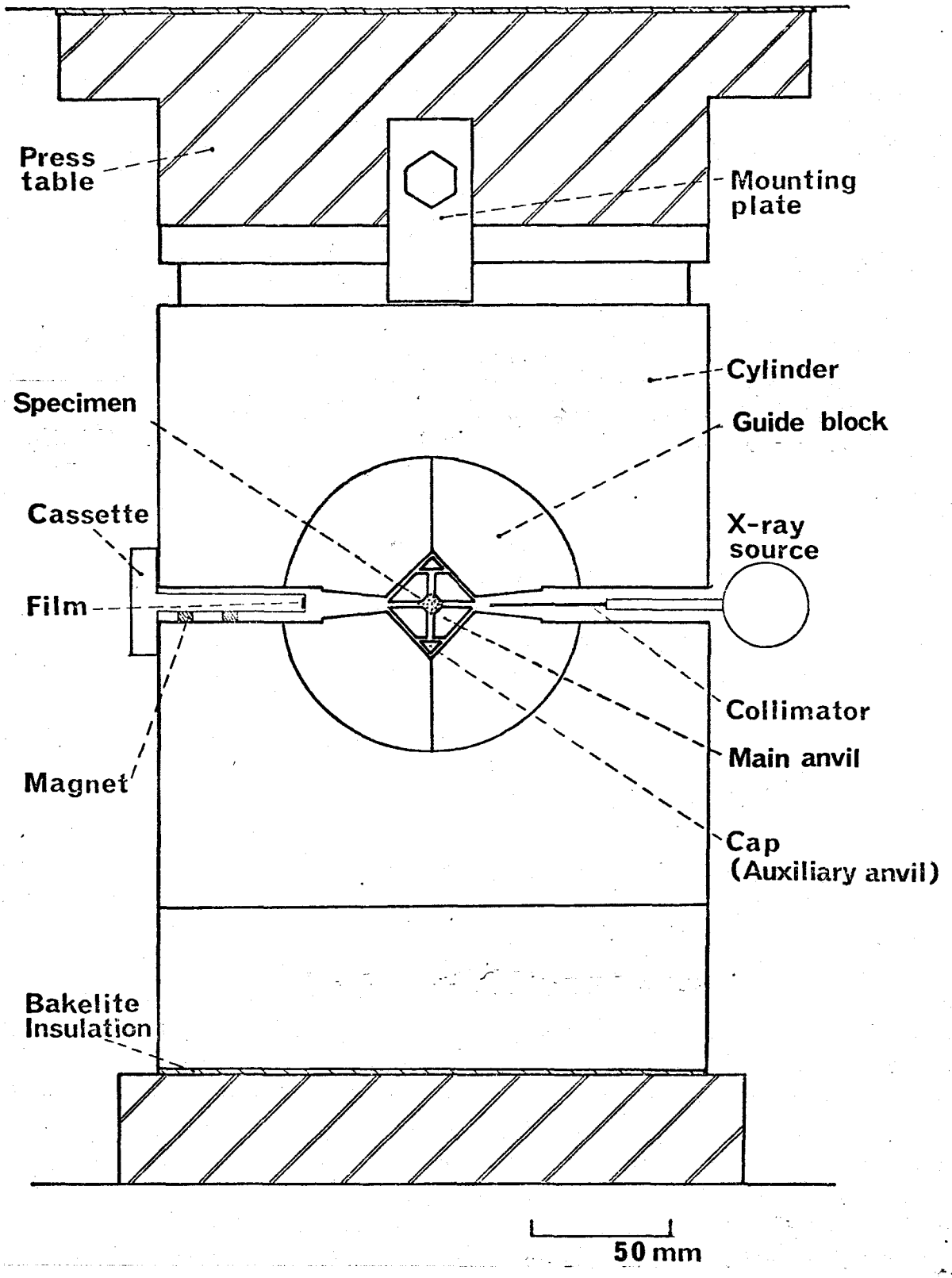

Fig. 1-10. Cross section of split-octahedron pressure vessel.

3.4) Measurement

Each of the anvil assemblages (1), (2) and (3), was compressed under various loads. The clearance between the main anvils was continuously measured by a clearance gage. After each compression, the anvil assemblage was taken out and the residual thickness of the spacers was measured by a micrometer. From the above observations, the alignment of main anvils was analyzed.

Next, the generated pressure was calibrated by measuring the electrical resistance of calibrant. As the calibrants, Bi, ZnTe, ZnS, GaAs, and GaP were used.

4. Results and Discussion

4.1) Alignment of main anvils

The condition of the anvil shrinkage was inspected after the application of external load upon the assemblage.

In case of assemblage (1) and octahedron B, a misalignment of the main anvils around the specimen occurred in a way as shown in Figs. 1-11 (a) and (b). The state of misalignment observed in octahedron A without the auxiliary anvils is shown in Figs. 1-12 (a) and (b). The mode of misalignment observed in the horizontal plane is different from that occurred in octahedron B. This kind of misalignment accompanied a nonuniform extrusion of sample.

In case of assemblage (2), namely with two auxiliary anvils, the misalignment as shown in Fig. 1-12 (a) disappeared in octahedron A. The misalignment as shown in Fig. 1-11 (b) still remained in octahedron B.

In addition to the above-mentioned misalignments, rotation of each main anvil as shown in Fig. 1-13 was observed in both octahedrons A and B. This rotation was caused by the torque arising from the friction as shown by the arrow in the diagram.

In case of assemblage (3), all the above-mentioned

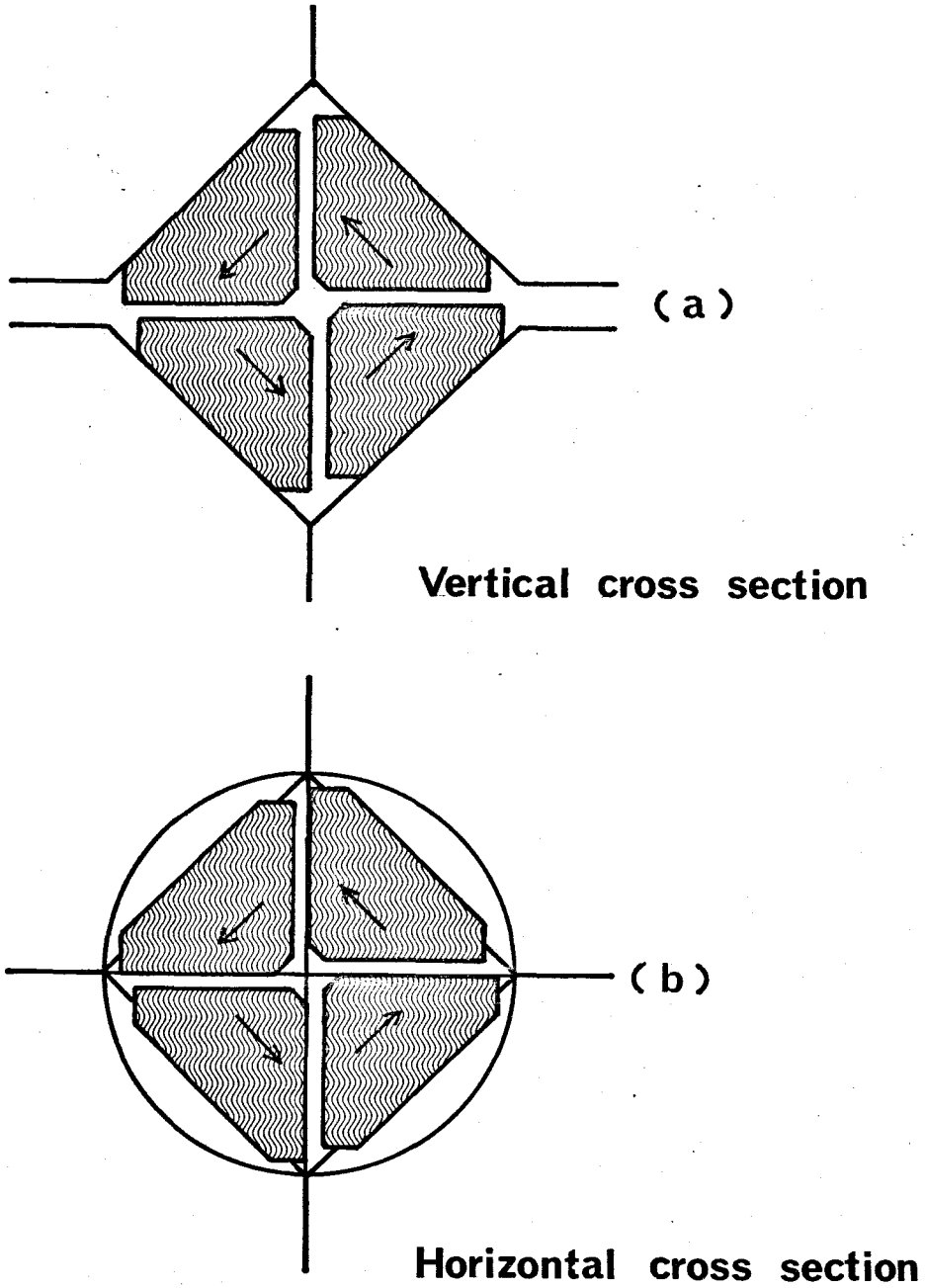

Fig. 1-11. Mode of misalignment in octahedron B.

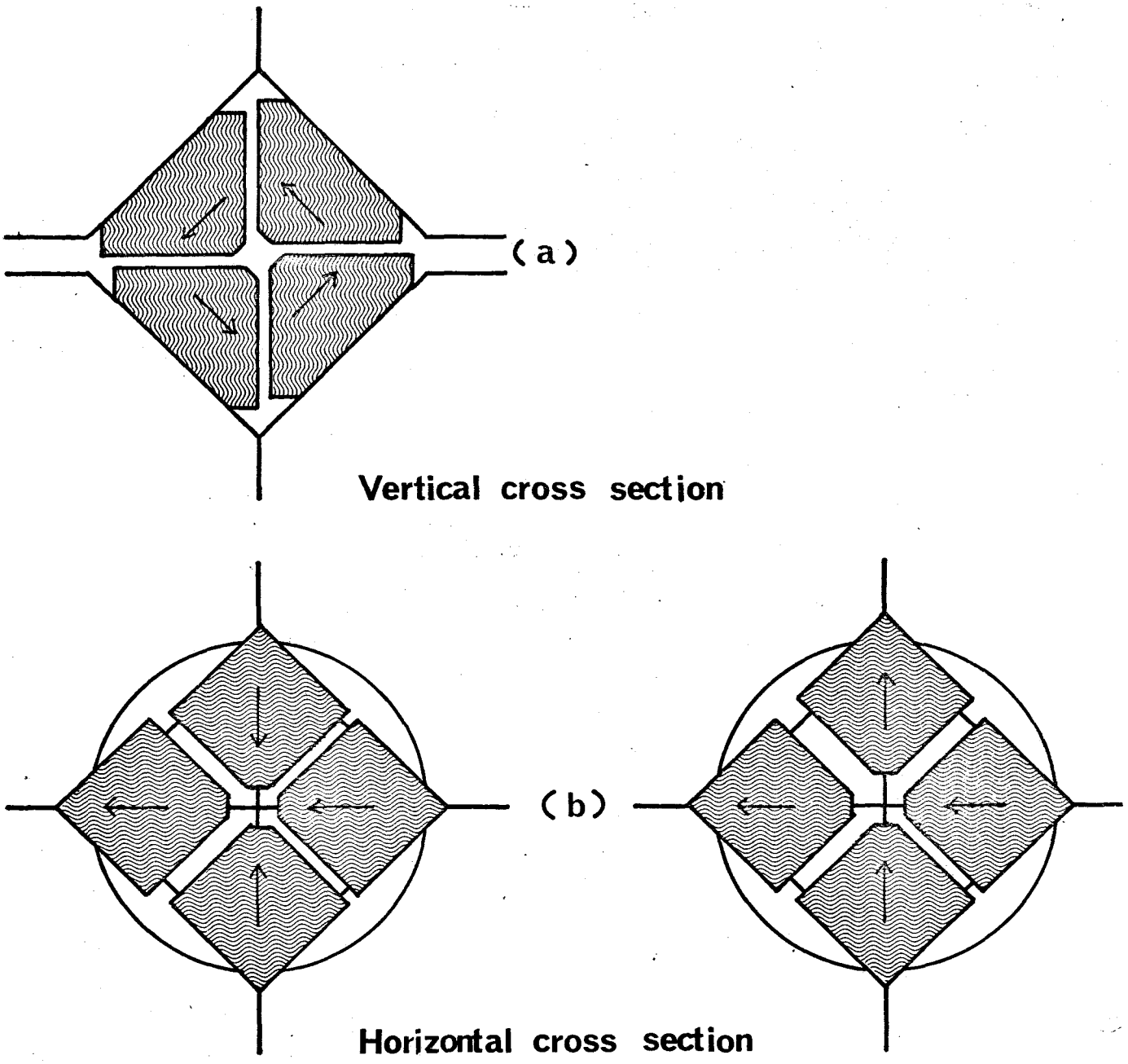

Fig. 1-12. Mode of misalignment in octahedron A.

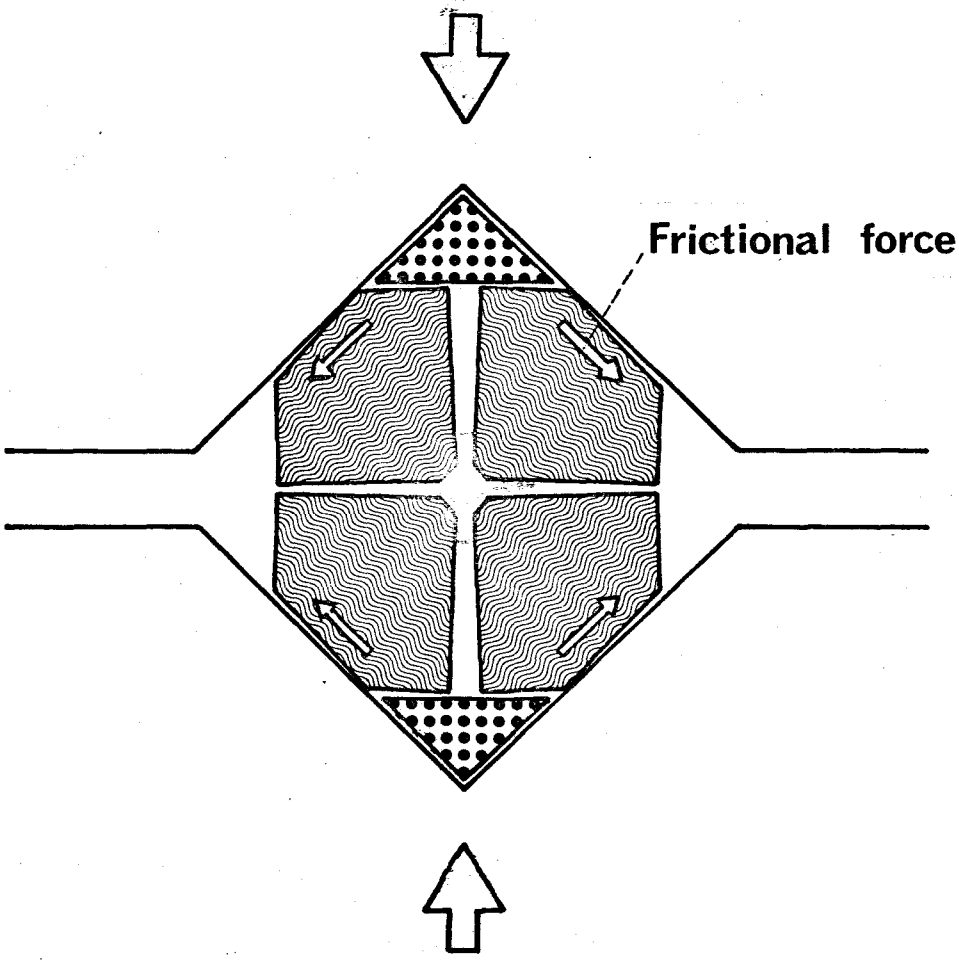

Fig. 1-13. Rotation of anvils caused by the frictional force.

misalignments and rotations vanished. The added four auxiliary anvils quite effectively prevented the rotation as well as the sliding.

4.2) Actual process of shrinkage in the anvil assemblage

Next to be discussed is the mechanism of anvil advancement realized in the assemblage (3).

Before compression, thin gap planes remained open between the main anvils and the outer guide blocks as shown in Fig. 1-14 (a). In the initial stage of the shrinkage, spacers on the auxiliary anvils were first compressed and the clearance of the gap planes began to decrease. The applied load was conveyed to the auxiliary anvils via cardboard spacers. Consequently, the main anvils were driven inwards uniformly and synchronously. On further increase of load, the guide blocks made contacts with the main anvils as shown in Fig. 1-14 (b). Then, both the main anvils and auxiliary anvils showed synchronous movements towards the center.

This synchronous shrinkage of anvil assemblage indicated that the uniaxial external force was converted smoothly into tetraxial forces surrounding the octahedron.

Accordingly, the clearance between one anvil and the neighboring anvils was kept equal everywhere in the entire anvil assemblage. This condition made the uniform compression inside the pressure transmitting medium.

The original stage of the assemblage before the compression and the final stage of the assemblage are shown in Photos 1-1 (a) and (b), respectively. The

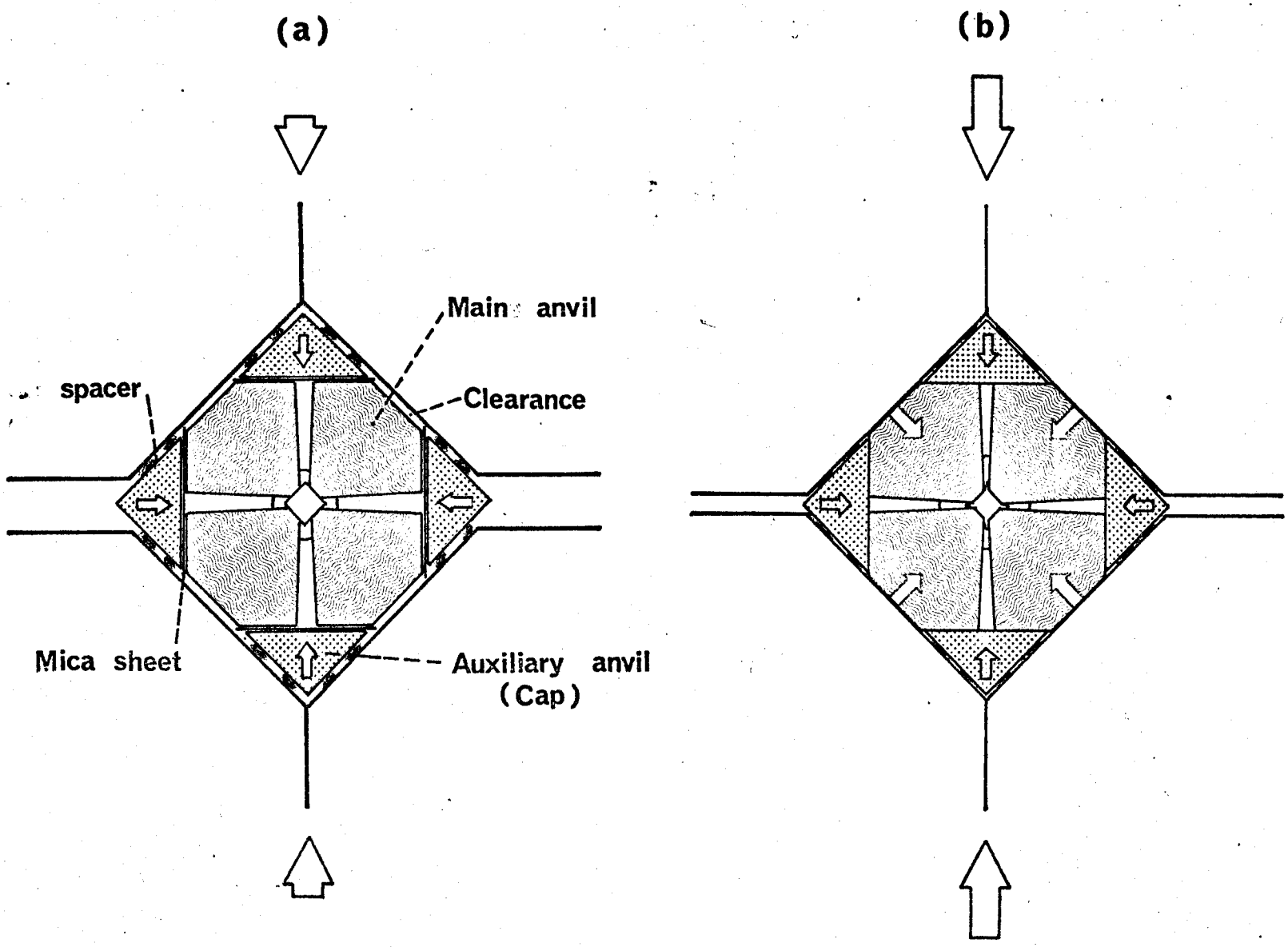

Fig. 1-14. Cross section of anvil assemblage; (a) the initial stage of shrinkage, and (b) the state on further increasing load.

(a)

(b)

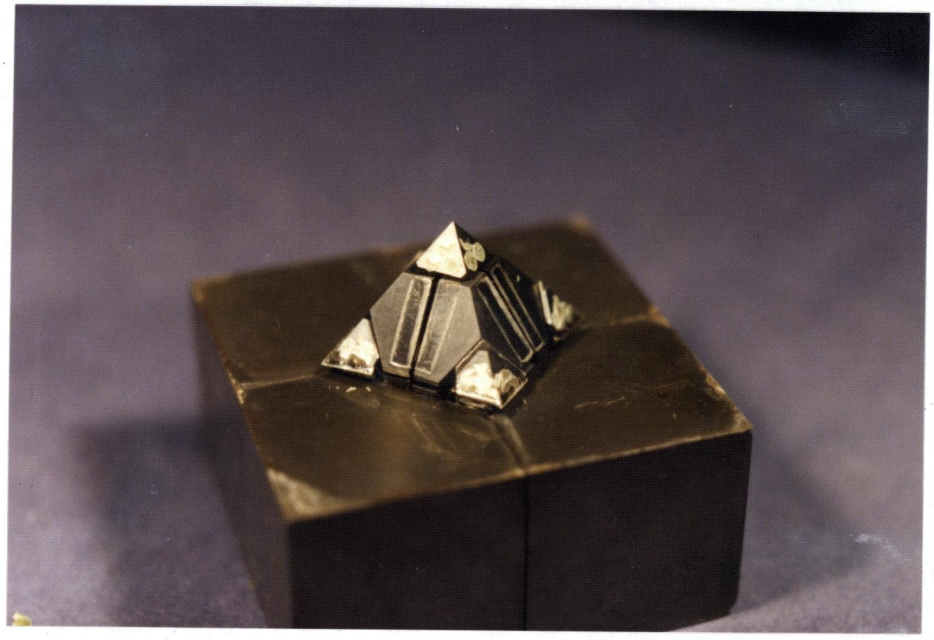

Photo 1-1. External view of anvil assemblage; (a) before compression and (b) after compression.

internal views of the assemblage are shown in Photos 1-2 (a) and (b).

In addition to the role to control the normal movement of the main anvils, the auxiliary anvils made lateral supports to the main anvils and hence increased their strength. Various materials and dimensions for the auxiliary anvil were tried and the final shape and substance, mentioned in Table 1-2, were selected so that the above role be accomplished.

(a)

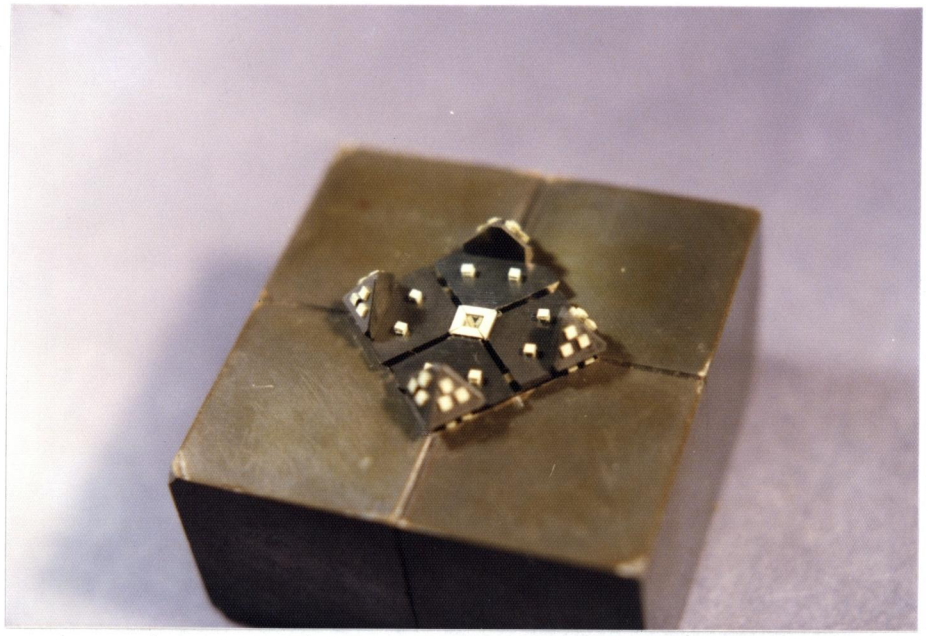

(b)

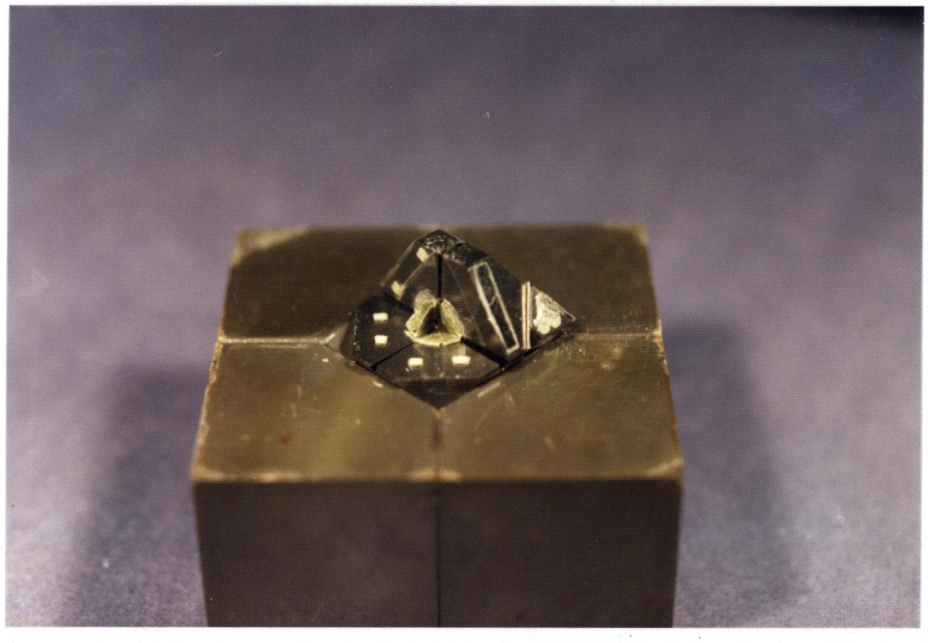

Photo 1-2. Internal view of anvil assemblage; (a) before compression and (b) after compression.

4.3) Efficiency of pressure generation

The generated pressure inside the medium was detected by an abrupt change in resistance, accompanied by phase transitions of calibrants (Bi, ZnTe, ZnS, GaAs, and GaP). The details relevant to the pressure value of each phase transition will be described in Part II.

4.3.1) Effect of the number of auxiliary anvils

The relations between the generated pressure and applied external load are shown in Fig. 1-15. In case of the assemblage (2), the clearance between the anvils in the vertical planes is larger than that in the horizontal plane. The result suggests that the force to shrink the anvil assemblage is still dominant in the vertical direction. Such shrinkage of anvil assemblage leads to an anisotropic compression of the pressure transmitting medium.

In case of the assemblage (3), the clearance between the adjoining main anvils is equal everywhere in the entire assemblage. As the result, a higher efficiency of pressure generation is expected.

4.3.2) Effect of changing the pressure transmitting medium

In Fig. 1-16 are shown two relations between the generated pressure and applied load, one being the relation

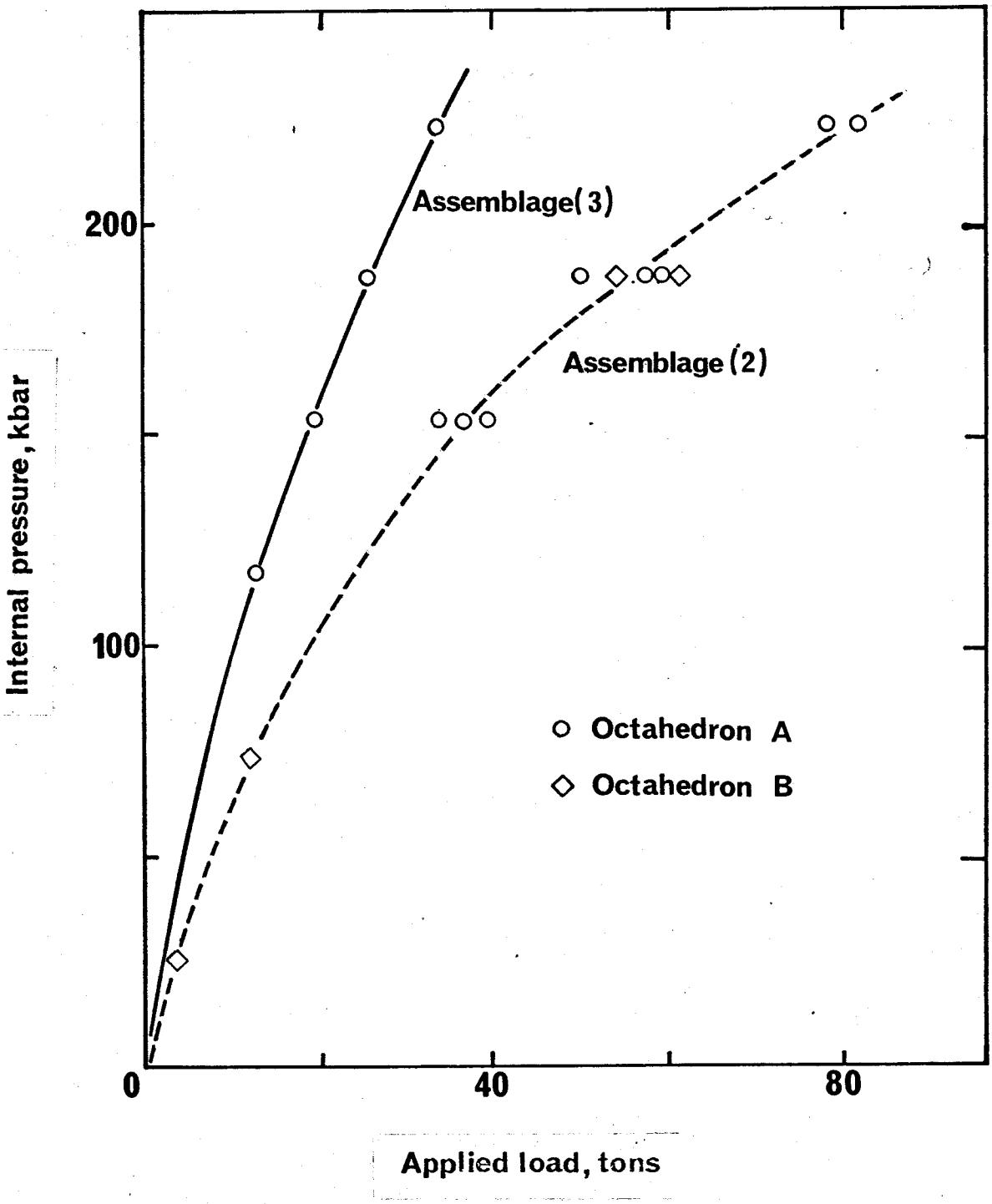

Fig. 1-15. Pressure calibration curves using the anvil assemblages (2) and (3). The medium is diamond.

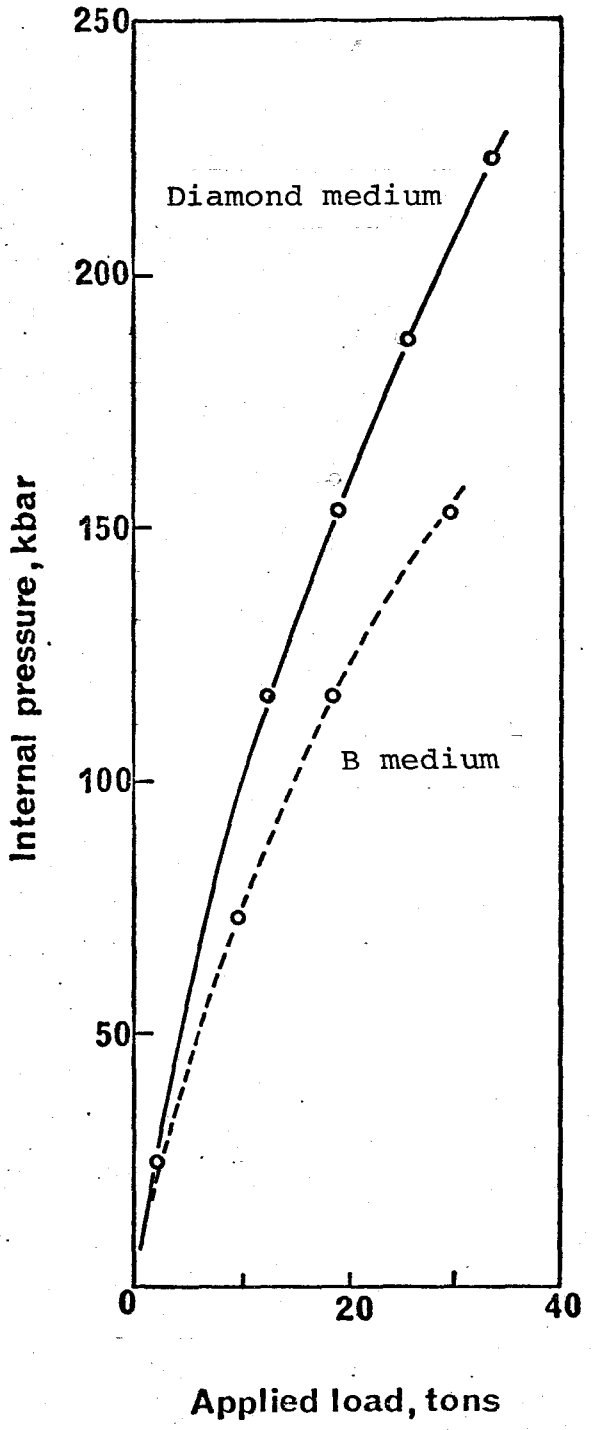

Fig. 1-16. Pressure calibration curves using pressure medium of diamond and B. The assemblage (3) in octahedron A is used.

when diamond powder was used as the pressure transmitting medium, and the other that when B powder was used. The spherical medium embedded inside the octahedron does not extrude into the clearance between the adjoining main anvils. It is, therefore, possible to compare the pressure transmitting efficiency of both the diamond and B powder directly. A higher rate of pressure generation is observed when diamond powder is used and this fact has been predicted by Kawai et al. (1975).

Since the incompressibility of B is much less than that of diamond, the efficiency of pressure intensification inside the B medium is lower than that inside the diamond medium.

It is expected that the force applied upon the outer surface of octahedral medium is effectively transmitted to the spherical aggregate of diamond powder and that an intensification of pressure inside the diamond aggregate is attained.

4.4) Application to x-ray diffraction experiments

A pressure vessel to compress an octahedral specimen was first developed by Kawai (1966) and modified into multistaged version afterwards (Kawai and Endo, 1970; Kawai et al., 1973). The x-ray diffraction studies have not been undertaken in these vessels because the design of the vessels has not permitted either the injection or the diffraction of x-rays.

The present vessel provides an entrance for incident x-rays and an exit for diffracted rays on the horizontal plane of split octahedron. It is necessary that the clearance in the horizontal plane should be retained at the highest pressure obtained in the present study.

Of three assemblages examined, the assemblage (3) permits the largest clearance in the horizontal plane, since the shrinkage of the anvil assemblage is most uniform.

The path of x-rays in case of the assemblage (3) in octahedron B is depicted in Fig. 1-17. Figure 1-17 (a) indicates diffraction angle surveyed in the horizontal plane. Divergence angle for the diffracted rays is provided in the vertical plane. It becomes wider when the front planes of main anvils are slanted outward as shown in Fig. 1-17 (b).

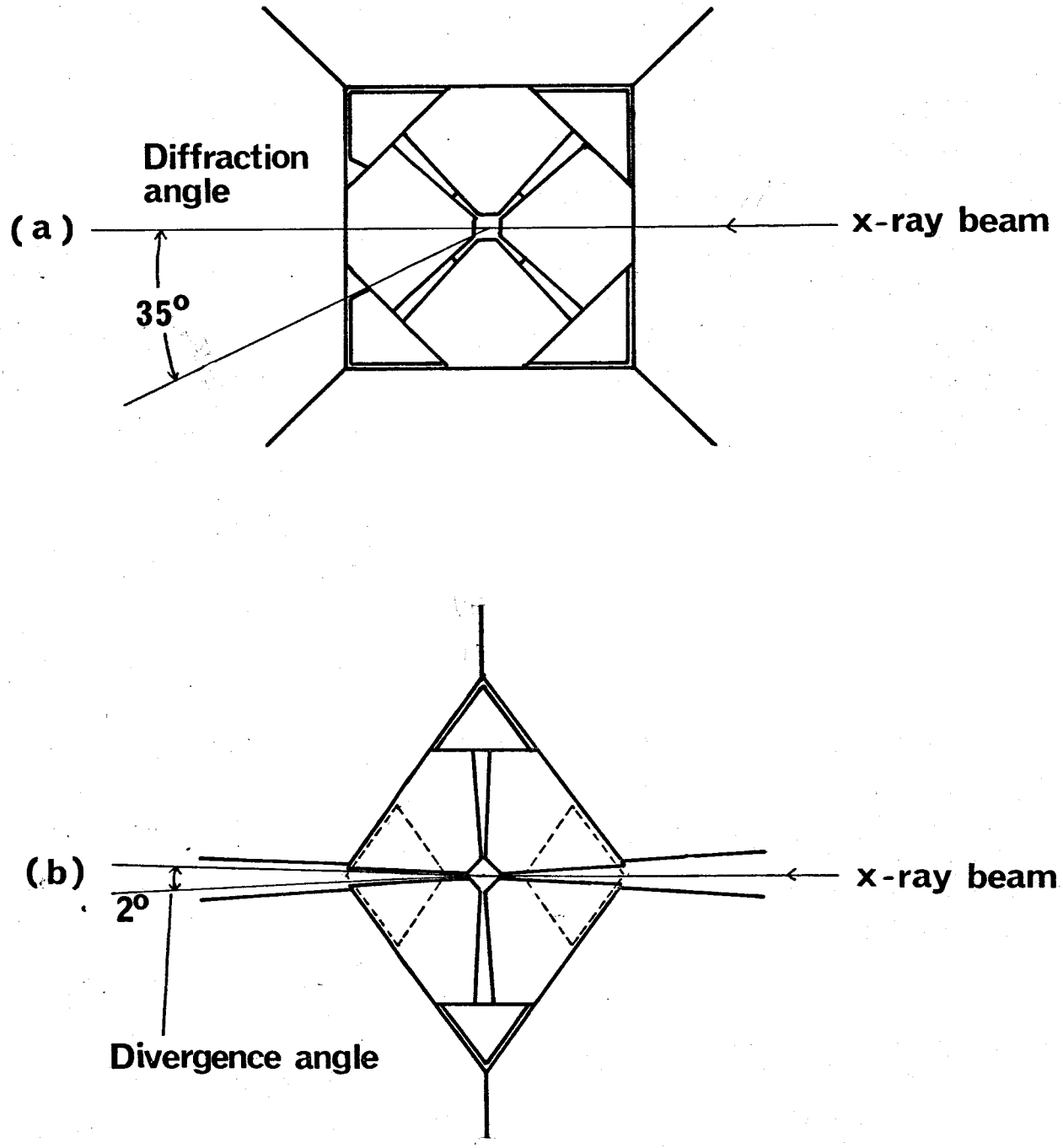

Fig. 1-17. Path of x-rays in the assemblage (3) of octahedron B ; (a) horizontal cross section, and (b) vertical cross section.

5. Conclusion

A new high pressure vessel of split-octahedron type is designed and constructed. Two types of splitting an octahedron into eight main anvil pieces are taken up. Three cases of anvil assemblage are examined in terms of the number of auxiliary anvils in each type, and the mechanism of anvil alignment is elucidated. This vessel is capable of generating quasi-hydrostatic pressures higher than 220 kbar. The use of this vessel makes it possible to undertake x-ray diffraction studies of specimen under pressure. Simultaneous measurement of electric resistance can be carried out.

Part II. PRESSURE FIXED POINTS ABOVE 100 KBAR

1. Introduction

In recent years there has been an increasing request to evaluate accurate magnitude of pressures acting on a substance.

Mechanically, one can simply define the pressure as the force loaded on a unit area. When the pressure P is uniform everywhere in the area,

$$P = F / S \qquad (2\text{-}1)$$

in which F is the force acting over an area S. The pressure, therefore, is estimated directly by measuring F and S. Representative equipment is mercury manometer or free-piston gage. This method enables the establishment of the primary scale of pressure. The primary scale is available only within the liquid pressure media, and the measurement becomes difficult when generated pressure is higher than 30 kbar since most of the liquids solidify and the pressures have to be transmitted via solids. In this case, some fraction of force acting on a specimen is in general consumed by the internal friction of solid medium. Therefore, the pressure should be evaluated by ways other than direct method.

Some of physical properties of substance are sensitive to compression and the measurements of these properties can be suitable for such an indirect dicision of pressure. Examples are ; (i) change of electrical resistance of metals or alloys, and (ii) shift of optical absorption. Since there exists no prediction pertinent to the pressure dependency of these properties, either the change of electrical resistance or that of optical absorption must be calibrated against the primary pressure scale. Hence these gages are referred to the secondary pressure scale. At higher range, where the primary scale no longer is available, the secondary gages must be correlated to another kind of pressure scale.

On the other hand, the pressure is defined from thermodynamics as

$$P = - \left(\partial A / \partial V \right)_T \qquad (2\text{-}2)$$

where A is the Helmholtz free energy and V is the volume, respectively. One can estimate the pressure acting upon a specific substance if the Helmholtz energy is derived theoretically in one hand and the volume is observed on the other.

Jamieson (1963) suggested the use of NaCl for this purpose. Decker (1965, 1971) calculated semi-empirical

equation of state for NaCl in a pressure range between 0 to 300 kbar at temperatures below 800°C. The scale thus determined by the help of Decker's equation is called the NaCl scale. In a high pressure vessel equipped with x-ray system, the generated pressure is estimable from the measurement of the lattice parameter (hence the volume) of NaCl and from Decker's equation. The NaCl scale, therefore, can be the primary gage even in the solid medium, and such secondary pressure scales as the electrical resistance and optical gages are possibly calibrated. The NaCl scale is also reliable for estimation of pressure at least up to 300 kbar, at which NaCl undergoes a transition into a denser phase (Bassett et al., 1968).

The above-mentioned primary and secondary gages are not always available in any kind of high pressure vessels. The use of primary gage is restricted to a low pressure range where liquids are stable. The optical gage is impossible to be used when either the anvil or the medium is opaque. The NaCl scale is not available in the pressure vessel which does not allow penetration of x-ray beam.

Another method is to measure pressures by the help of 'fixed points'. This is based on the observations of

pressure-induced phase transition in metals (Bi, Sn, etc.), alloys (Fe-Co, etc.), or semiconductors (ZnS, etc.). First, the pressures, at which the phase changes occur, are determined by a primary scale. These pressures are called fixed points. Once a generated pressure versus external force relation is obtained in terms of fixed points, the pressure inside the vessel is known by only measuring the external force.

In Part II of this study, the determination of various pressure fixed points are described on the basis of NaCl scale. Difference of pressure media investigated in Part I is reexamined and the best assemblage in the vessel is shown. Final values of the fixed points are introduced, using this assemblage.

2. Comparison of NaCl scale with other methods of pressure measurement

In this section we will discuss the above-mentioned NaCl scale and the indirect methods of pressure measurement such as the electrical resistance and the optical scales.

2.1) NaCl scale

Decker tried to evaluate the lattice energies of potential and vibrational for NaCl on the basis of Mie-Grüneisen equation of state. He calculated the Grüneisen constant, attractive and repulsive forces in the lattice, using appropriate assumption and experimental values. His equation of state is successful to relate the compressibility of NaCl to pressures working on this crystal (1965, 1971).

The pressure values determined by the equation of state agreed well with the experimental data (Bridgman, 1940, 1945), the error being less than 3 % up to 100 kbar. The pressure values above 150 kbar obtained by the shock wave experiments (Fritz et al., 1971) agreed well with the calculated pressures within an error less than ± 3 kbar.

The calculation by Weaver et al. (1971) based on the Hildebrand equation was also in a good agreement with Decker's calculation within 0.1 % around 200 kbar.

2.2) Electrical resistance scale

Balchan and Drickamer (1961) reported resistance jumps of several metals by compressions up to 550 kbar using the supported opposed anvils. The determinations of pressures were based on the extrapolation of decrease in electrical resistance of Pt, In, and Pb, which was calibrated against several fixed points below 100 kbar. Above 100 kbar, only one correction was made using the jump accompanied by a phase transition of Fe. The resistance change indicated that the transition of Fe occurred at 133 kbar, showing a good agreement with a shock compression experiment at 131 kbar (Bancroft et al., 1956). Then, they proposed that this is one of the resistance scale above 100 kbar.

Meanwhile, a number of fixed points were determined by free-piston gage and by NaCl scale. It became clear that the pressure values of many fixed points below 100 kbar had been overestimated (Lloyd, 1971). So Drickamer (1970) revised his scale of calibration downwards. The calibration was based on the x-ray diffraction analysis of NaCl, Al, Ag, and MgO. This new calibration is called new Drickamer scale, while the earlier calibration based on the resistance scale is called old Drickamer scale.

2.3) Optical scale

Many optical properties such as the absorption peak shift and refractive index show quite linear changes with increasing pressure. Recently, a shift of the wavelength of ruby R-fluorescence line at 6942 Å with increasing pressure has been taken into account (Forman et al., 1972; Barnett et al, 1973). The experiment was carried out in a gem-quality opposed diamond-anvil cell. Small fragments of ruby were placed at the interface between the diamond opposed anvils. The powder of NaCl was compressed simultaneously. Since both the wavelength data on the ruby R-line and the x-ray data on NaCl were obtainable, the wavelength shift of R-line was calibrated against the pressure estimable from the compression of NaCl. The pressure dependency of wavelength shift of ruby R-line is almost constant up to 195 kbar (Piermarini et al., 1975).

3. Experiment

An x-ray system was combined with the high pressure vessel described in Part I. Figure 2-1 shows the schematic diagram of the x-ray system.

The x-ray beam of MoKα obtained at 50 kV with 20 mA and filtered with Zr foil was used. This beam provided a low diffraction angle, relatively small absorption in air, and small absorption due to medium and cardboard spacers.

The diffraction angle (2θ) from 0° to 180° was available in case two auxiliary anvils were used, while the angle from 0° to 35° was available in case all auxiliary anvils were used.

Stainless steel tube was used as a collimator. Its inner diameter was 0.4 mm. The length was 40 mm. The collimator permitted a divergence angle of 1.14°.

For the detection of the diffracted rays, a Debye-Scherrer camera with the radius of 55 mm was used. The positions of diffraction lines on the film were read by a comparator.

The spacer and pressure-transmitting medium should be as transparent as possible to the x-ray beam. The cardboard was found to be transparent to the x-ray beam in the present case.

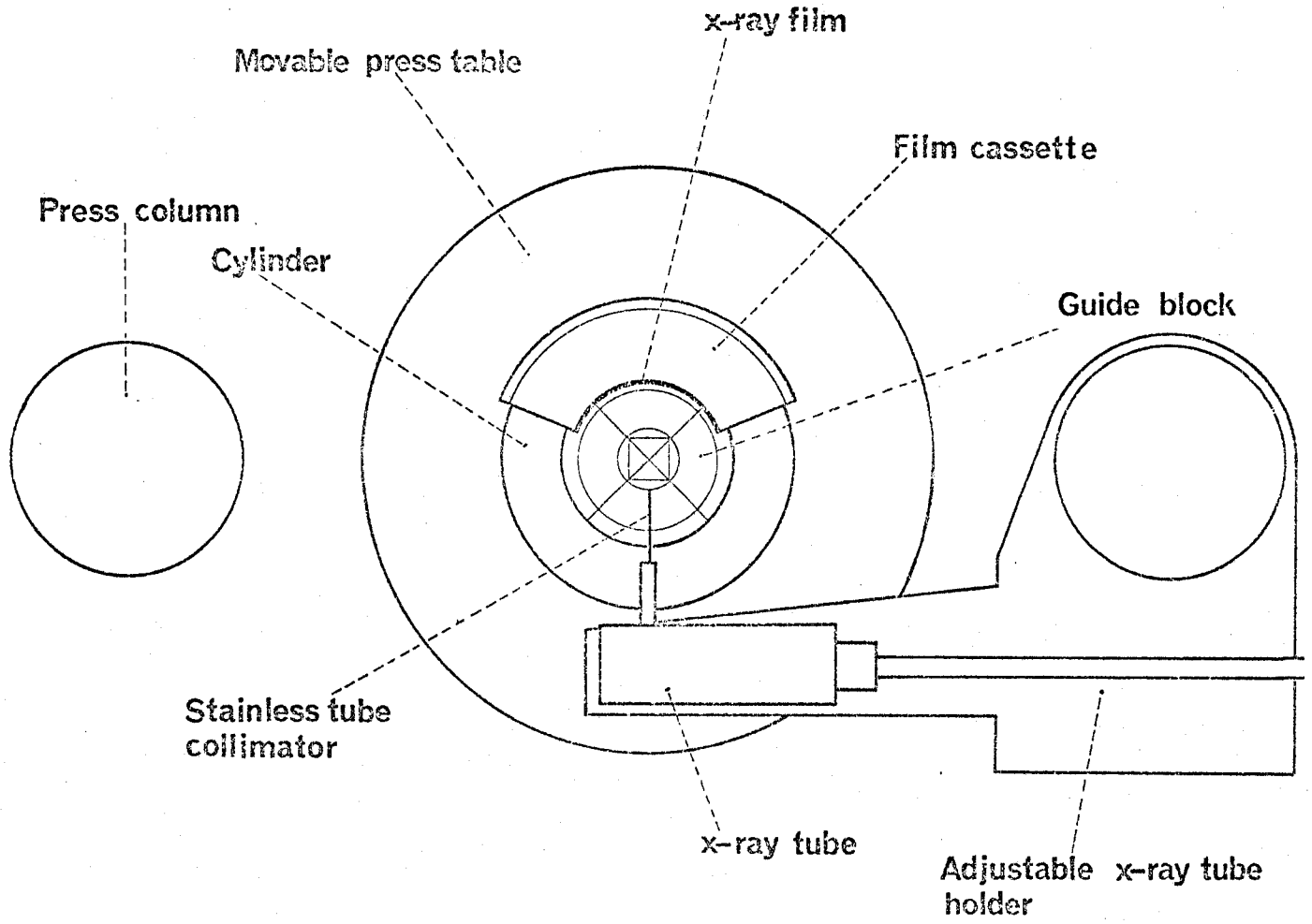

Fig. 2-1. X-ray system combined with the high-pressure apparatus.

Amorphous B powder admixed with epoxy resin has been used as the pressure transmitting medium for x-ray studies by many researchers. In this experiment we employed amorphous B, diamond, LiH, and g-BN* powder.

A medium block with pyramidal shape as shown in Fig. 2-2 was prepared by consolidation of admixture of B powder and epoxy resin (see Part I). In the bottom of the pyramid was made a hemispherical hollow space which was then filled with the medium powder. Next a small rectangular block of NaCl was plunged into the medium hemisphere. A pair of Pt foils was placed next to the NaCl block in order to reduce the aperture of the incident x-ray beam. Another pyramid containing a calibrant, as described in Section 3.2 of Part I, was prepared. When the two pyramids were adjoined at each basal plane, an octahedral medium was completed.

The calibrants employed were single crystals of ZnTe, ZnS, GaAs, and GaP. Table 2-1 tabulates the source, purity, and impurities of each calibrant crystal. Each crystal had been grown from the melt. The calibrants were known to exhibit polymorphic transition accompanied by a change of electronic state from semiconductor to metal at a certain pressure above 100 kbar.

The sample of NaCl was Merck "suprapur" grade with the purity higher than 99.998 %.

---

* hexagonal graphite-like BN

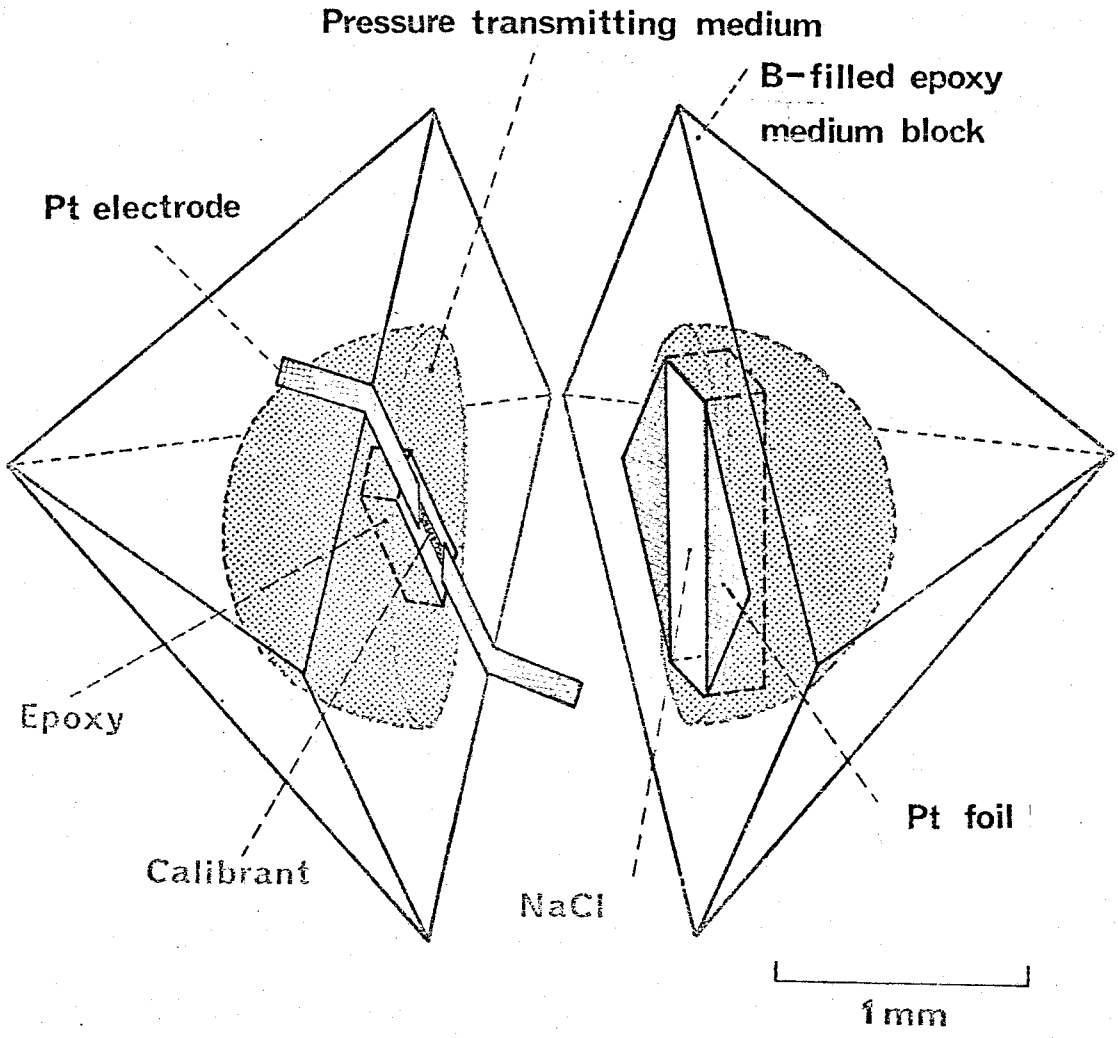

Fig. 2-2. Sample assembly for simultaneous measurements of x-ray and electrical resistance.

Table 2-1. Description of the samples

Sample	Source	Purity (%)	Impurities* (ppm)
ZnTe	Prof. S. Narita (Osaka University)	99.99	Mg, 1; Cu, 5; Fe, 0.8; Ga, 3; Al, 3; Ca, 3; Si, 80
ZnS†	Dr. S. Block (National Bureau of Standards)	99.999	Si, 5; Mg, 1; Cu, 1
GaAs	Monsanto Chemical Co., Ltd.	99.999	Mg, 3; Cu, 3; Si, 3; Al, 1; Ca, 0.8
GaP§	Dr. J. A. Van Vechten (Bell Laboratories)	99.99	Fe, 0.8; Si, 3; Al, 5; Ca, 1; Pb, 5; Mg, 30

* Analyzed by spectroscopic emmission.

† The same sample was studied in the diamond-anvil cell and cubic anvil apparatus (private communication; Block, 1978).

§ The same sample was studied in the diamond-anvil cell (Piermarini, 1975).

The electrical resistance of the calibrant crystal was continuously measured as a function of applied external load. As soon as a drop of resistance accompanied by polymorphic transition was observed, the elevation of external load was stopped and the x-ray diffraction photograph of not the calibrant but the coexisting NaCl was obtained. The exposure time was from 3 to 20 hours depending on the applied external load. The lattice constant of the compressed NaCl powder was measured from the diffraction photograph. The pressure on the powder was estimated when the obtained lattice constant was put into Decker's equation of state for NaCl.

4. Results and Discussion

4.1) Pressure fixed points

The abrupt drop of resistance for each calibrant is shown in Figs. 2-3 (a) to (n). At the point indicated by a closed circle in each diagram, the x-ray measurement of NaCl was started. The resistance exhibited a continuous decrease by several orders of magnitude during the prolonged exposure time.

The x-ray diffraction pattern taken for each transition is shown in Photos 2-1 to 2-4, respectively. The change in lattice constant, $-\Delta a / a_0$, and the obtained pressures for the transition of ZnTe, ZnS, GaAs, and GaP are all tabulated in Table 2-2. With respect to each transition in ZnTe, ZnS, and GaAs, we have different pressure values corresponding to the varieties of media, diamond, B, LiH, and g-BN. For GaP, only diamond and B media were used.

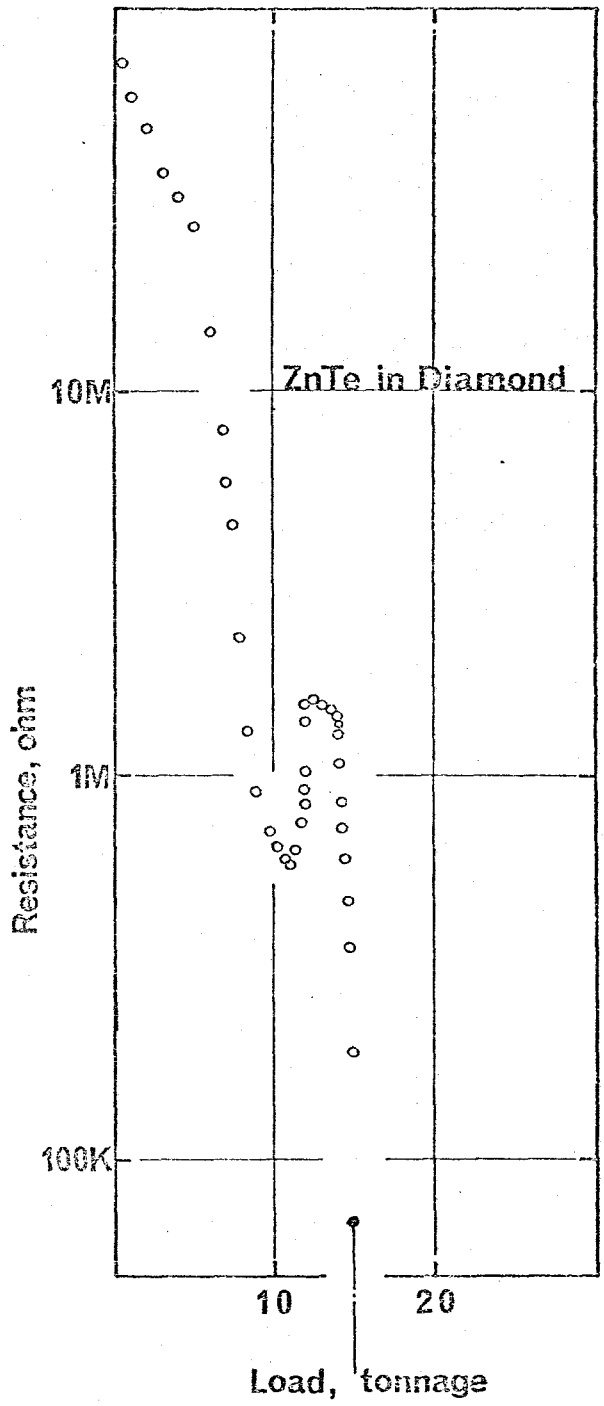

Fig. 2-3 (a). Resistance-external load curve for ZnTe inside diamond medium.

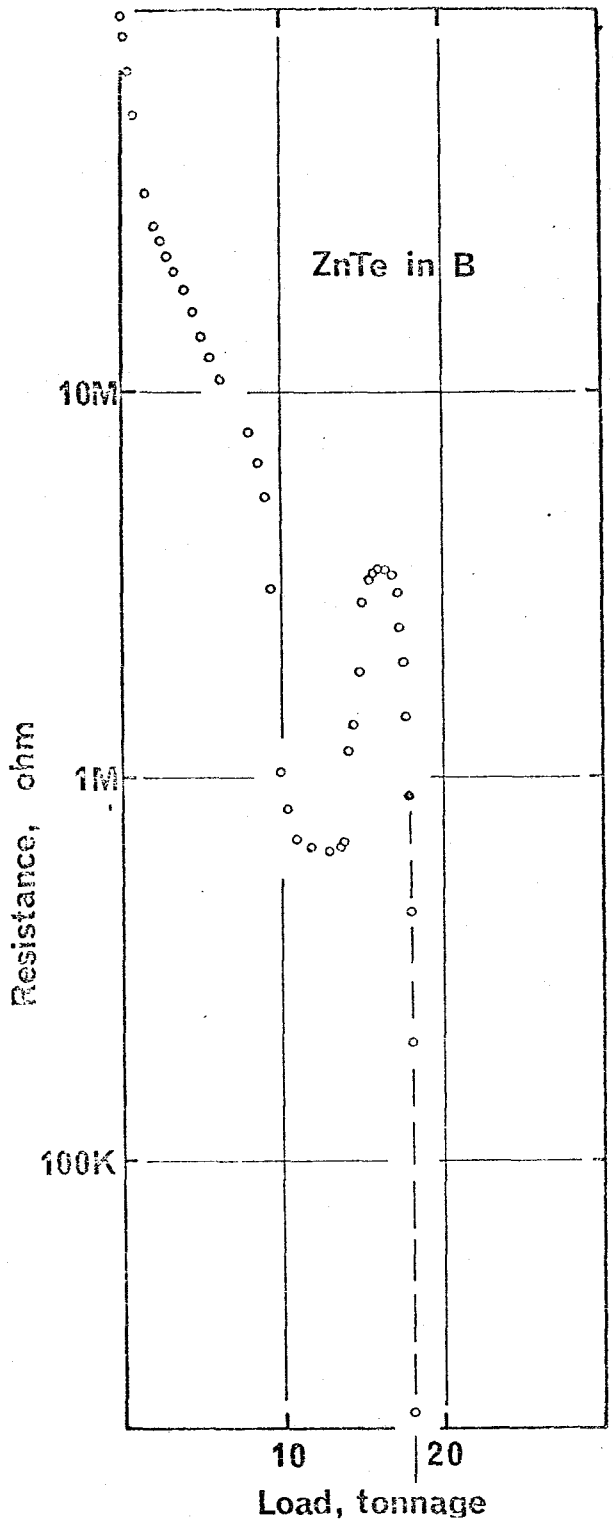

Fig. 2-3 (b). Resistance-external load curve for ZnTe inside B medium.

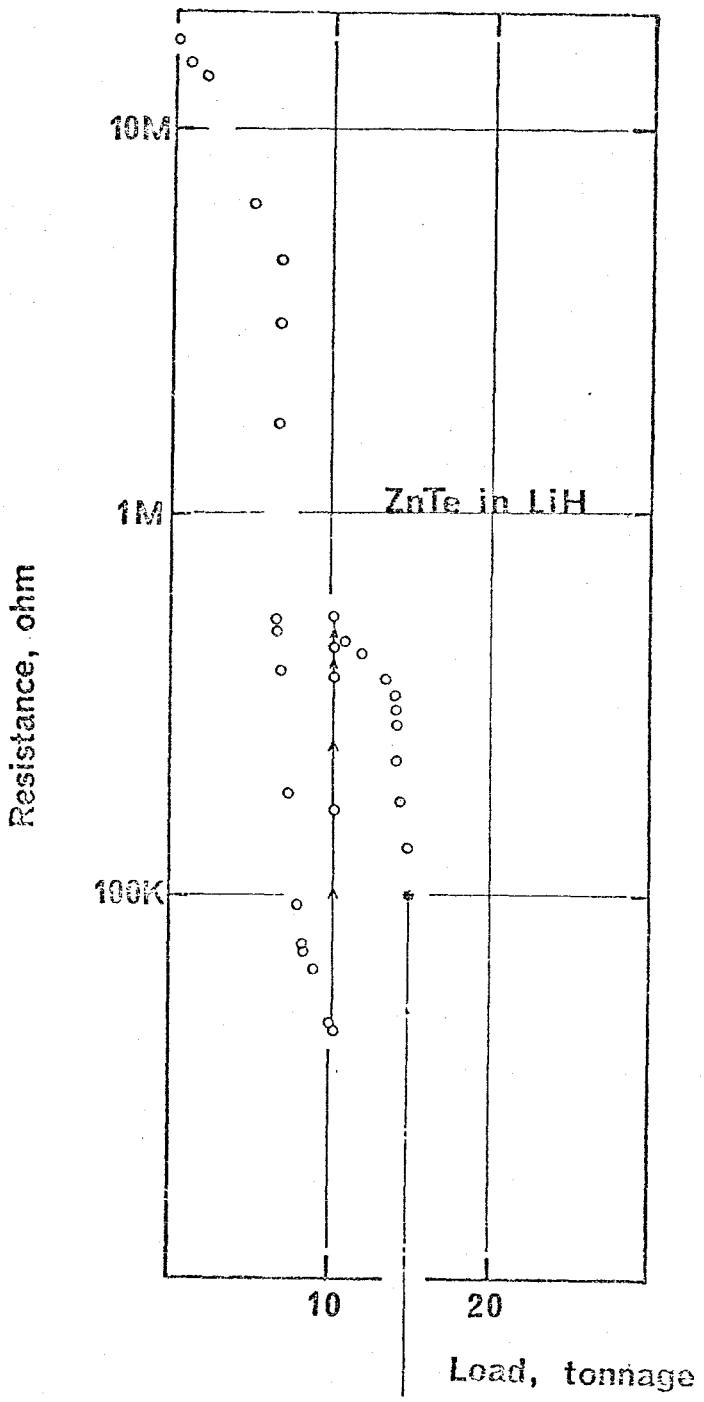

Fig. 2-3 (c). Resistance-external load curve for ZnTe inside LiH medium.

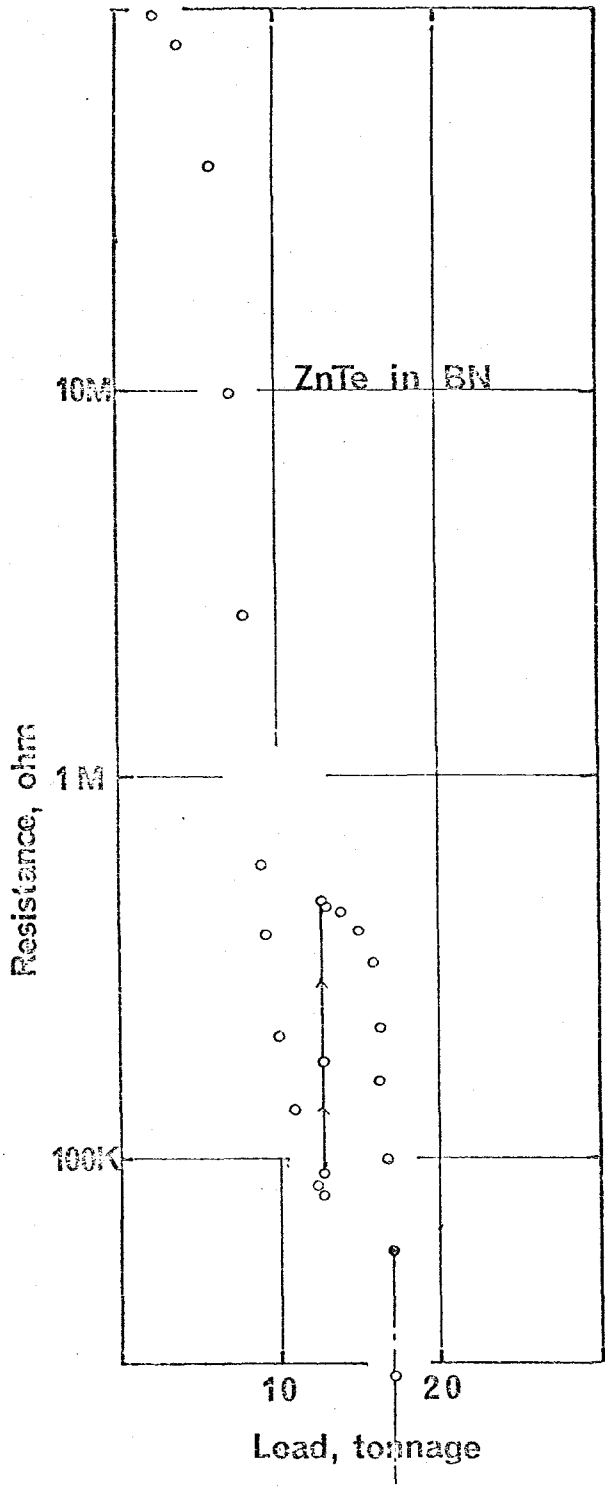

Fig. 2-3 (d). Resistance-external load curve for ZnTe inside BN medium.

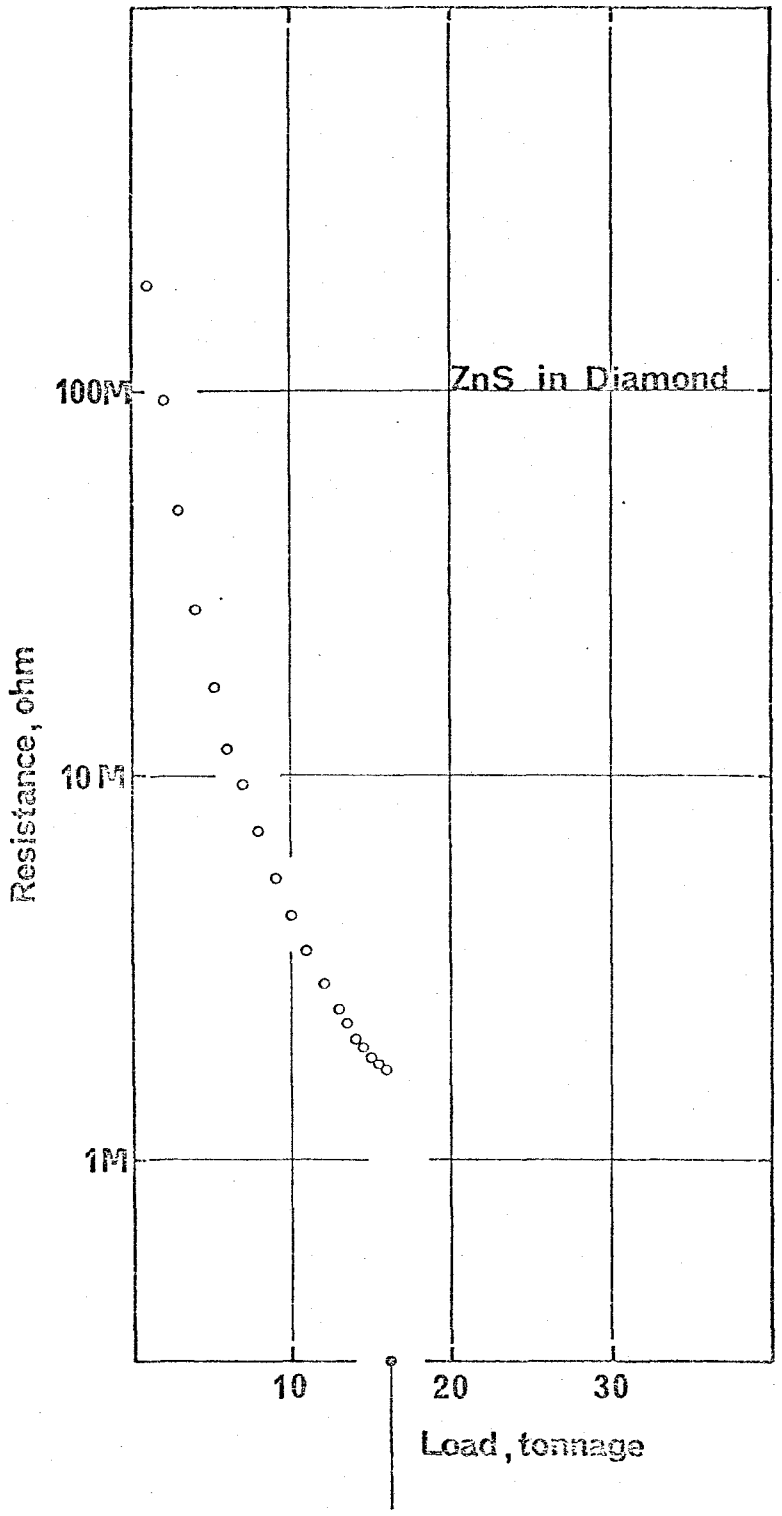

Fig. 2-3 (e). Resistance-external load curve for ZnS inside diamond medium.

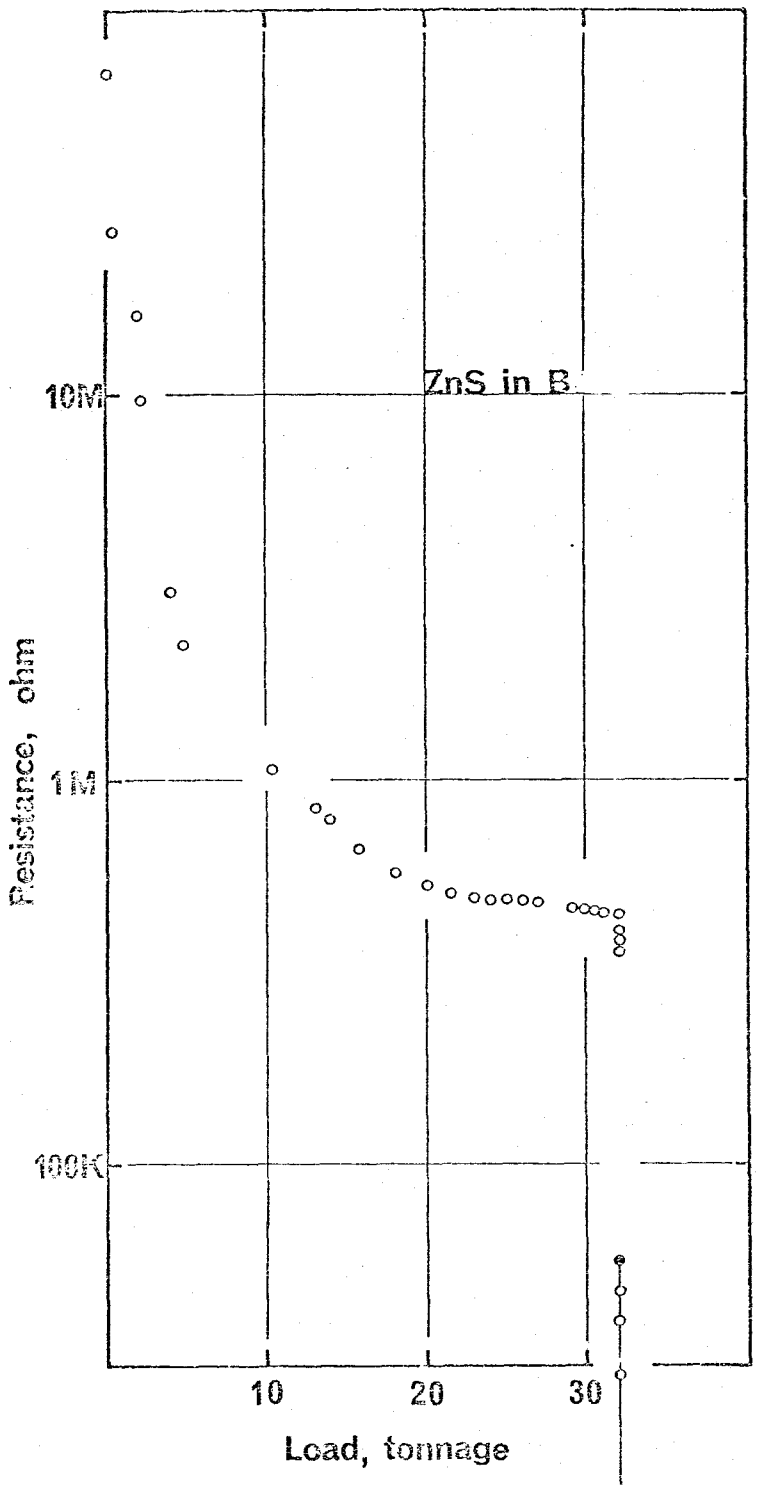

Fig. 2-3 (f). Resistance-external load curve for ZnS inside B medium.

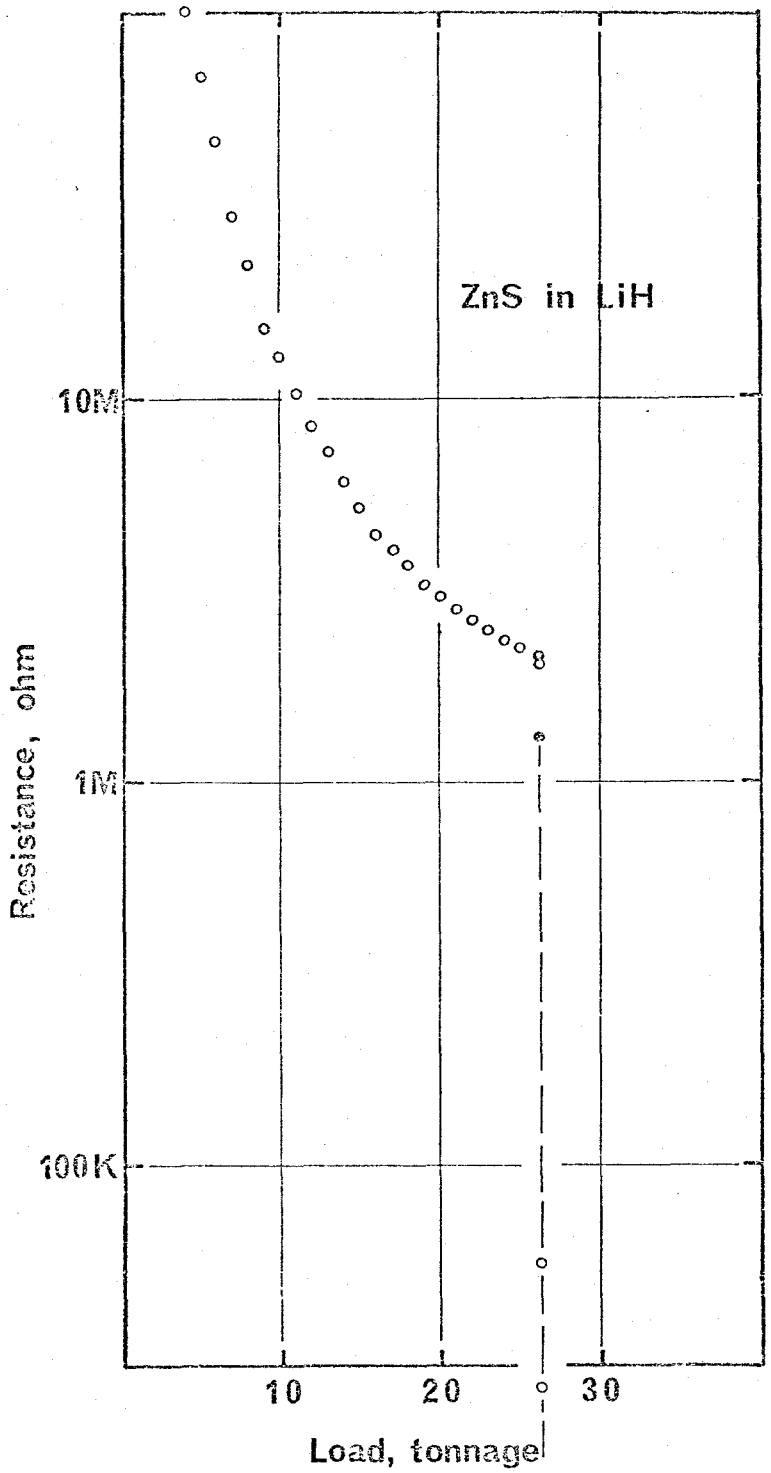

Fig. 2-3 (g). Resistance-external load curve for ZnS inside LiH medium.

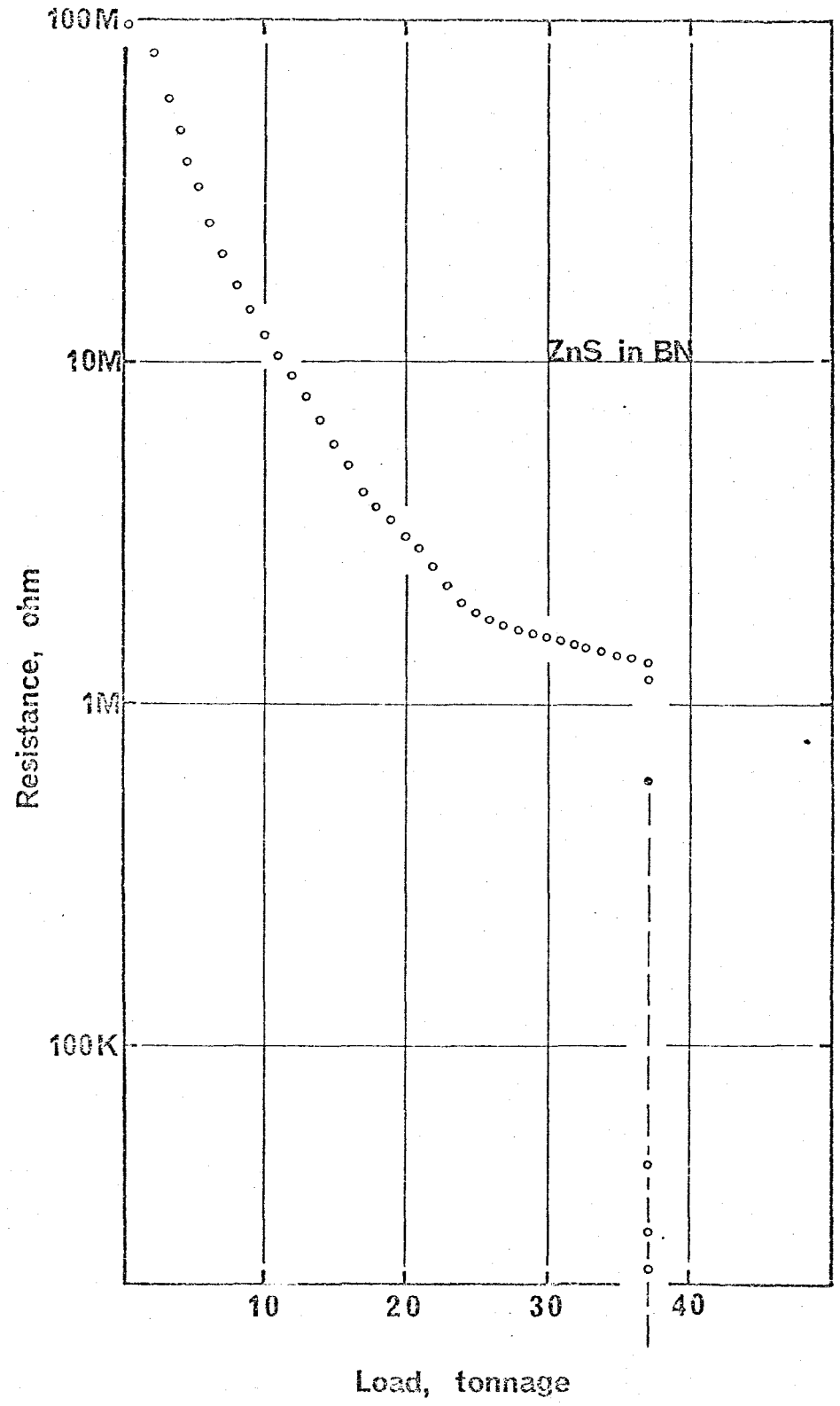

Fig. 2-3 (h). Resistance-external load curve for ZnS inside BN medium.

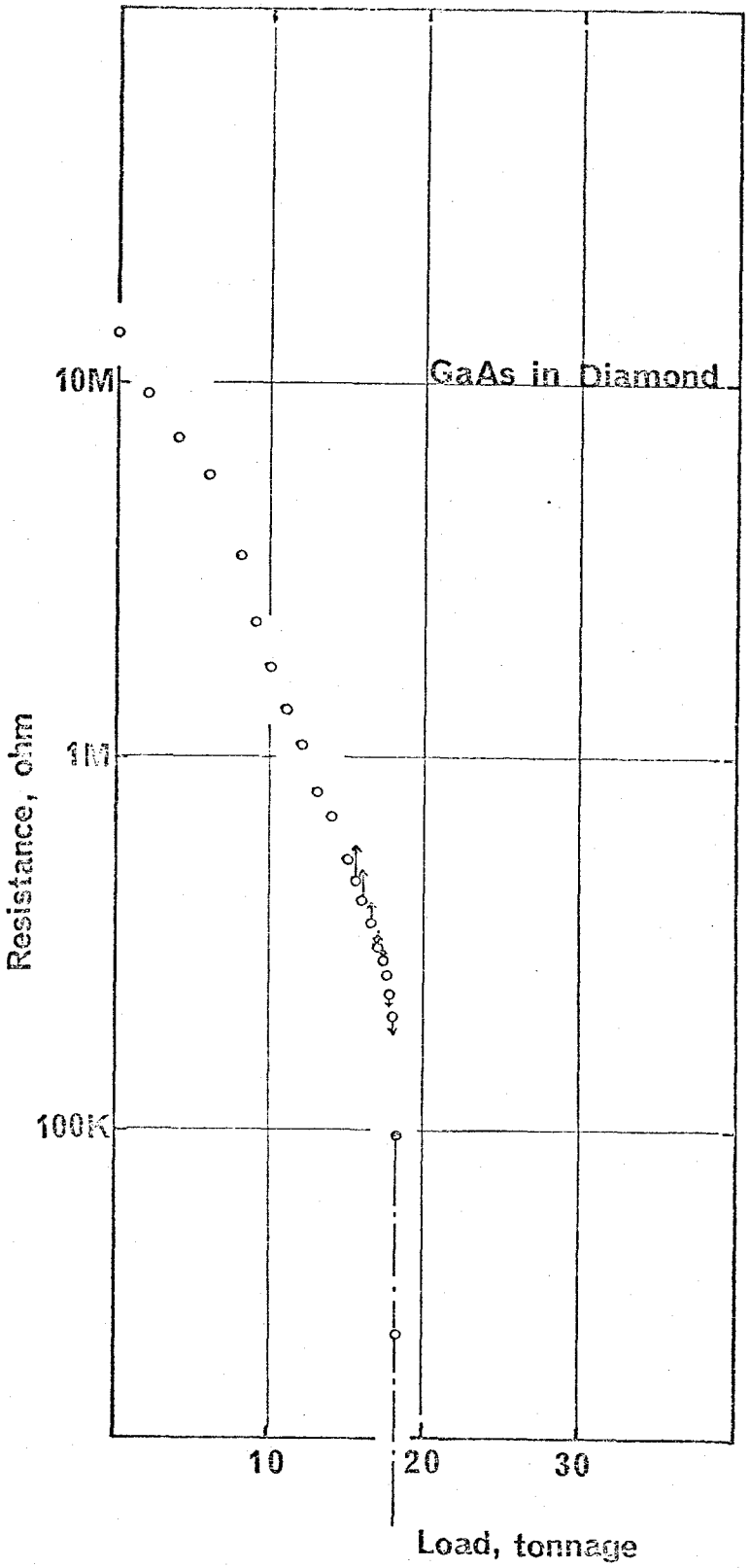

Fig. 2-3 (i). Resistance-external load curve for GaAs inside diamond medium.

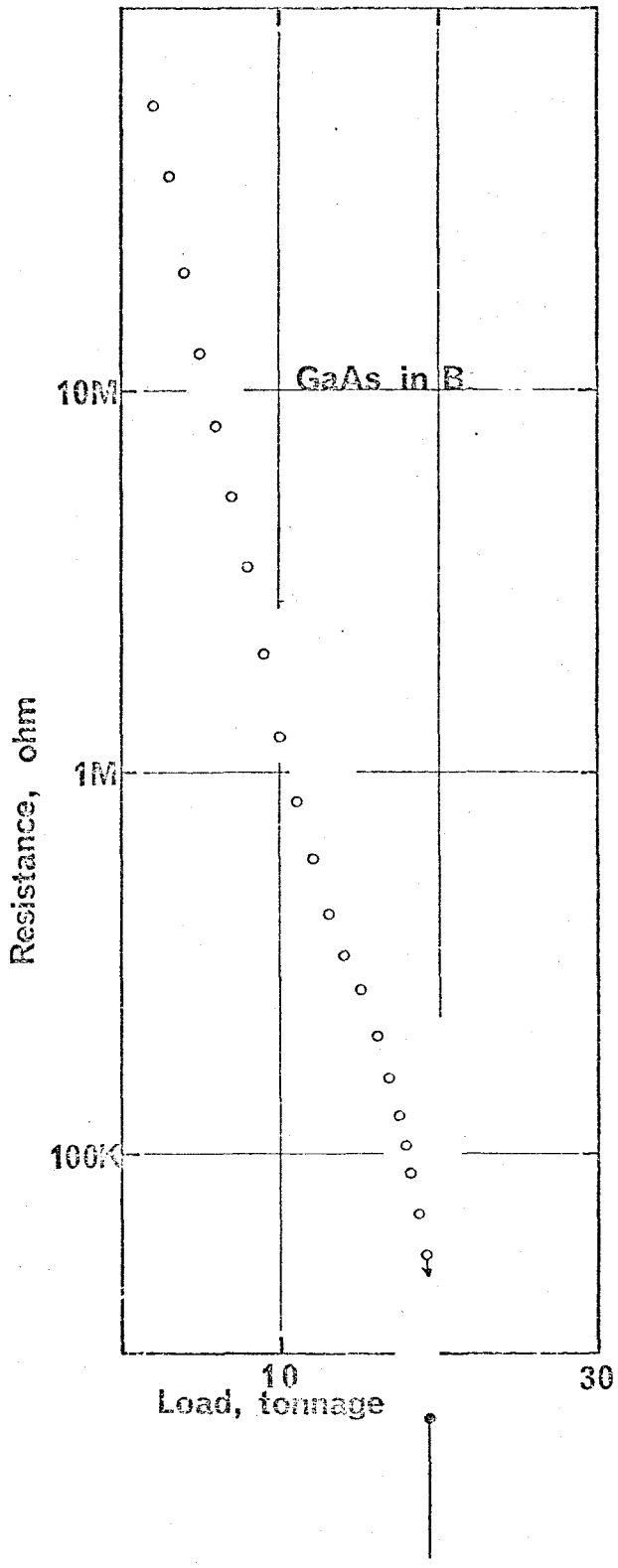

Fig. 2-3 (j). Resistance-external load curve for GaAs inside B medium.

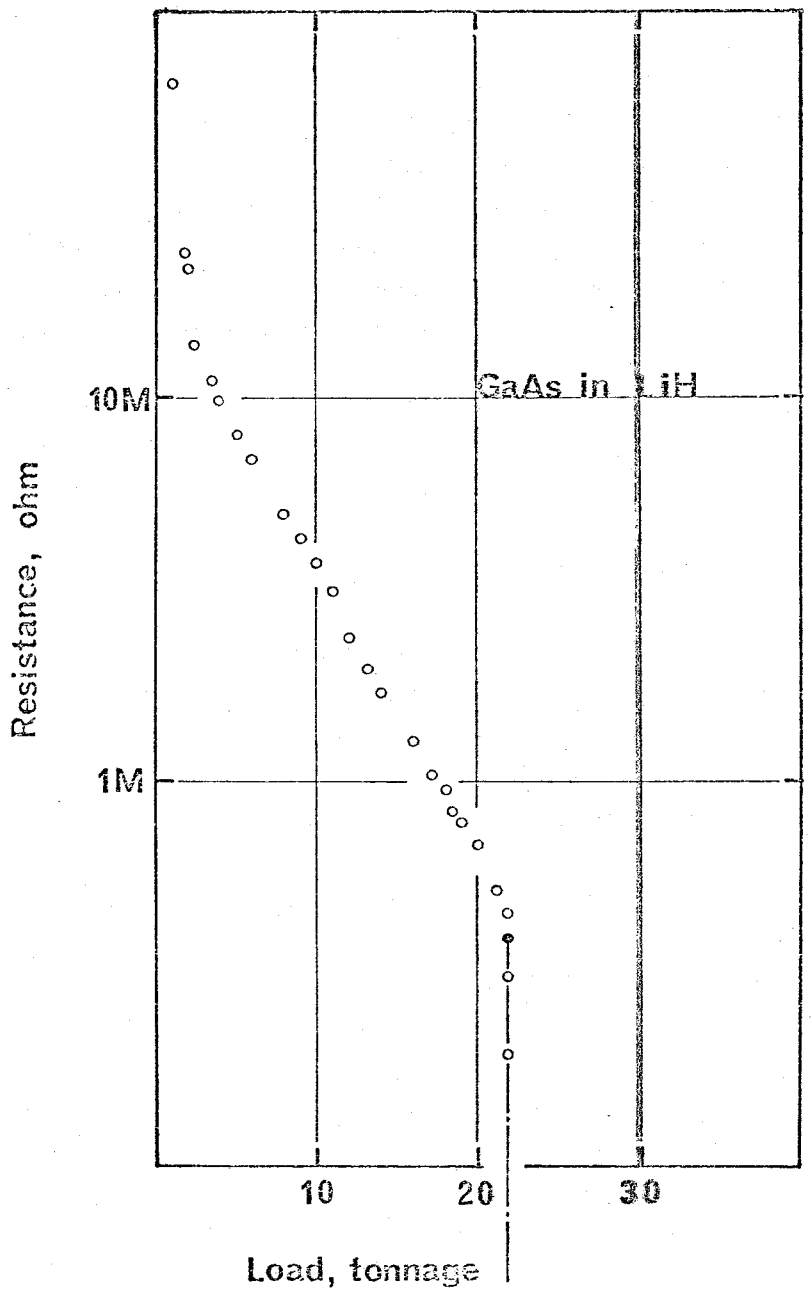

Fig. 2-3 (k). Resistance-external load curve for GaAs inside LiH medium.

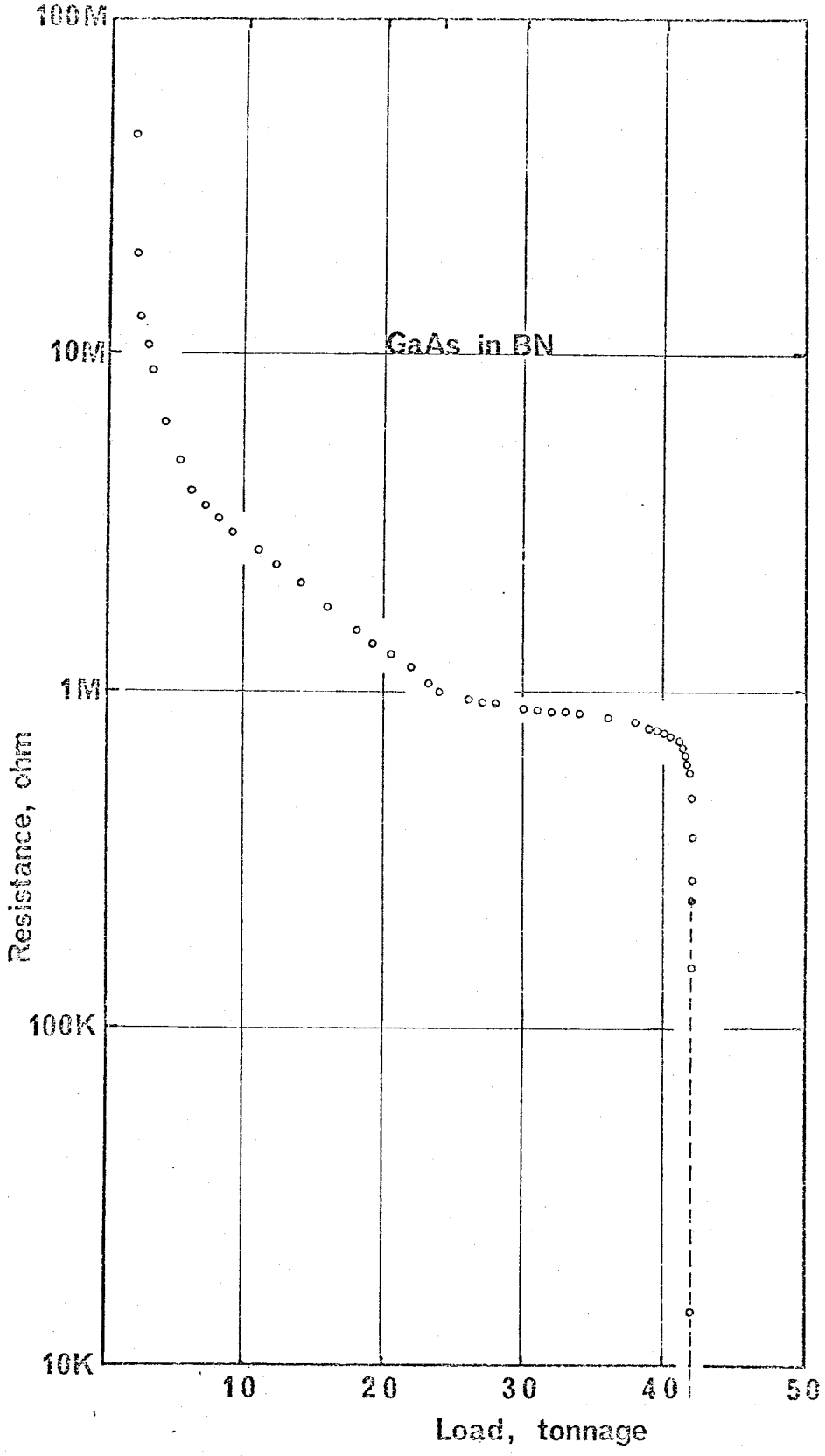

Fig. 2-3 (1). Resistance-external load curve for GaAs inside BN medium.

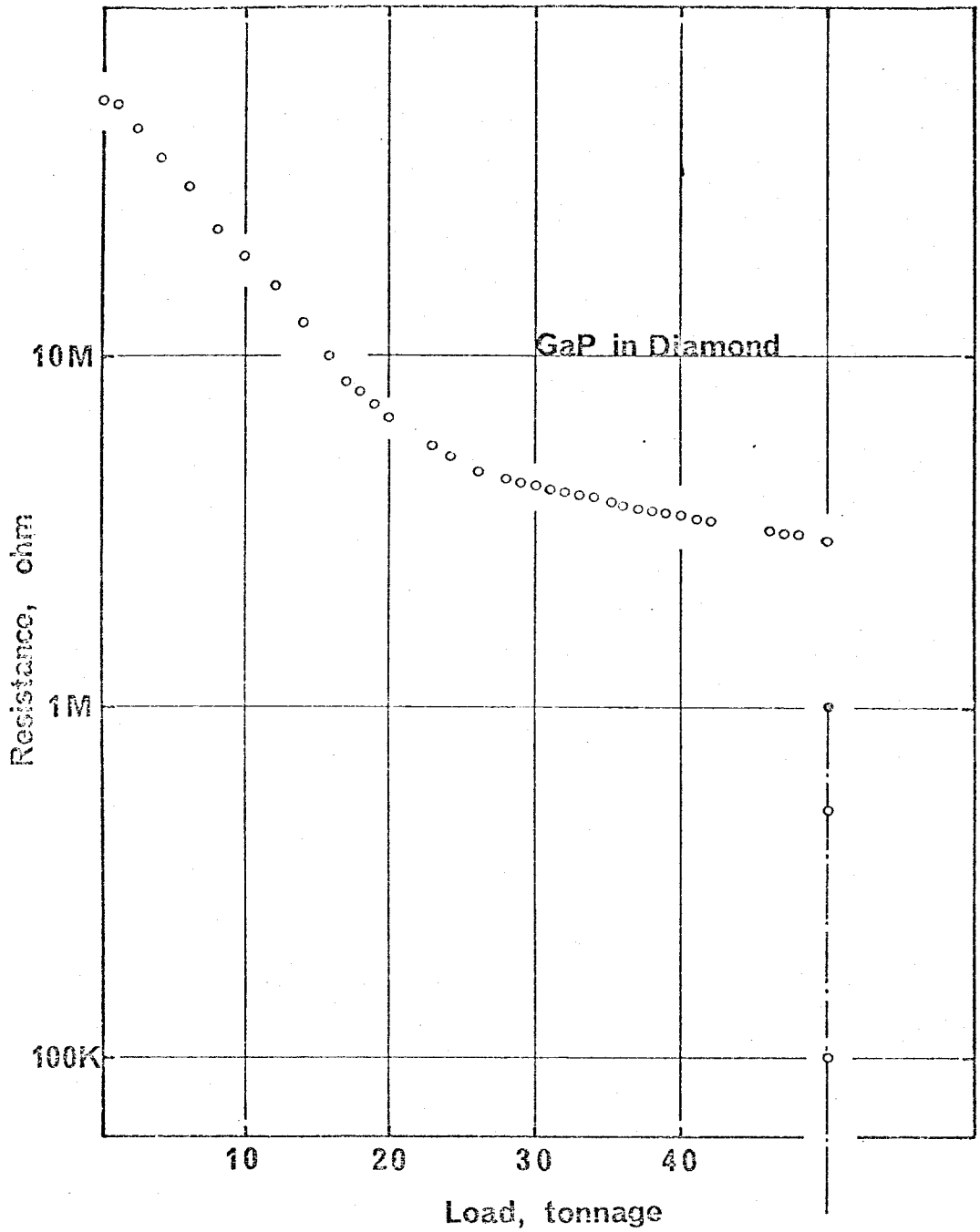

Fig. 2-3 (m). Resistance-external load curve for GaP inside diamond medium.

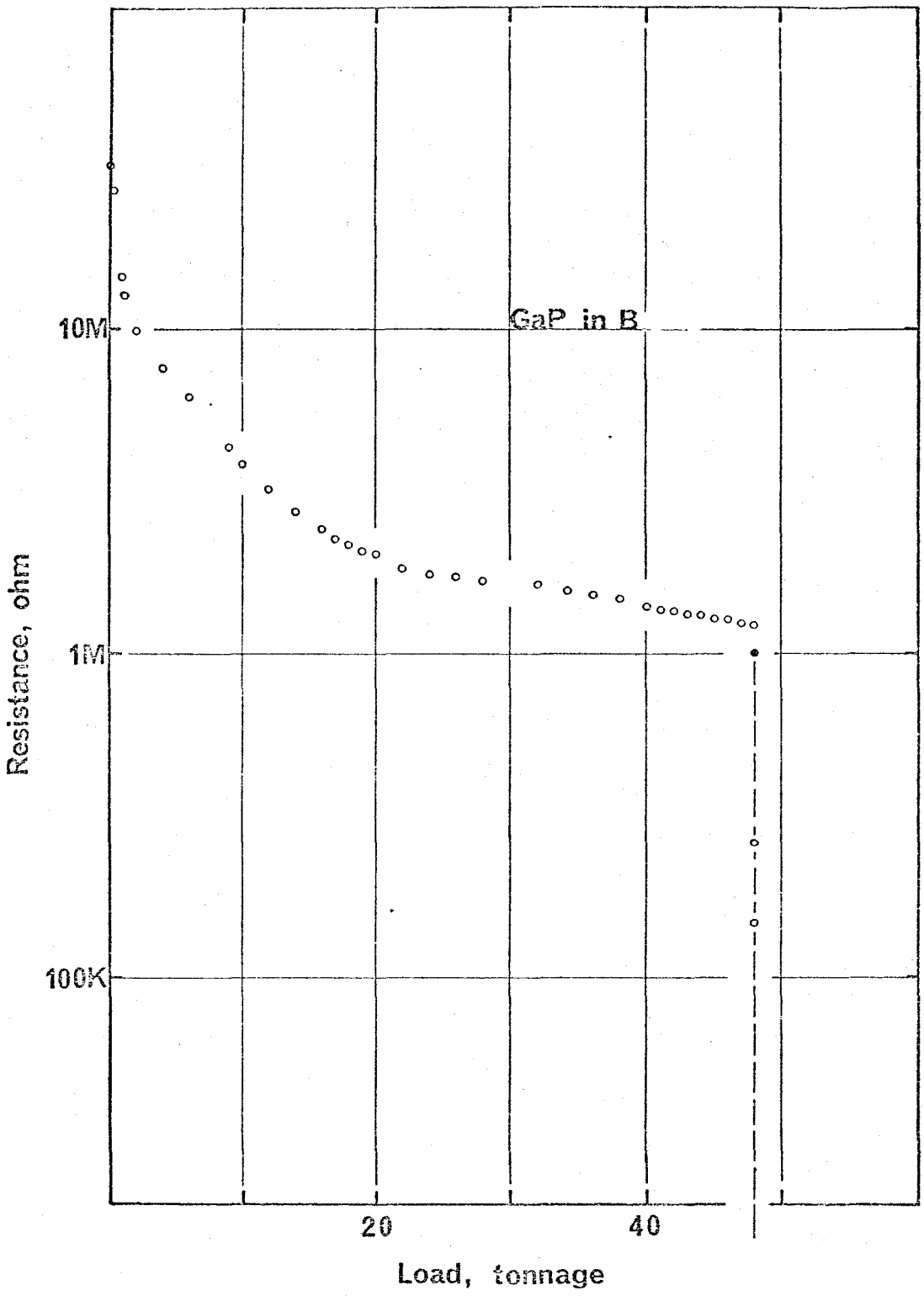

Fig. 2-3 (n). Resistance-external load curve for GaP inside B medium.

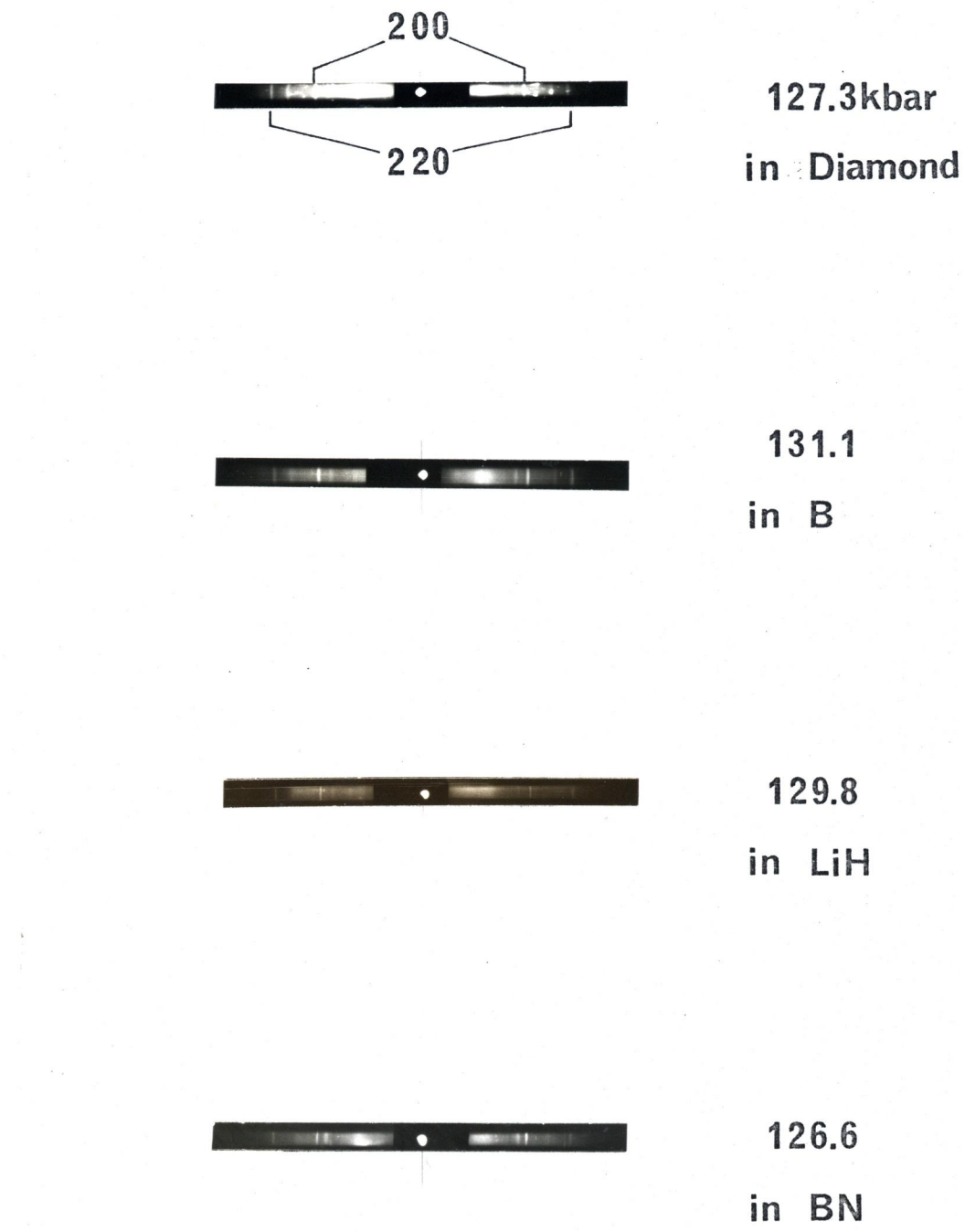

Photo 2-1. Diffraction patterns of NaCl at the transition pressure of ZnTe.

ZnS

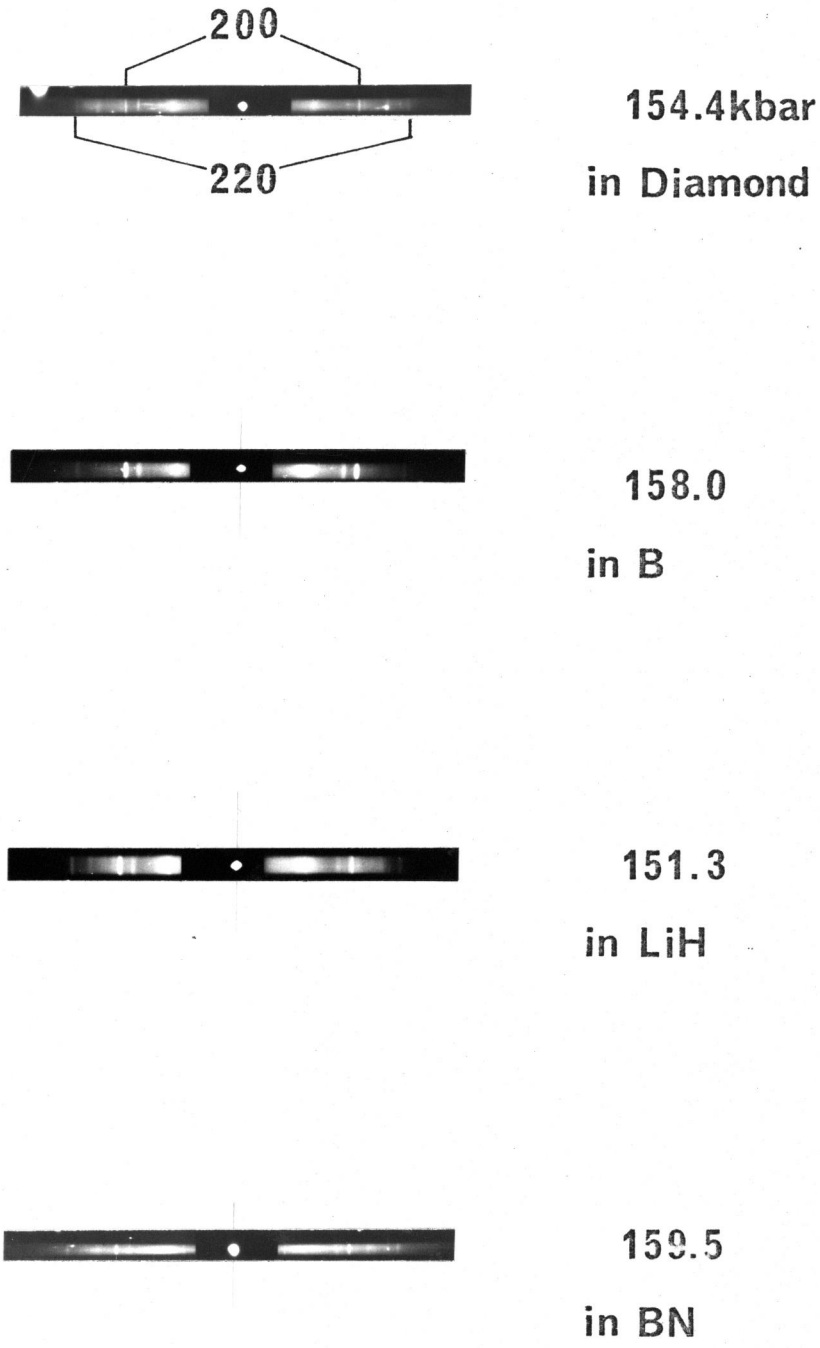

Photo 2-2. Diffraction patterns of NaCl at the transition pressure of ZnS.

GaAs

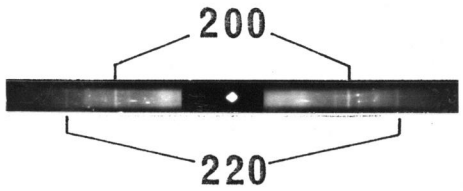

176.5kbar
in Diamond

190.0
in B

188.3
in LiH

186.7
in BN

Photo 2-3. Diffraction patterns of NaCl at the transition pressure of GaAs.

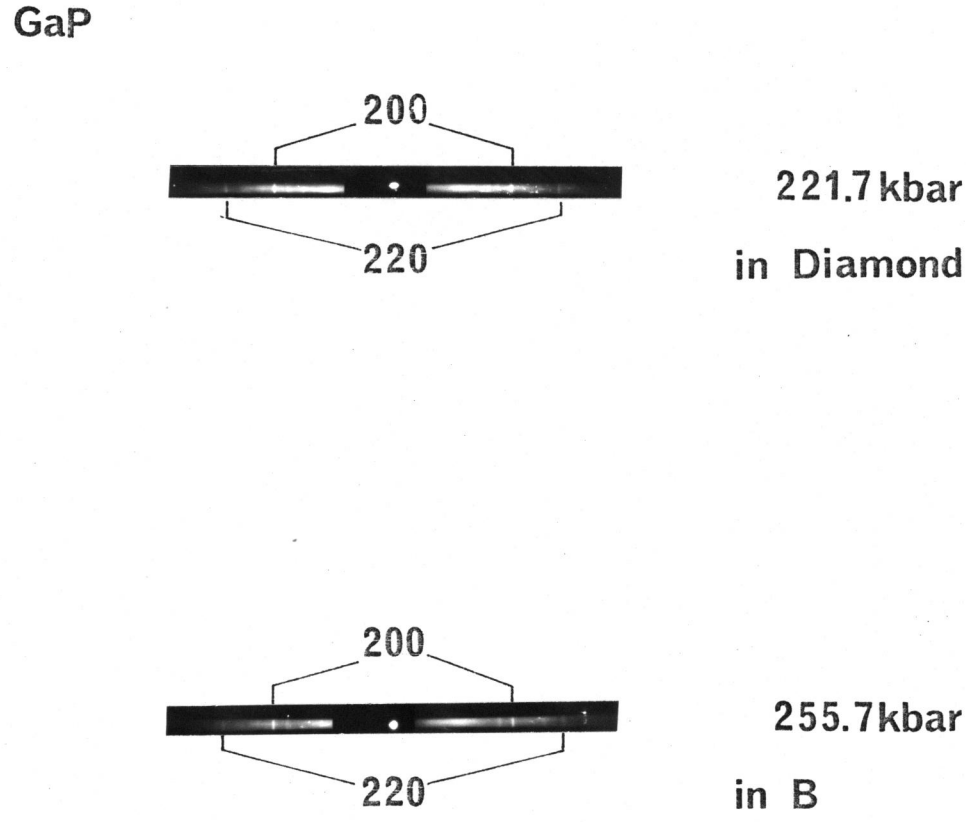

Photo 2-4. Diffraction patterns of NaCl at the transition pressure of GaP.

Table 2-2. Transition pressure of ZnTe, ZnS, GaAs, and GaP, each determined in various pressure media.

	Medium							
	Diamond		B		LiH		g-BN	
Calibrant	$-\Delta a / a_0$	P_t(kbar)	$-\Delta a / a_0$	P_t(kbar)	$-\Delta a / a_0$	P_t(kbar)	$-\Delta a / a_0$	P_t(kbar)
ZnTe	0.0875	127.3 ± 6.0	0.0894	131.1 ± 6.0	0.0885	129.8 ± 6.1	0.0866	126.6 ± 5.9
ZnS	0.0974	154.3 ± 6.8	0.0987	158.0 ± 6.9	0.0964	151.3 ± 6.7	0.0990	159.5 ± 7.0
	0.0964	151.3 ± 6.7			0.0964	151.0 ± 6.7		
	0.0975	154.4 ± 6.8						
GaAs	0.1045	175.0 ± 7.4	0.1088	190.0 ± 7.9	0.1083	188.3 ± 7.8	0.1078	186.7 ± 7.8
	0.1061	180.0 ± 7.7	0.1081	187.7 ± 7.8				
	0.1047	176.5 ± 7.5						
GaP	0.1176	221.7 ± 8.8	0.1245	249.4 ± 9.5				
	0.1171	219.8 ± 8.7	0.1260	255.7 ± 9.7				

$-\Delta a / a_0$: Compression of NaCl

P_t(kbar): Transition pressure

4.2) Analysis of errors

The experimental errors attached to the values in Table 2-2 will be analysed in this Section.

The error in the determination of lattice constant arises from various factors such as :

(i) determination of the camera radius,

(ii) shift of the specimen,

(iii) shift of camera,

(iV) reading error,

(v) change in the position of diffraction line due to the absorption of the beam within the specimen.

4.2.1) Determination of the camera radius

In the present work the camera radius was determined on each experiment according to the following procedure.

The diffraction patterns of NaCl were obtained intermittently during the course of the approach of guide blocks just before the compression began. The approach of guide blocks was measured by a dial gage. Figure 2-4 shows typical plots of the distance between a pair of diffraction lines due to (200), S_{200}, as a function of dial gage reading. An almost constant value of S_{200} was observed before the compression as seen in the

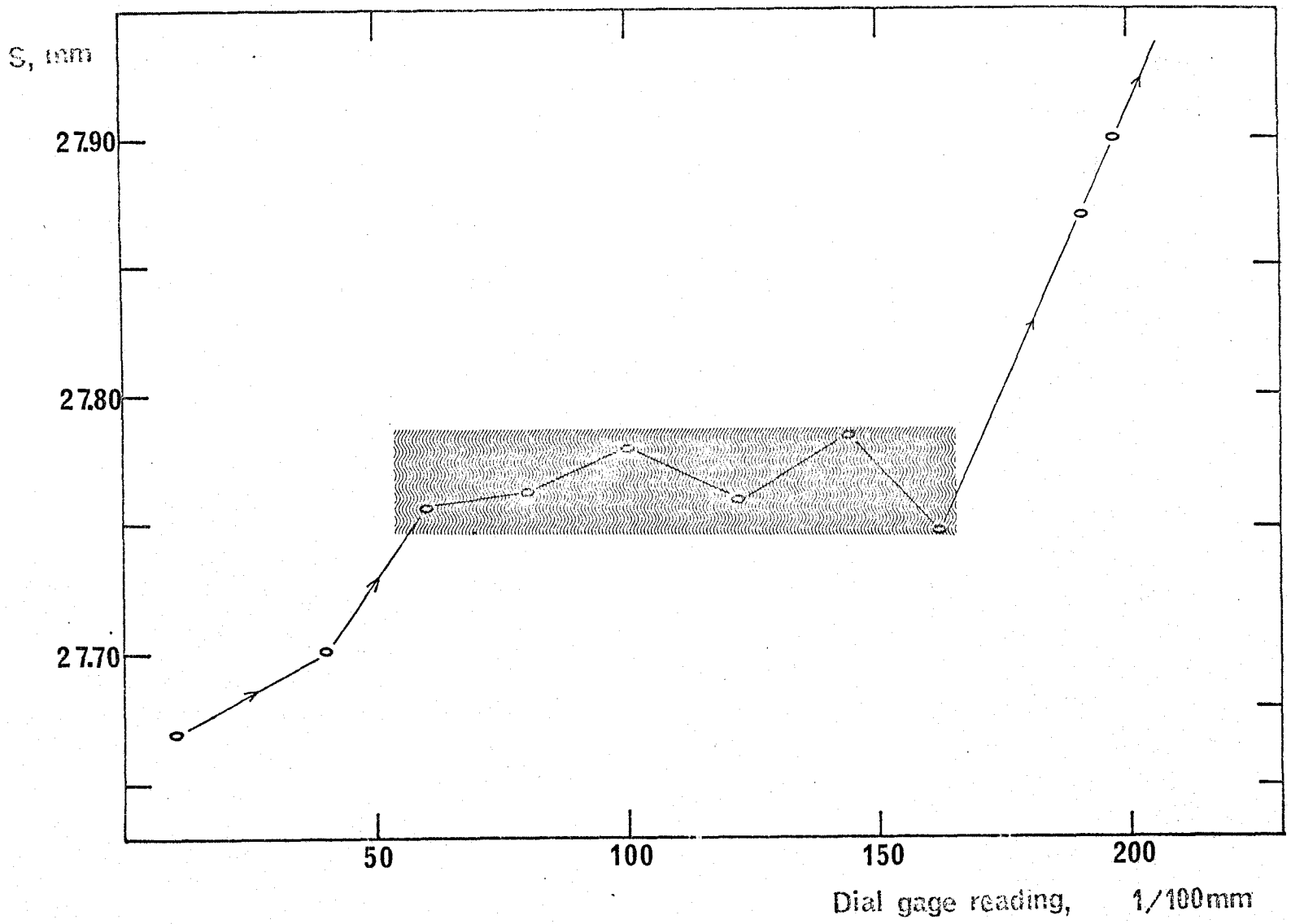

Fig. 2-4. Distance between a pair of diffraction lines due to (200), S_{200}, versus dial gage reading.

shaded region in Fig. 2-4, followed by a sudden increase due to the start of compression. From the data in the shaded region, we had the mean value, $\bar{S}$. The radius of the camera, R, is related to $\bar{S}$ by

$$R = \bar{S} \,/\, 4\theta_{200} \qquad (2\text{-}3)$$

where θ_{200} is expressed by the Bragg's equation

$$d_{200} = \lambda \,/\, 2 \sin \theta_{200} \,. \qquad (2\text{-}4)$$

In Eq. (2-4), d_{200} is the spacing of (200) planes in NaCl given in the ASTM card and λ is the wavelength of the MoKα beam. From Eqs. (2-3) and (2-4) we have an equation,

$$R = \frac{\bar{S}}{4 \sin^{-1} \dfrac{\lambda}{2d_{200}}} \qquad (2\text{-}5)$$

which finally gives the camera radius.

The error in the determination of the camera radius, ΔR, is estimated from the relation obtained by differentiating Eq. (2-5),

$$\Delta R = \frac{\Delta \bar{S}}{4 \sin^{-1} \dfrac{\lambda}{2d_{200}}} \,, \qquad (2\text{-}6)$$

in which $\Delta \bar{S}$ is given by the width of the fluctuation of S_{200} in the shaded region in Fig. 2-4. The value of

0.04 mm for $\Delta\bar{S}$ gives rise to the error of 0.08 mm in the determination of the camera radius.

4.2.2) Shift of the specimen

For the estimation of specimen shift, the following experiment was carried out. The x-ray diffraction analyses were undertaken right after releasing pressure as well as just before pressurizing. On each diffraction photograph thus obtained, we observed the Debye-Scherrer rings whose distances were not equal to each other. The discrepancy in the distance, ΔS, was obtained from another experiment in which diamond was used as a specimen and its diffraction was observed. If diamond is assumed to be incompressible by compression of low grade and also if a difference in the position of lines before and after compression of diamond is observed, this difference represents ΔS.

The shift of the specimen, Δx, is calculated by the relation (see Fig. 2-5),

$$\Delta x = \Delta S / 2 \sin 2\theta_D \qquad (2\text{-}7)$$

where $2\theta_D$ is the diffraction angle related to the (111) diffraction lines of diamond. In the present work Δx was found to be 0.03 mm. This value is less than the error in the camera radius.

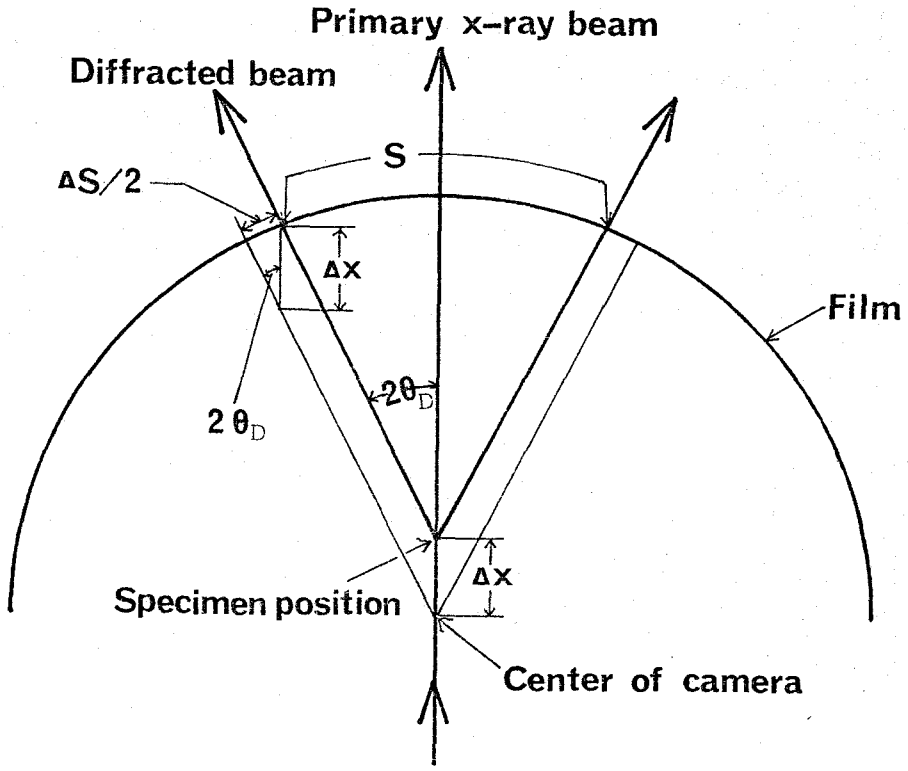

Fig. 2-5. Schema showing the relation between ΔS/2 and Δx.

Figure 2-6 shows the case in which the specimen shifts from the original position P_a to the position P_b as pressure increases. The arc A has a radius R originated from the point P_a, while the arc B has a radius R' from the point P_b. The diffracted rays from P_b are collected on the film along the actual arc A, although the ideal pattern should be collected on the film along an authentic arc B whose radius is R'.

Therefore, for a given diffraction angle of 2θ, we observe the lines with distance S on the arc A, which should be seen on the arc B with distance S'. When we put the shift of specimen as Δx, then

$$R = R' + \Delta x \ . \qquad (2\text{-}8)$$

It follows that,

$$S = 2\theta (R - \Delta x) \qquad (2\text{-}9)$$

and

$$S' = (2\theta - \Delta\theta) R \ . \qquad (2\text{-}10)$$

The difference, ΔS, between S and S', is expressed as

$$\Delta S = \Delta\theta R - 2\theta \Delta x. \qquad (2\text{-}11)$$

Using Eqs. (2-9) and (2-11) it comes out that

$$\frac{\Delta S}{S} = \frac{\Delta\theta R - 2\theta \Delta x}{2\theta (R - \Delta x)} \ . \qquad (2\text{-}12)$$

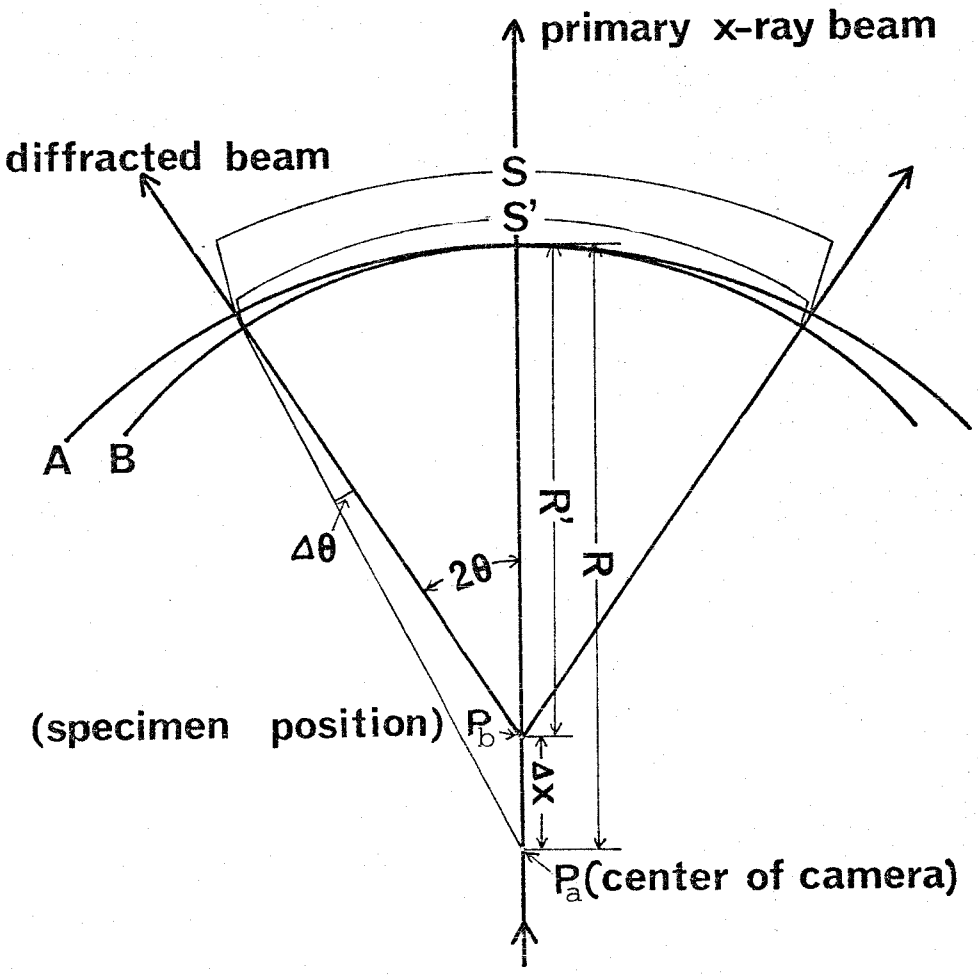

Fig. 2-6. Schema showing two arcs in case the specimen shifts from the center of camera, P_a to a position P_b.

The following relation is obtainable from Fig. 2-6,

$$\frac{\Delta x}{\sin \Delta\theta} = \frac{R}{\sin (180 - 2\theta)}, \qquad (2\text{-}13)$$

Putting Eq. (2-13) into Eq. (2-12) we obtain the followig equation,

$$\Delta S/S = \frac{\sin^{-1}\{\frac{\Delta x \cdot \sin(180-2\theta)}{R}\}}{2\theta(R-\Delta x)} - \frac{\Delta x}{R-\Delta x}. \qquad (2\text{-}14)$$

The error in the distance arising from the discrepancy of actual and authentic arcs is estimated from Eq. (2-14) to be about one order of magnitude smaller than the other errors. Therefore it can be neglected.

4.2.3) Shift of camera

The camera cassette was mounted on the periphery of the lower cylinder as shown in Fig. 1-10. When load was applied upon the cylinder, it deformed. In the present device, the load was applied parallel to the axis of the cylinder. The cylinder, therefore, expanded radially according to the Poisson's effect.

The expansion of the cylinder while it was loaded was measured by strain gage. On the periphery of the lower cylinder the strain gages were placed at three points, each being separated to each other by an angle $\pi/2$.

As shown in Fig. 2-7, the amount of expansion increases almost linearly with increasing the load. Upon decreasing the load, the cylinder contracts reversibly. Therefore the expansion of the cylinder occurs in an elastic fashion. Using the least square method, the slope in Fig. 2-7 is determined to be 1.58×10^{-6} mm/ton. From this slope we can correct the amount of the shift of camera with the change in the applied load. The value is negligible compared with the other errors even when we apply the load up to 100 tons.

4.2.4) Reading error

A standard deviation of 0.1 % , arising from the reading error was obtained for the precision of the d_{200} spacing.

4.2.5) Errors due to the absorption

The error can be neglected since the thickness of the specimen is too small to absorb the x-ray beam.

4.2.6) Sum of the errors

From the above discussion it turns out that the errors to be taken into account involve only the items (i)determination of camera radius, (ii) shift of the specimen, and (iv) reading error.

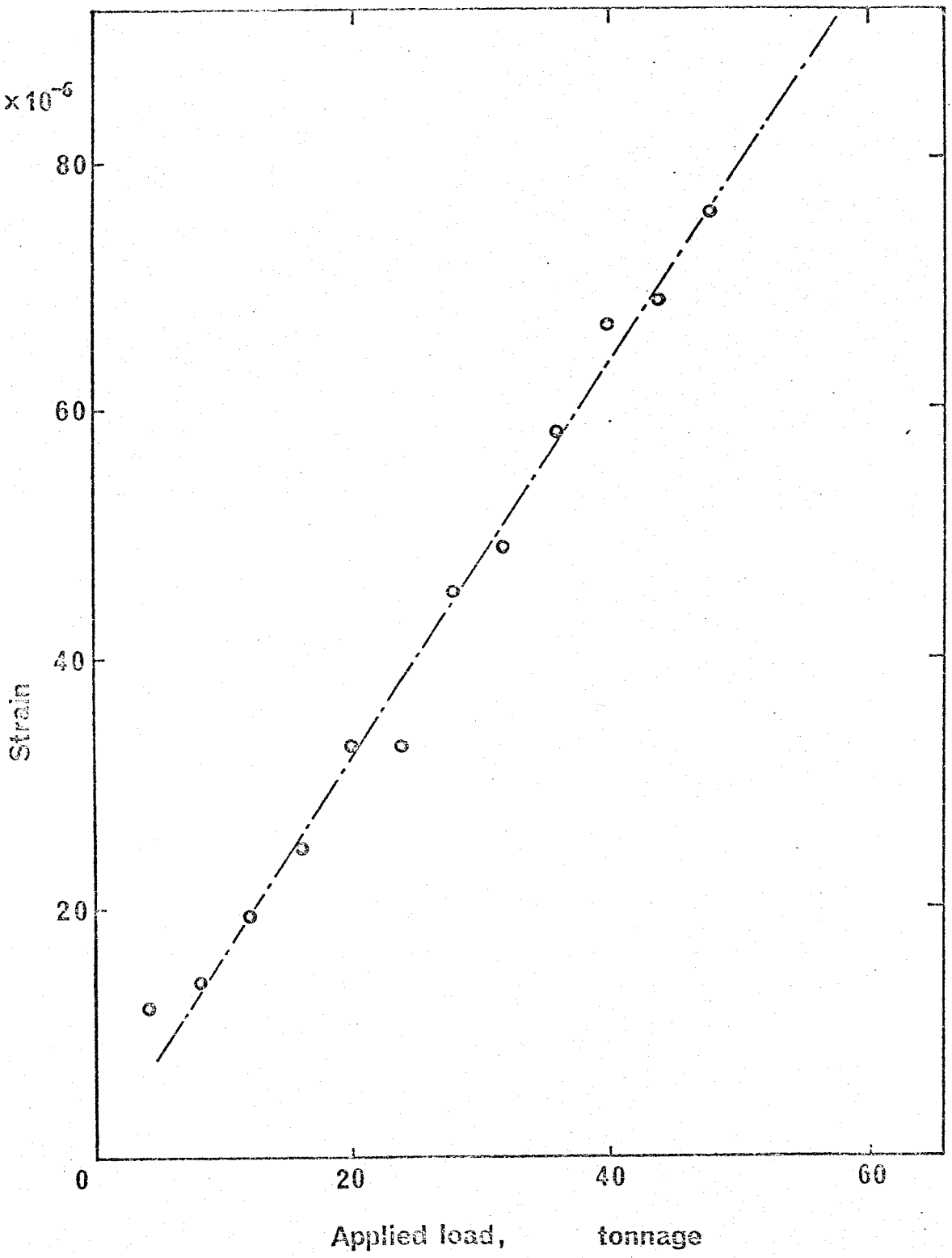

Fig. 2-7. Strain versus applied load relation, showing a linear expansion of the cylinder.

On differentiating the generalized form of Eq.(2-3), we have

$$\Delta\theta/\theta = \Delta R/R + \Delta S_S/S + \Delta S_R/S . \qquad (2\text{-}15)$$

The first term in Eq. (2-15) is the error (i), concerned with the determination of camera radius. The second term concerns the error (ii) caused by the specimen shift. The third term arises from the reading error (iv). By using Eq. (2-7) , Eq. (2-15) becomes

$$\Delta\theta/\theta = \Delta R/R + \Delta x\cdot\sin\theta\cdot\cos\theta/\theta\cdot R + \Delta S_R/S. \qquad (2\text{-}16)$$

On the other hand, the next equation can be derived from the generalized form of Eq. (2-4) ,

$$\Delta d / d = \cot\theta\cdot\Delta\theta . \qquad (2\text{-}17)$$

Putting $\Delta\theta$ in Eq. (2-16) into Eq. (2-17), then we have

$$\Delta d/d = \cot\theta(\Delta R\cdot\theta/R + \Delta x\cdot\sin\theta\cdot\cos\theta/R + \Delta S_R\cdot\theta/S) . \qquad (2\text{-}18)$$

Figure 2-8 shows $\Delta d / d$ versus θ for different values of ΔS and Δx, while ΔR is kept fixed. The value $\Delta d/d$ smoothly decreases with increasing θ. The accurate lattice constant can, therefore, be obtained using the diffraction line with higher Miller indices, in coinci-

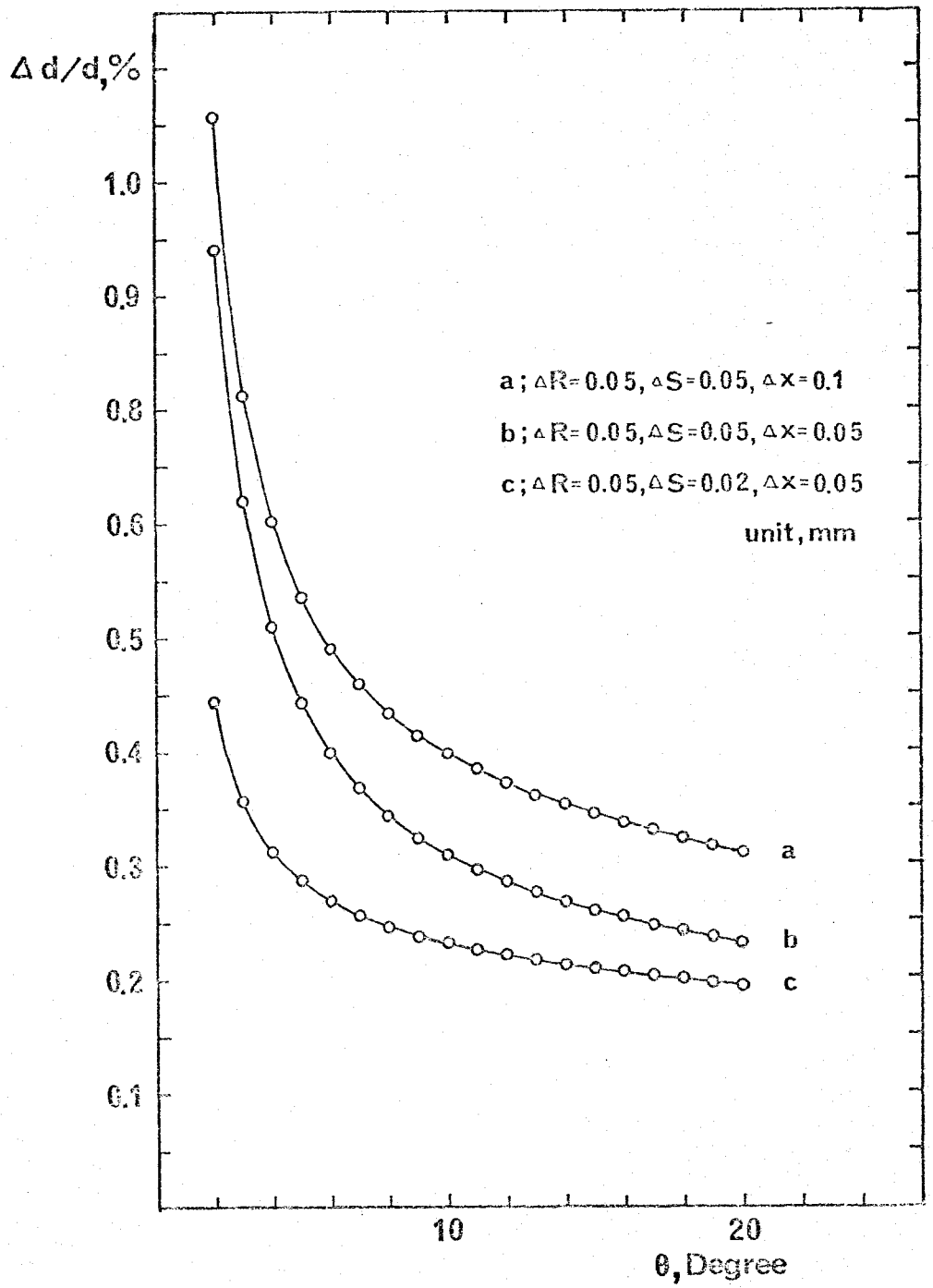

Fig. 2-8 . Δd/d versus θ for different values of Δx, ΔS, and ΔR.

dence with the general concept.

At higher pressure, however, broadening of the diffraction line with higher Miller indices occurs caused by the nonhydrostatic compression inside the solid medium. This line broadening gives rise to an additional reading error. Therefore, ΔS_r varies with the change in diffraction angle. In this study, we obtain the relation between ΔS_r and θ as,

$$\Delta S_R/4\theta \cdot R = 0.722 \times 10^{-3}. \qquad (2\text{-}19)$$

Furthermore, from the result in Section 4.2.1, the error in the determination of camera radius is

$$\Delta R/R = 1.46 \times 10^{-3}. \qquad (2\text{-}20)$$

From the result in Section 4.2.2, the error arising from the specimen shift is

$$\Delta x/R = 0.137 \times 10^{-3}. \qquad (2\text{-}21)$$

Putting Eqs. (2-19), (2-20), and (2-21) into Eq. (2-18), we finally obtain the error in the determination of lattice constant as,

$$\Delta d/d = \cot\theta\{(1.46\times10^{-3}+0.722\times10^{-3})\cdot\theta+0.274\times10^{-3}\cdot\sin2\theta\}. \qquad (2\text{-}22)$$

Using Eq. (2-22), the error in the present experiment is accurately evaluated as shown in Fig. 2-9. The error estimation curve in Fig. 2-9 is different from that in Fig. 2-8. The error in the determination of lattice constant at high pressure turns out to be almost constant in the entire region of the diffraction angle between 0 and 20°. In case we use MoKα rediation, almost all diffraction lines are observable in this region. A great accuracy can thus be attained by using the diffraction lines with lower Miller indices. The error in d-spacing in this study is estimated to be 0.26 %.

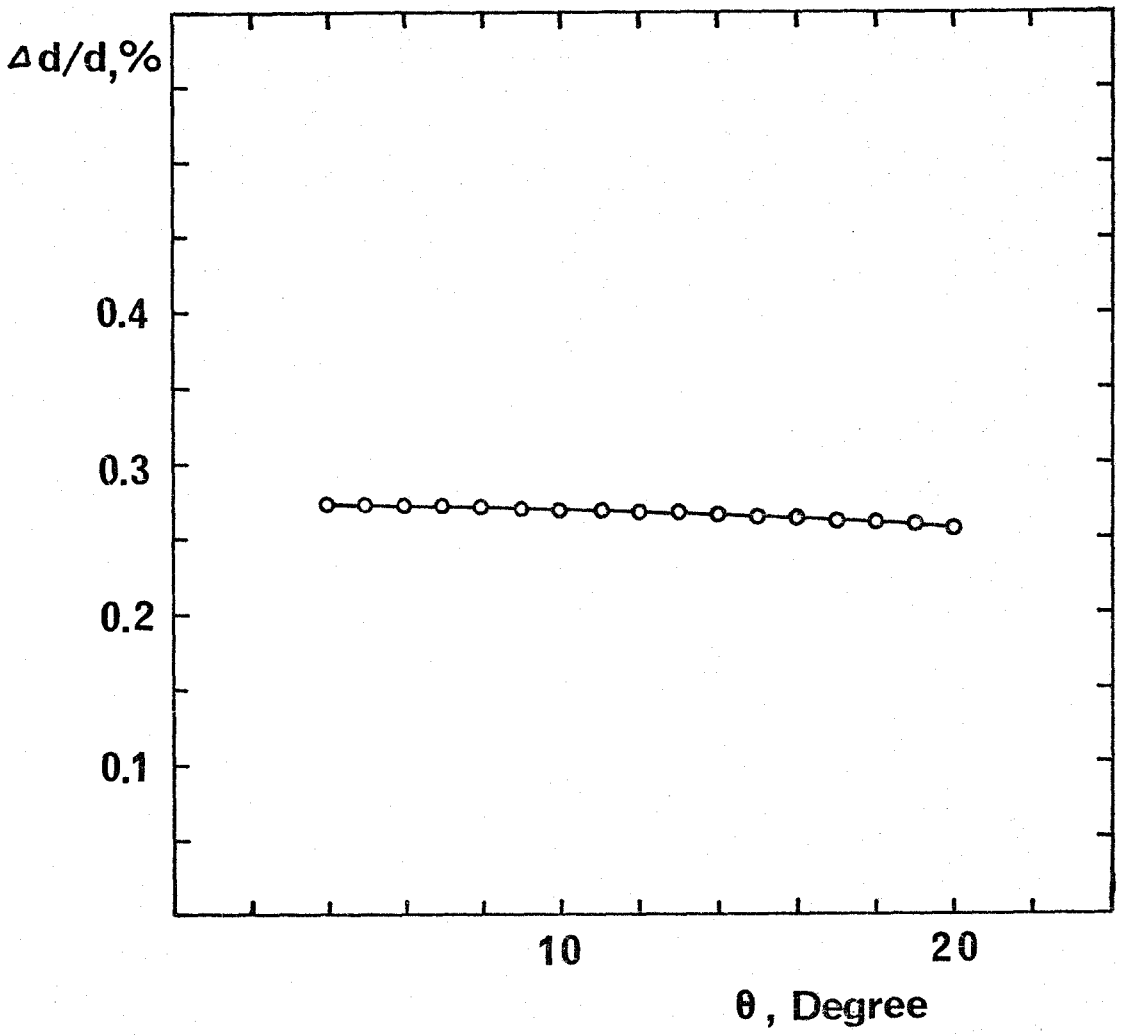

Fig. 2-9 . The sum of the errors in d-spacing versus θ in the present x-ray measurement.

4.3) Hydrostaticity

As a measure to know hydrostaticity inside the pressure medium, the discrepancy of lattice parameter of NaCl determined from two diffraction lines were examined. The discrepancy would become zero if the NaCl crystals were compressed in a virtually hydrostatic condition (Singh and Kennedy, 1974). Figure 2-10 shows the discrepancy of the lattice parameter of NaCl determined from the two diffraction lines (200) and (220), each obtained inside four different pressure media. The data points lies in the region within the experimental errors arising from the x-ray system except for the case of diamond. The specimen in the present pressure media are, therefore, compressed in a nearly hydrostatic condition.

However, we can perceive from Fig. 2-10 that a small discrepancy is observed. This suggests that inside the diamond medium the pressure deviates from the hydrostatic condition, although the amount is close to experimental uncertainty.

Difference due to pressure medium is also seen in the measurement of electric resistance. As seen in the case of GaAs embedded inside the diamond medium, the resistance decreased monotonously until it approached to the transition point. At pressures near to the transition, the increment of load was carefully made

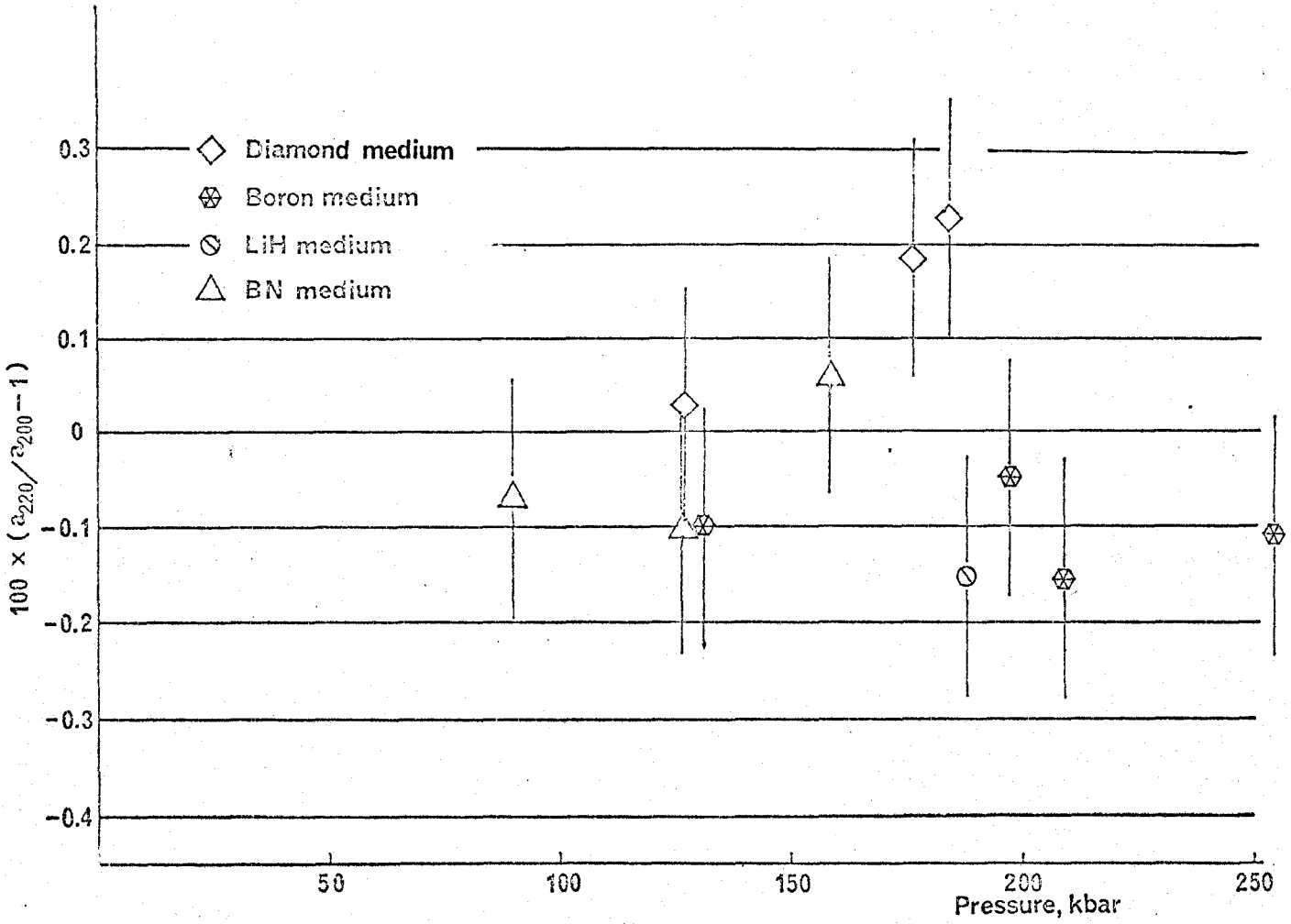

Fig. 2-10. Discrepancy of the lattice parameter of NaCl determined from the (200) and (220) lines inside various pressure media.

stepwise. After each increment the load was fixed for 5 minutes, during which was observed a slight increase of resistance by an amount as shown by the arrow in Fig. 2-3 (i). This amount decreased gradually and became zero as the load was increased further. Next to be observed was a small decrease in resistance. The resistance did not show any further decrease unless the load was stepped up. After this precursor the resistance dropped very sharply by several orders of magnitude, showing the transition into the metallic state. This anomalous behavior was not observed in other media. Similar trend is seen in the case of Si (Minomura and Drickamer, 1962).

For the sake of comparison, the electric resistance of GaAs was measured inside NaCl medium. As shown in Fig. 2-11 a very sharp drop of resistance without a precursor was observed inside this soft medium.

Another influence due to nonhydrostaticity is known on the apparent transition pressure of covalent crystals as evidenced in Si by Minomura and Drickamer (1962). It follows that the transition pressure measured in non-hydrostatic condition would become lower than that in perfect hydrostatic condition.

As seen from Table 2-2, the transition pressure of

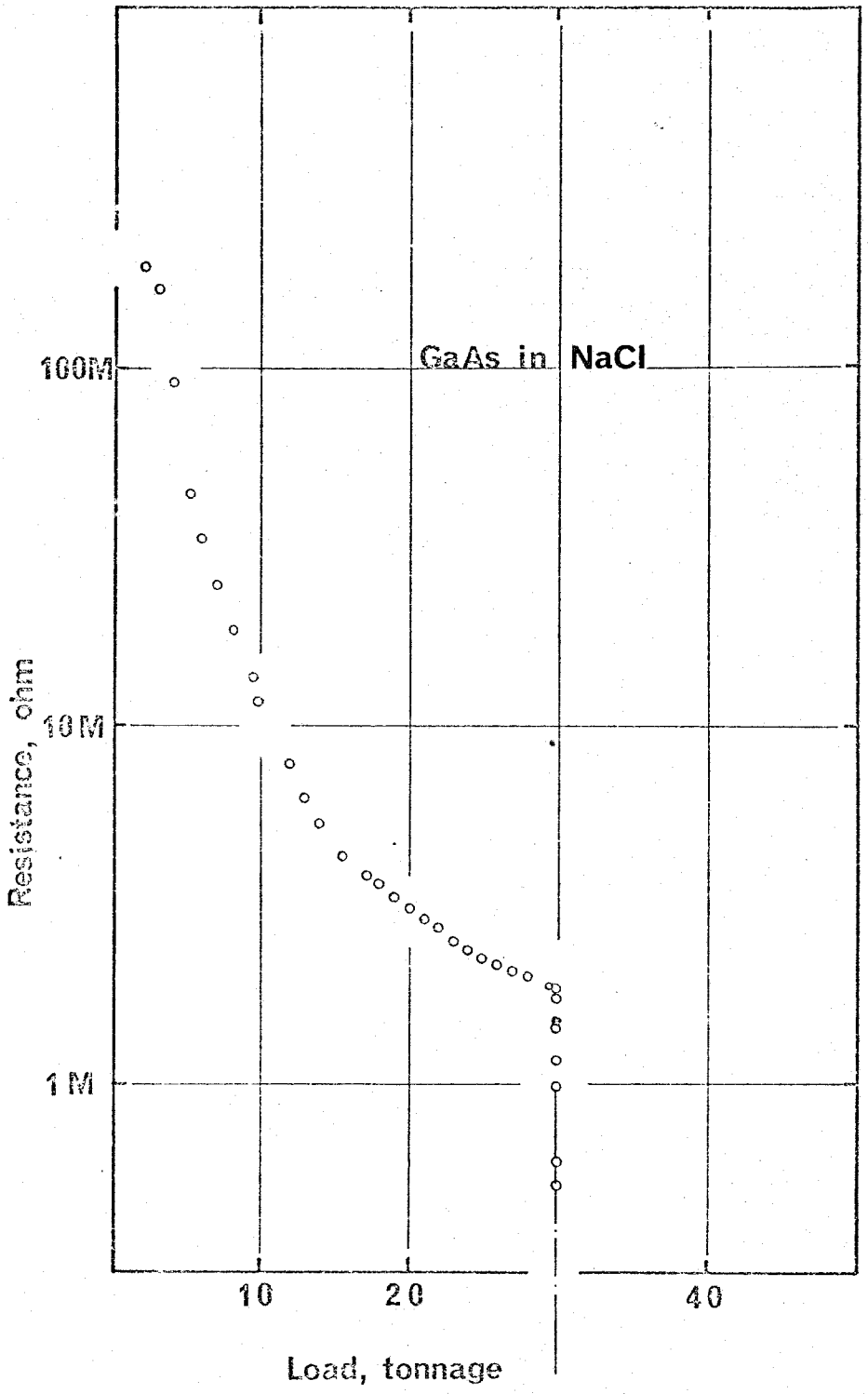

Fig. 2-11. Resistance-external load curve for GaAs inside NaCl medium.

GaAs observed inside the diamond medium is lower than that in the B medium, the difference being larger than the limit of experimental error. For GaP, the transition pressure observed in the diamond medium is again lower than that inside the B medium.

For ZnTe and ZnS, the difference in the transition pressure inside various media is within the experimental uncertainty. This suggests that in the pressure region below the ZnS transition, the pressure inside the diamond medium remains similar to that realized in the other three media.

4.4) Comparison with other fixed points data

In Table 2-3 are shown experimental results for the semiconductor-metal transitions in ZnTe, ZnS, GaAs, and GaP. An inaccordance is seen in the results and this can be attributed to the differences of devices and of pressure transmitting media used.

4.4.1) ZnTe

Samara and Drickamer (1962) observed the semiconductor-metal transition in ZnTe. Their report showed a hump to appear in the curve showing logarithm of resistance versus applied pressure relation. The hump was assumed to appear at 65-70 kbar. Next the resistance became maximum at 120 kbar before the final drop of resistance was seen.

No study has been made so far for the determination of transition pressure of ZnTe by means of NaCl x-ray measurement.

In the present experiment, there existed no hump but a minimum occurred at 75 kbar. As shown in Table 2-2, the semiconductor-metal transition pressure observed in each pressure transmitting medium lies in a range 127 to 131 kbar, which is within the experimental error.

Table 2-3. Comparison of transition pressures

Substance	Transition pressure (kbar)	Apparatus	Pressure scale	Reference
ZnTe	140-145	WC Drickamer anvil	new Drickamer	Drickamer (1970)
ZnS	180-185	WC Drickamer anvil	new Drickamer	Drickamer (1970)
	150 ± 5	diamond anvil	ruby	Piermarini and Block (1975)
	162 ± 4	cubic	NaCl	Yagi and Akimoto (1976, 1977)
GaAs	180-185	WC Drickamer anvil	new Drickamer	Drickamer (1970)
	180 ± 8	diamond anvil	ruby	Piermarini (1975)
	193 ± 5	cubic	NaCl	Yagi and Akimoto (1976, 1977)
	167 ± 18	shock wave	Hugoniot	Goto et al. (1976)
	170 ± 5	diamond anvil	NaCl	Yu et al. (1978)
GaP	220 ± 10	diamond anvil	ruby	Piermarini and Block (1975)
	220	Bridgman anvil	extrapolation (fixed points)	Homan et al. (1975)
	230-240	diamond Drickamer anvil	extrapolation (load/area)	Bundy (1975)
	>233	cubic	NaCl	Yagi and Akimoto (1977)

4.4.2) ZnS

Very high transition pressure of 240-250 kbar was reported for ZnS by Samara and Drickamer (1962). The value was later revised at 180-185 kbar according to the new Drickamer scale (1970).

Piermarini and Block (1975) confirmed the same transition in an opposed diamond-anvil cell. In their experiment, the transition was assumed to take place when the optically transparent ZnS crystal became opaque. The pressure at the transition was measured by the shift of the wavelength of ruby R-line. The transition pressure reported was 150 ± 5 kbar.

In a cubic anvil apparatus, Yagi and Akimoto (1976, 1977) determined the transition pressure from the simultaneous measurements of the electrical resistance change of ZnS and of the x-ray diffraction of NaCl. The transition pressure was 162 ± 4 kbar. More recently, the same samples as used in the present study have been compressed both in the diamond-anvil cell and in the cubic anvil apparatus by the above authors (private communication; Block, 1978). The transition pressure determined in each device has been substantially the same as reported earlier, respectively.

The transition pressure is observed at 153 kbar in the diamond medium, at 158 kbar in the B medium,

at 151 kbar in the LiH medium, and at 160 kbar in the g-BN medium, respectively in this study.

4.4.3) GaAs

Minomura and Drickamer (1962) first discovered the transition in GaAs at 240-250 kbar. The new Drickamer scale (Drickamer, 1970) reevaluated this pressure to be 180-185 kbar.

Next, Piermarini and Block (Piermarini, 1975) determined in the diamond-anvil cell the transition pressure to be 180 ± 8 kbar.

Goto et al. (1976) observed the transition at a pressure of 167 ± 18 kbar, which was generated dynamically by shock wave method.

The transition pressure determined in the cubic press was 193 ± 5 kbar (Yagi and Akimoto, 1976, 1977).

Yu et al.(1978) determined the transition pressure of GaAs to be 170 ± 5 kbar in the diamond-anvil cell. The pressure was determined by the NaCl scale.

The transition pressure has also been examined in the present study in various media as shown in Table 2-2. The highest pressure is 189 kbar in the B medium, while the lowest is 177 kbar obtained in the diamond medium, the difference in the pressure being more than 12 kbar.

4.4.4) GaP

Minomura and Drickamer (1962) examined a possibility of transition of GaP. Despite of the repeated experiments the transition was not observed.

Onodera et al. (1974) succeeded to prove an existence of this transition using split-sphere high pressure vessel. Homan et al. (1975) and Bundy (1975) reexamined the transition using different pressure vessels.

Piermarini and Block (1975) determined that the transition occurred at 220 ± 10 kbar. In the course of their experiments, they compressed the same crystal of GaP as used in the present study (Piermarini, 1975). They used the diamond-anvil cell and the ruby scale.

Yagi and Akimoto (1977) investigated the transition up to 233 kbar but they could not detect it, and no report has been appeared on the successful NaCl x-ray study of the semiconductor-metal transition of GaP.

In the present work, the repeated experiments using the B pressure medium have shown that the transition pressure lies at pressure around 250 kbar, one experiment showing it to be at 249 kbar and the other at 257 kbar, respectively. In the diamond medium, however, the transition is found at 221 kbar, which is the average of the two experiments using the diamond medium. This value shows a fairly good agreement to the data by Piermarini and Block (1975).

4.4.5) Further comparison

As described above, the same samples (ZnS and GaP) have been studied by both the present octahedral vessel and the diamond-anvil cell. We can, therefore, exclude an effect due to the difference of samples such as inherent impurities or defects. The inconsistency in the transition pressure is attributable to the nature of pressure environment, method of detection of transition, or the scale with which the pressure is determined, or their combination. It is quite difficult at present to analyse them quantitatively except for the problem of pressure scale.

Nevertheless, a very rough feature is perceivable. Since the transition pressure determined in the present diamond medium is closer to that measured in the diamond-anvil cell, the pressure generated in the diamond cell is considered to be accompanied by nonhydrostatic component. The present B, LiH, and g-BN media can generate quite a hydrostatic pressure as noted in Section 4.3. The pressure fixed points determined in these media are therefore preferable. The transition pressures of ZnTe(129.2 kbar), ZnS (155.0 kbar), GaAs(188.2 kbar), and GaP(252.6 kbar), each being the average of the values determined by the use of these media, form a new set of pressure scale above 100 kbar.

5. Conclusion

Progress is made in the design and the construction of device for manipulating simultaneous measurements of x-ray diffraction of NaCl and electric resistance of several semiconductors under pressure above 100 kbar. Pressures required for metallic transitions of several semiconductors are determined by the correlations of lattice shrinkage of NaCl due to compression, which is theoretically evaluated by an equation of state of this substance. The same kind of transition of GaP is also obtained at 253 kbar. Errors arised from the experimental procedures are precisely examined and hydrostatic compressions of samples are thoroughly discussed. It is concluded that all the results are accurate enough to use them as the best fixed points on the universal scale of pressure standard. The final values being :

ZnTe: 129.2 kbar ZnS: 155.0 kbar

GaAs: 188.2 kbar GaP: 252.6 kbar.

GENERAL CONCLUSION

1) A new high pressure vessel of split-octahedral type is designed and constructed. This vessel is capable of generating a quasi-hydrostatic pressures in excess of 250 kbar.

2) The use of this vessel makes it possible to undertake x-ray diffraction of samples under pressures above 100 kbar. Simultaneous measurements of their electric resistances are successful in a trial to detect the phase transitions of these substances from semiconductive to metallic states.

3) Fixed points, by which the pressures generated in a vessel are evaluated, are revised by the present investigation, the standard values proposed being :

ZnTe ----- 129.2 ± 6.1 kbar

ZnS ----- 155.0 ± 6.8 kbar

GaAs ----- 188.2 ± 7.8 kbar

GaP ----- 252.6 ± 9.6 kbar.

4) Semiconductor to metal transition of GaP is expected to be a new fixed point around 250 kbar but has not been accurately estimated. First determination of the fixed point is made in this study. The value is propounded at 252.6 ± 9.6 kbar.

REFERENCES

Balchan, A. S., and H. G. Drickamer, Rev. Sci. Instrum., 32, 308 (1961).

Bancroft, D., E. L. Peterson, and S. Minshall, J. Appl. Phys., 27, 557 (1956).

Barnett, J. D., and H. T. Hall, Rev. Sci. Instrum., 35, 175 (1964).

Barnett, J. D., S. Block, and G. J. Piermarini, Rev. Sci. Instrum., 41. 1 (1973).

Bassett, W. A., T. Takahashi, and P. W. Stook, Rev. Sci. Instrum., 38, 37 (1967).

Bassett, W. A., T. Takahashi, H. K. Mao, and J. Weaver, J. Appl. Phys., 39, 319 (1968).

Block, S., Report on round-robin study of ZnS (April, 1978).

Bridgman, P. W., Proc. Amer. Acad. Arts Sci., 74, 21 (1940).

Bridgman, P. W., Proc. Amer. Acad. Arts Sci., 76, 1 (1945).

Bundy, F. P., Rev. Sci. Instrum., 46, 1318 (1975).

Cohn, W. M., Phys. Rev., 44, 326 (1933).

Contre, M., High Temp. High Pressures, 1, 339 (1969).

Decker, D. L., J. Appl. Phys., 36, 157 (1965).

Decker, D. L., J. Appl. Phys., 42, 3239 (1971).

Drickamer, H. G., Rev. Sci. Instrum., 41, 1667 (1970).

Forman, R. A., G. J. Piermarini, J. D. Barnett, and S. Block, Science, 176, 284 (1972).

Freud, P. J. and P. N. LaMori, Trans, Amer. Cryst. Assoc., 5, 155 (1969).

Freud, P. J. and C. B. Sclar, Rev. Sci. Instrum., 40, 434 (1969).

Frevel, L. K., Rev. Sci. Instrum., 6, 214 (1935).

Fritz, J. N., S. P. Marsh, W. J. Carter, and R. G. McQueen, "Accurate Characterization of the High-Pressure Environment", P. 201, NBS Spec. Publ. No. 326 (1971).

Goto, T., Y. Syono, J. Nakai, and Y. Nakagawa, Solid State Commun., 18, 1607 (1976).

Homan, C. G., D. P. Kendall, T. E. Davidson, and J. Frankel, Solid State Commun., 17, 831 (1975).

Inoue, K. and T. Asada, Jpn. J. Appl. Phys., 33, 776 (1973).

Jacobs, R. B., Phys. Rev., 54, 468 (1938).

Jamieson, J. C., A. W. Lawson, and N. O. Nachtrieb, Rev. Sci. Instrum., 30 , 1016 (1959).

Jamieson, J. C., and A. W. Lawson, J. Appl. Phys., 33, 776 (1962).

Jamieson, J. C., Science, 139, 1291 (1963).

Kapitanov, E. V., V. N. Panyushkin, L. F. Vereshchagin, E. N. Yakovlev, V. I. Novokshonov, and V. V. Evdokimova, High Temp. High Pressures, 7, 555 (1975).

Kawai, N., Proc. Jpn. Acad., 42, 385 (1966).

Kawai, N., and S. Endo, Rev. Sci. Instrum., 41, 1178 (1970).

Kawai, N., M. Togaya, and A. Onodera, Proc. Jpn. Acad., 49, 623 (1973).

Kawai, N., A. Onodera, S. Mizukami, and A. Ohtani, Proc. Jpn. Acad., 51, 650 (1975).

Lawson, A. W., and N. A. Riley, Rev. Sci. Instrum., 20, 763 (1949).

Lawson, A. W., and F. Y. Tang, Rev. Sci. Instrum., 21, 815 (1950).

Lloyd, E. C., "Accurate Characterization of the High-Pressure Environment", p. 314, NBS Spec. Publ. No. 326 (1971).

Mao, H. K., P. M. Bell, J. W. Shanner, and D. J. Stein, J. Appl. Phys., 49, 3276 (1978).

Mii, J., I. Fujishiro, M. Senoo, and K. Ogawa, High Temp. High Pressures, 5, 155 (1973).

Minomura, S., and H. G. Drickamer, J. Phys. Chem. Solids, 23, 451 (1962).

Ohtani, A., S. Mizukami, M. Katayama, A. Onodera, and N. Kawai, Jpn. J. Appl. Phys., 16, 1843 (1977).

Onodera, A., N. Kawai, K. Ishizaki, and I. L. Spain, Solid State Commun., 14, 803 (1974).

Perez-Albuerne, E. A., K. F. Forsgren and H. G. Drickamer, Rev. Sci. Instrum., 35, 29 (1964).

Piermarini, G. J., private communication to A. Onodera (1975).

Piermarini, G. J., and S. Block, Rev. Sci. Instrum., 46, 973 (1975).

Piermarini, G. J. S. Block, J. D. Barnett, and R. A. Forman, J. Appl. Phys., 46, 2774 (1975).

Samara, G. A., and H. G. Drickamer, J. Phys. Chem. Solids, 23, 457 (1962).

Singh, A. K., and G. C. Kennedy, J. Appl. Phys., 45, 4686 (1974).

Weaver, J. S., T. Takahashi, and W. A. Bassett, "Accurate Characterization of the High-Pressure Environment", p. 189, NBS Spec. Publ. No. 326 (1971).

Yagi, T., and S. Akimoto, J. Appl. Phys., 47, 3350 (1976).

Yagi, T., and S. Akimoto, "High Pressure Research : Applications to Geophysics", p. 573, eds. M. H. Manghnani and S. Akimoto, Academic Press, New York (1977).

Yu, S. C., I. L. Spain, and E. F. Skelton, Solid State Commun., 25, 46 (1978).